



THE UNIVERSITY OF
WAIKATO
Te Whare Wānanga o Waikato

Research Commons

<http://researchcommons.waikato.ac.nz/>

Research Commons at the University of Waikato

Copyright Statement:

The digital copy of this thesis is protected by the Copyright Act 1994 (New Zealand).

The thesis may be consulted by you, provided you comply with the provisions of the Act and the following conditions of use:

- Any use you make of these documents or images must be for research or private study purposes only, and you may not make them available to any other person.
- Authors control the copyright of their thesis. You will recognise the author's right to be identified as the author of the thesis, and due acknowledgement will be made to the author where appropriate.
- You will obtain the author's permission before publishing any material from the thesis.

Paleoliquefaction in Late Pleistocene alluvial sediments in the Hauraki and Hamilton basins

A thesis submitted in partial fulfilment
of the requirements for the degree

of

Masters of Science (Research)

in Earth Sciences

at

The University of Waikato

by

Melissa Anita Kleyburg

The University of Waikato
2015



THE UNIVERSITY OF
WAIKATO
Te Whare Wānanga o Waikato

Dedicated to my brother Pieter Kleyburg
Who taught me to embrace every obstacle in life with a smile
You are forever in my heart

Abstract

Liquefaction susceptibility of the Late Pleistocene Hinuera Formation volcanogenic sediments is of interest to the engineering community as it is unclear whether materials of this age will still be prone to activation by cyclic stresses. Screening methods suggest a low susceptibility to liquefaction, yet instrumental tools such as Cone Penetrometer Tests (CPT) imply a much greater susceptibility. Recognising paleoliquefaction features in the geological record provides evidence of paleoseismicity.

The Hinuera Formation was deposited by an active braided alluvial system of the ancestral Waikato River during the late Pleistocene, with the bulk of sediments located in the Hauraki Basin (deposited before c. 22,000 calendar years ago) and in the Hamilton Basin (deposited mainly c. 22,000 to c. 18,000 calendar years ago). Lithofacies in the Hinuera Formation include unconsolidated gravels, gravelly sands, sands, and silts, with interbedded peats. The deposits are complex structurally both laterally and vertically because of the migration of channels laterally during low-angle fan-building. Previous studies on post-sedimentary features of the Hinuera Formation identified uncommon secondary sedimentary structures that at the time were of uncertain origin, either from non-seismic or seismic triggers.

Excavations into the Hinuera Formation at two sites showed definitive evidence of paleoliquefaction features: a sand quarry on Aspin Road (site 15) and Endeavour Primary School (site 16). These sites showed earthquake-induced injection structures (sand dikes) intruding through several lithological layers, including an organic layer. Through cross-cutting relationships, maximum age of occurrence for the injection structures are determined. A seismic event causing liquefaction occurred sometime after c. $20,749 \pm 204$ calendar years ago (95% probability range) at site 15 and after c. $19,964 \pm 222$ calendar years ago (95% probability range) at site 16.

The instrumental CPT data provides a valid method of predicting liquefaction potential. However, the sedimentary materials are highly variable over short distances and so liquefaction is therefore localised; it is difficult to infer ground conditions more than a few metres from a CPT site without further ground-truth information. Sites of known paleoliquefaction features show Factor of Safety (FS) values of 0.25 to 0.5 for the critical layers, these are values that predict liquefaction. Liquefaction Potential Index (LPI) values that are calculated present high risks of liquefaction occurring and calculated liquefaction severity number (LSN) values show minor to moderate expression of liquefaction. Field observations and CPT_u based predicted liquefaction are therefore in keeping.

Key conditions observed at the two sites with identified paleoliquefaction features included the presence of silts associated with organic-rich materials. High levels of organic material reflect impeded or slow flowing drainage associated with overbank silt deposition, and thus are indicative of the elevated water tables required for liquefaction. The liquefaction structures observed are both at locations where the modern (pedological) soils (Te Rapa and Te Kowhai soil series) occurred in topographic depressions on the Hinuera Surface. Therefore this relationship enabled the development of a soil-landscape model using the modern soil pattern to tentatively predict, areas of higher susceptibility to liquefaction.

Acknowledgements

Firstly, I would like to express my utmost appreciation to my supervisors Dr Vicki Moon, Professor David Lowe and Emeritus Professor Campbell Nelson. Vicki, your support and guidance throughout this experience has been remarkable. Thank you for allowing me to choose a topic I am really interested in, and also for answering “a million” questions every time you came into the office – I hope now you’ll be able to go to tea break in peace. David, your positivity, extensive knowledge about anything and everything, proficient editing, enthusiastic attitude are all things I aspire to myself. Cam, your expert knowledge and field assistance are greatly appreciated.

I’m very grateful for the financial assistance received from the Waikato Regional Council, and from the School of Science (Earth Sciences group), University of Waikato. Your support made this project possible. I also thank the quarry owners and field site managers who allowed me access to field sites, the Waikato Radiocarbon Dating Laboratory, and AECOM.

I am profoundly grateful to Andrew Holland at HD Consultants. Thank you for your mentorship and industry expertise. I really appreciated the time and effort you’ve put into helping out a geo student understand complex engineering concepts.

To my main “homegirls” Amy Jane Christophers (Big Red/Clifford) and Camillia Pauline Garae (Ni-Vanuatu princess) – thanks for your in-depth discussion about thesis- and (especially) non-thesis related topics. Your friendship and madness made life ever so more exciting. I honestly don’t think I would have made it through without you both. Thanks to my fellow Earth Science MSc students for helping out, in particular Megan Saunders and Emma Bagley, with assistance in the field.

Jason, you’re always there when I need you most. Thank you for editing, insightful suggestions and continuous belief in me. I am a better person because of you.

I would like to express my sincere gratitude to my family and friends for your support and encouragement throughout this project. To my biggest financial investors, Mum and Dad, your love and guidance have always encouraged me to seek what I enjoy.

Table of Contents

Abstract	v
Acknowledgements	vii
Table of Contents	ix
List of Figures	xii
List of Tables	xvii
Chapter 1 Introduction	1
1.1 Background to the problem of liquefaction.....	1
1.2 Summary of existing research	2
1.3 Aims and objectives	4
Chapter 2 Literature Review	5
2.1 Introduction	5
2.2 Soil liquefaction	5
2.2.1 Flow (static) liquefaction	5
2.2.2 Cyclic (softening) liquefaction.....	6
2.3 Paleoliquefaction	7
2.3.1 Soft-sediment deformation.....	8
2.4 Ground effects	13
2.5 Liquefaction assessment.....	14
2.5.1 Cyclic Stress Ratio	15
2.5.2 Cyclic Resistance Ratio (CRR).....	15
2.6 Study area	24
2.6.1 Hinuera Formation	24
2.6.2 Hauraki Basin.....	26
2.6.3 Hamilton Basin	28
2.6.4 Historical Earthquakes	29
2.7 Canterbury Earthquake Sequence 2010-2012	31
2.8 Summary	33
Chapter 3 Methods	35
3.1 Introduction	35
3.2 Site selection.....	35
3.3 Facies analysis	36

3.3.1	Site descriptions	36
3.3.2	Geological description	37
3.3.3	Lithofacies and paleoenvironment interpretation.....	38
3.4	Soft sediment deformation	38
3.5	Particle size analysis.....	39
3.6	Liquefaction assessment.....	39
3.7	Radiocarbon dating.....	40
3.7.1	CPTu-based soil analysis	40
3.7.2	CPTu cyclic liquefaction analysis	42
3.7.3	Minimum PGA.....	44
Chapter 4 Lithofacies analysis of the Hinuera Formation		47
4.1	Introduction	47
4.2	Hauraki Basin	48
4.2.1	Site 1 – Private property (Kevin Nola’s Sandpit)	48
4.2.2	Site 2 – McPhersons Sand Supply	49
4.2.3	Site 3 – Daltons Sand Ltd	50
4.2.4	Site 4 – Private property (Ian Settle’s Sandpit).....	51
4.2.5	Site 5 – Wilsons Sand	52
4.2.6	Site 6 – Manawaru Sandfill and Livestock Ltd.....	54
4.2.7	Site 7 – Tirau Sand Quarry.....	55
4.3	Hamilton Basin.....	57
4.3.1	Site 8 – Landcycle	57
4.3.2	Site 9 – Monavale Sand Quarry	58
4.3.3	Site 10 – Perry Resources	60
4.3.4	Site 11 – Waikato Aggregates.....	60
4.3.5	Site 12 – Coombes Sand	61
4.3.6	Site 13 – Porritts Sand Quarry	62
4.3.7	Site 14 – IH Wedding and Sons Waikato Ltd.....	63
4.3.8	Site 15 – Quarry on Aspin Road	64
4.3.9	Site 16 – Endeavour Primary School	66
4.3.10	Site 17 – Waikato Expressway (Cambridge section).....	66
4.4	Summary	67
Chapter 5 Paleoliquefaction		71
5.1	Introduction	71

5.2	Site 15 – Quarry on Aspin Road	71
5.2.1	Injection structures	71
5.2.2	Particle size analysis	74
5.2.3	Radiocarbon dating	78
5.2.4	Liquefaction assessment.....	78
5.3	Site 16 – Endeavour Primary School.....	90
5.3.1	Injection structures	90
5.3.2	Particle size analysis	93
5.3.3	Radiocarbon dating	94
5.3.4	Liquefaction assessment.....	95
5.4	Summary	106
Chapter 6 Discussion		107
6.1	Introduction	107
6.2	Soft-sediment deformation	107
6.2.1	Possible evidence of paleoliquefaction	107
6.2.2	Definitive evidence of paleoliquefaction	108
6.3	Liquefaction assessment.....	111
6.3.1	Site 15 – Quarry on Aspin Road	111
6.3.2	Site 16 – Endeavour Primary School	112
6.3.3	Calculation methods.....	113
6.3.4	Aging factor	114
6.4	Soil-landscape model	115
6.4.1	Limitations	118
6.5	Summary	118
Chapter 7 Conclusion		121
7.1	Paleoliquefaction	121
7.2	Liquefaction assessment.....	122
7.3	Summary	123
7.4	Recommendations for future study	124
References		125

List of Figures

Figure 1.1: Location map highlighting the study area: Hamilton and Hauraki basins (McCraw, 2011).	2
Figure 2.1: Typical morphology of paleoliquefaction features from Obermeier <i>et al.</i> (2005) modified after Obermeier (1996).	8
Figure 2.2: Structures of different seismites. (a) Ball-and-pillow structures (Moretti & Ronchi, 2011). b) Individual pseudo-nodules and flame structures (Rana <i>et al.</i> , 2013). (c) Dish-and-pillar structures, field observation (left) and schematic diagram (right) (Ghosh <i>et al.</i> , 2012). (d) Clastic sand dike from the Darfield Earthquake (Almond <i>et al.</i> , 2010).	10
Figure 2.3: Reconstruction of pre-deformed stratigraphy (initial system) to the deformed system, showing regular and irregular deformations from massive (1) and cross-bedded (2) strata (Moretti & Ronchi, 2011).	12
Figure 2.4: Context-based analysis from lacustrine deposits in the Sant’ Arcangelo Basin, Italy with sketches of the soft-sediment deformation and their associated driving forces and trigger agent (Moretti & Sabato, 2007).	13
Figure 2.5 Standard Penetration Test (SPT) procedure based on the ASTM standard (Mayne <i>et al.</i> , 2001).	17
Figure 2.6: Cone Penetration Test (CPT) procedure with important measuring variables (Mayne <i>et al.</i> , 2001).	19
Figure 2.7: Soil Behaviour Type (SBT) chart for normalised cone resistance and friction ratio with the various soil types defined by SBT index (I_c). From Robertson (2010a), modified version of Robertson and Wride (1998).	21
Figure 2.8: Relationship between CSR and q_{cIN} for historical earthquakes producing liquefaction and no liquefaction events to determine threshold CRR for CPT which is the CPT clean-sand base curve indicated on graph.	22
Figure 2.9: Correlation between CSR and V_{s1} for shear-wave measurements for historical liquefaction and non-liquefaction events. Curved boundary is defined as CRR for differing fine contents (Andrus & Stokoe, 2000).	24
Figure 2.10: Location of the Kerepehi Fault and sections (Beanland & Berryman, 1986).	28
Figure 2.11: Comparison of liquefaction severity between the (a) Darfield earthquake and the (b) Christchurch earthquake (Maurer <i>et al.</i> , 2014).	32
Figure 3.1: Locality map of sites visited in the Hamilton and Hauraki basins. Site numbering defined in chapter 4.	36
Figure 3.2: Comparison between Udden-Wentworth scale and NZGS (2005) grain size criteria. Arrows show similarities.	37
Figure 4.1: Physiographic and lithofacies model for Hinuera Formation from Hume <i>et al.</i> , (1975). A1: Large trough cross-bedded, rhyolitic and pumiceous gravelly and slightly gravelly quartzofeldspathic sands. A2: Planar cross-bedded, gravelly sands (same texture as A1). B. Fine trough cross-bedded sands. C1: Poorly defined horizontally stratified (often appears structureless), rhyolitic sandy gravels. C2: Horizontal to gently dipping laminae, gravelly sands. D: Horizontal laminae	

pumiceous silts. E: Horizontal laminae to massive peats and peaty pumiceous silts.	48
Figure 4.2: (a) Stratigraphic section at Kevin Nola’s Sandpit showing horizontal bedding near upper boundary in S1. Person is 1.8 m tall. (b) Contact between G1 and S1. Arrows point to pseudo-nodules. Scale pencil 14 cm long.....	49
Figure 4.3: Light grey, soft sediment deformation (arrow) intruding through Z1 at section at McPhersons Sand Supply. Cutting tool 30 cm long.	50
Figure 4.4: S4 overlain by Z1 at Daltons Sand quarry. S4 contains fine cross-beds (arrow) and is interpreted as a minor channel. Cutting tool 30 cm long.....	51
Figure 4.5: The inactive sandpit at site 4 contains weakly cemented surficial sand wash and vegetation cover on facies XBS1 and Z2. Person 1.6 m tall.....	52
Figure 4.6: (a) Large quarry: facies XBS1 and Z1 at Wilson Sand, XBS1 contains a thick orange iron stained bed. Person 1.8m tall. (b) Small quarry: interbedded gravelly sands and sandy silt (S1 & Z1). Cutting tool 30 cm long.	53
Figure 4.7: (a) Stratigraphic section of Manawaru Sandfill deposits. Person 1.7 m tall, tape measure 2 m long. (b) Heavily stained and consolidated XBS1a (manganese) and XBS1b (iron) facies. Cutting tool 30 cm long.	55
Figure 4.8: (a) Small possible liquefaction structure (arrow) in facies Z1 at Tirau Sand Quarry. Also note evidence of a water table. Scale 8 cm long. (b) Inferred pyroclastic deposit with pumice clasts (arrows) at Tirau Sand Quarry. Cutting tool 30 cm.	57
Figure 4.9: (a) Stratigraphic sequence of the active quarry section at Landcycle. Person 1.7 m tall. (b) Stratigraphic sequence of the inactive quarry section at Landcycle with a thick white tephra deposit (Z2). Tape measure 2 m long.	58
Figure 4.10: A section of the Monavale Sand Quarry stratigraphic sequence containing the interbedded S2 and Z1 overlain by XBS1. Colluvium to the left of the sequence contains possible rotated blocks (see arrow, faint light brown material) that may have resulted from quarrying. Cutting tool 30 cm long.	59
Figure 4.11: Section through the Perry Resources quarry face, encompassing all facies identified (XBS1, Z1 and Z2). Water table is evident as the pond.....	60
Figure 4.12: (a) Quarry face at Waikato Aggregates including all facies (XBS1, Z1 and Z2) noted. Person 1.7 m tall. (b) Upper part of the section seen in (a) showing Z1 and two paleosol beds (arrowed). Person 1.7 m tall.	61
Figure 4.13: (a) Facies XBS1 at Coombes Sand with thick iron stained bed. (b) Facies Z1 irregular contact to XBS1 and depression structure due to eroded out material. Cutting tool 30 cm long.	62
Figure 4.14: Rhyolitic XBG1 facies with large gravel clasts at Porritts Sand. Cutting tool 30 cm long.	63
Figure 4.15: Trough cross-bedding of facies XBG1 at IH Wedding and Sons Waikato quarry. Cutting tool 30 cm long.	64
Figure 4.16: Sections at the Quarry on Aspin Road. (a) Quarry face. Niwashi cutting tool 30 cm long. (b) Injection structures (arrows). Water table adjacent to section indicating shallow water table. Cutting tool 30 cm long.	65

Figure 4.17: Injection structures at site 16. (a) Source bed and water table at locality i. (b) Injection structure across excavated floor. Cutting tool 30 cm long.....	66
Figure 4.18: Facies Z4 and XBS1 at the Waikato Expressway, Cambridge section showing deformation structure (arrow) from syn-depositional processes. Cutting tool 30 cm long.	67
Figure 5.1: Cross-sectional view of injection structures found at the Quarry on Aspin Road, Cambridge. (a) Schematic diagram of injection structures and surrounding stratigraphic units, refer to key. Injection-1 stalls at the Sand-2 and Sand-3 boundary. (b) Field observations, cutting tool 30 cm.	72
Figure 5.2: Stratigraphy at Quarry on Aspin Road, Cambridge, emphasising the stratigraphic units the injection structures intrude through (refer to key in Figure 5.1). Injection structure-1 tapers from injection structure-2 and intrudes through Silt-1 and Sand-2. Injection structure-2 intrudes through Silt-1, Organic silt, Silt-2 and stalls halfway in Sand-2.	73
Figure 5.3: Longitudinal view of injection structures including all units in previous stratigraphic column (Figure 5.2) at Quarry on Aspin Road. Injection structure-2 dimensions: width 2 cm, vertical height 10 cm and horizontal length of 1.20 m (*total length of injection structure; this is not captured in image) (a) Schematic diagram, “X” defines sample locations (refer to key in Figure 5.1). (b) Field observations, cutting tool ~ 30 cm.	73
Figure 5.4: Cross-sectional view of injection structure-2 cross-cutting the organic silt layer and indicating its connection to Sand-1, providing field evidence as the source bed. (a) Schematic diagram (refer to key in Figure 5.1). (b) Field observation, cutting tool ~ 30 cm in length.	74
Figure 5.5: Cumulative plots of particle size at Quarry on Aspin Road for (a) stratigraphic units: Sand-1, Sand-3, Injection-1, Injection-2a and Injection-2b; and (b) stratigraphic units: Silt-1, Organic silt, Silt-2 and Sand-2. Bold inner boundaries define a high possibility of liquefaction occurring and outer dotted boundary define a possibility of liquefaction occurring (boundaries reproduced by NZGS (2010) modified from MTJ (1999))......	75
Figure 5.6: Site location of injection structures, CPTus, and radiocarbon samples of organic silt location for Quarry on Aspin Road.	79
Figure 5.7: Plots exported from CPeT-IT presenting corrected cone resistance (q_t), friction ration (R_f) and pore water pressure (u_2) at the Quarry on Aspin Road. (a) CPTu-1. (b) CPTu-2.....	80
Figure 5.8: Depth verses shear strength plots exported from CPeT-IT for a) CPTu-1 and b) CPTu-2 at the Quarry on Aspin Road.	81
Figure 5.9: Non-normalised soil behaviour type plots for a) CPTu-1 and b) CPTu-2 at the Quarry on Aspin Road. Bold black box indicates critical layers for each CPTu test. Depths defining critical layer for CPTu-1: 1.73 to 5.64 m and CPTu-2: 3.19 to 6.81m.	82
Figure 5.10: ULS (1 in 500 year return period) cyclic liquefaction plots at the Quarry on Aspin Road, imported from CLiq (GeoLogismiki, 2006). (a) CPTu-1 and (b) CPTu-2. Liquefaction parameters: M_{eff} 5.9, ground water table 0 m and PGA 0.25, calculation method Idriss and Boulanger (2008), bold black box defining critical layer. CRR and CSR plot: red line is the CSR, purple line is CRR. LPI plot:	

green zone is “low risk”, orange zone is “high risk” and red zone is “very high risk” of liquefaction occurring.	84
Figure 5.11: ULS (1 in 500 year return period) cyclic liquefaction plots at the Quarry on Aspin Road, imported from CLiq (GeoLogismiki, 2006). a) CPTu-1 and b) CPTu-2. Liquefaction parameters: M_{eff} 5.9, ground water table 0 m and PGA 0.25, calculation method Boulanger and Idriss (2014), bold black box defining critical layer. CRR plot: red line is the CSR, purple line is CRR. LPI plot: green zone is “low risk”, orange zone is “high risk” and red zone is “very high risk” of liquefaction occurring.	85
Figure 5.12: Parametric graphs of PGA calculated for (a) settlement, (b) LPI and (c) LSN using calculation method Idriss and Boulanger (2008) for site 15.	87
Figure 5.13: Parametric graphs of PGA verses (a) settlement, (b) LPI and (c) LSN using calculation method Boulanger and Idriss (2014) for site 15.	89
Figure 5.14: Cross-sectional view of pit at locality i, Endeavour Primary School, north Hamilton. (a) Schematic diagram of injection structure intruding through sand, peat and silt beds (see key in Figure 5.1). Dimensions: width of 3 cm, vertical height of 1.10 m and 3.30 m for the path travelled on the excavated floor (above the pit). (b) Field observation. (c) Stratigraphy of pit sequence at locality i.	91
Figure 5.15: Cross-sectional view looking above pit at locality i, for Endeavour Primary School. (a) Schematic diagram of multiple paleoliquefaction features across the excavated floor, injection structure from pit splays into different directions (see key in Figure 5.1). (b) Field observation, field book ~ 30 cm in length.	92
Figure 5.16: Cross-sectional view of small pit at locality ii. (a) Schematic diagram of injection structures intruding through a silt and sand layer (see key in Figure 5.1). (b) Field observations, cutting tool ~ 30 cm. Injection structures with widths of 2 cm and vertical height of 30 cm.	92
Figure 5.17: Endeavour Primary School cumulative plots of particle size analysis for stratigraphic units: Sand and Injection. Bold inner boundaries define a high possibility of liquefaction occurring and outer dotted boundary define a possibility of liquefaction occurring (boundaries reproduced by NZGS (2010) modified from MTJ (1999)).	93
Figure 5.18: Site location of injection structures and CPTus at site 16.	95
Figure 5.19: Basic plots exported from CPeT-IT presenting corrected cone resistance (q_c), friction ration (R_f) and pore water pressure (u_2) at Endeavour Primary School. (a) Locality i- CPTu-6. (b) Locality-ii CPTu-3.	96
Figure 5.20: Shear strength verses depth plots for (a) CPTu-6 - locality i and (b) CPTu-3 (locality ii). Exported from CPeT-IT for Endeavour Primary School. See appendix 3 for other estimated plots.	97
Figure 5.21: Soil behaviour type plots for locality i, CPTu-6 (left) and locality ii, CPTu-3 (right) at Endeavour Primary School. Bold black box indicates critical layers for each CPTu test. Depths defining critical layer for CPTu-6: 3.00 to 3.70 m and CPTu-3: 3.60 to 4.00 m.	98
Figure 5.22: ULS (1 in 500 year return period) cyclic liquefaction plots at Endeavour Primary School, imported from CLiq (GeoLogismiki, 2006). (a) CPTu-6 and (b) CPTu-3. Liquefaction parameters: M_{eff} 5.9, ground water table 0 m and	

PGA 0.22, calculation method Idriss and Boulanger (2008), bold black box defining critical layer. CRR plot: red line is the CSR, purple line is CRR. LPI plot: green zone is “low risk”, orange zone is “high risk” and red zone is “very high risk” of liquefaction occurring. 100

Figure 5.23: ULS (1 in 500 year return period) cyclic liquefaction plots at Endeavour Primary School, imported from CLiq (GeoLogismiki, 2006). (a) CPTu-6 and (b) CPTu-3. Liquefaction parameters: M_{eff} 5.9, ground water table 0 m and PGA 0.22, calculation method Boulanger and Idriss (2014), bold black box defining critical layer. CRR plot: red line is the CSR, purple line is CRR. LPI plot: green zone is “low risk”, orange zone is “high risk” and red zone is “very high risk” of liquefaction occurring. 101

Figure 5.24: Parametric graphs of PGA verses (a) settlement, (b) LPI and..... 103

Figure 5.25: Parametric graphs of PGA verses (a) settlement, (b) LPI and (c) LSN using calculation method Boulanger and Idriss (2014) for site 16. 105

Figure 6.1: Relationship of FS verses aging factor for (a) site 15 and (b) site 16. Below FS=1, liquefaction is predicted to occur..... 115

Figure 6.2: Map of soils likely to be more prone to liquefaction (pink-purple colours) on the basis of a soil-landscape model of the Hamilton and Hauraki basins. 117

List of Tables

Table 2-1: Criteria-based trigger identification for a seismic agent summarised from Owen and Moretti (2011).....	11
Table 2-2: Soil profile name according to the Vs (Wair <i>et al.</i> , 2012).....	23
Table 2-3: Historical Earthquakes within the Waikato Area.	30
Table 3-1: Site subsoil classification scheme (McVerry <i>et al.</i> , 2006; Standards New Zealand, 2004).....	41
Table 3-2: Maximum depth limits: Table 3.2 from NZS1170.5: 2004 (Standards New Zealand, 2004).	41
Table 3-3: Peak ground coefficients for a 1000 year return period ($C_{0,1000}$) and effective magnitudes (M_{eff}) for towns and cities in the Hamilton and Hauraki basins (from Table 6A.1: NZTA, 2014).....	43
Table 3-4: Summary of liquefaction parameters, used in CLiq for Hamilton and Cambridge.	44
Table 4-1: Lithofacies identified and their interpreted paleoenvironment.....	47
Table 4-2: Summary table of sites with no definite evidence of paleoliquefaction	68
Table 5-1: Mode, mean, sorting, skewness and kurtosis of the lithologies surrounding the injection structures (organised according to stratigraphic sequence) and of the injection structures (samples organised from source bed to loss in sequence) at Quarry on Aspin Road. Measurements of particle size are determined using Udden-Wentworth scale, values in phi units (ϕ) unless stated.....	77
Table 5-2: Radiocarbon dates for organic silt at site 15.....	78
Table 5-3: Summary of minimum PGA results for site 15.	86
Table 5-4: Calculated liquefaction parameters for site 15 using Idriss and Boulanger (2008).	88
Table 5-5: Calculated liquefaction parameters for site 15 using Boulanger and Idriss (2014).	90
Table 5-6: Mode, mean, sorting, skewness and kurtosis at locality i, Endeavour Primary School. Measurements of particle size are determined using Udden-Wentworth scale, values in phi units (ϕ) unless stated.	94
Table 5-7: Radiocarbon date for peat material at site 16 (Endeavour Primary School).	94
Table 5-8: Summary of minimum PGA results for site 16	102
Table 5-9: Calculated liquefaction parameters for site 16 using Idriss and Boulanger (2008).	104
Table 5-10: Calculated liquefaction parameters for site 16 using Boulanger and Idriss (2014).	106
Table 6-1: Correlation and classification of soil series.....	118

Chapter 1

Introduction

1.1 Background to the problem of liquefaction

Events in Christchurch during the 2010–2011 earthquake sequence have highlighted liquefaction as a potential hazard for communities across New Zealand. The liquefaction process occurs in saturated, non-cohesive sediments (typically those dominated by fine sand to coarse silt). Increased pore water pressure induced by cyclic stresses leads to a complete loss of shear strength in the affected sediments; the materials become a fluid with sediment grains suspended in water. Earthquakes with a magnitude greater than M_w 5.5 are the common trigger for liquefaction. Loss of bearing strength, differential settlement, and sand boils (which are formed as the liquefied sediment escapes upwards to the ground surface) are common features of liquefaction. Young, loose sedimentary sequences in environments with high water tables are the most prone to liquefaction. In general, ‘modern’ (< 500 years) and Holocene (< 11,700 years) sediments are recognised as being most at risk of liquefaction. However, a few cases of liquefaction in older (Late Pleistocene) sediments have also been recorded.

The Late Pleistocene Hinuera Formation is a very low angled, braided alluvial fan sequence consisting of volcanogenic (quartzofeldspathic) gravels, sands, silts, and interbedded peats. Deposition occurred in the Hamilton and Hauraki basins and evidence suggests deposition occurred between c. 25,000 to c. 18,000 calendar (cal.) years ago (e.g. McCraw, 2011). Much of the Hamilton and Hauraki basins (Figure 1.1) are underlain by the Hinuera Formation. The Hinuera Formation partly infills both basins, with the Hamilton Basin being an oval-shaped depression that extends from near Te Awamutu to Taupiri and the Hauraki Basin extending from Tirau to the Firth of Thames. This area is of interest to the engineering community as it is unclear whether materials of this age will still be prone to activation by cyclic shear stresses, which are forces most commonly induced by earthquakes.

The Hinuera Formation forms much of the modern land surface (see chapter 2) and hence is the foundation of many structures for both the Hamilton and Hauraki basins. Therefore, understanding the liquefaction susceptibility of the Hinuera Formation is essential for assessing the risk associated with liquefaction in this part of the Waikato Region.

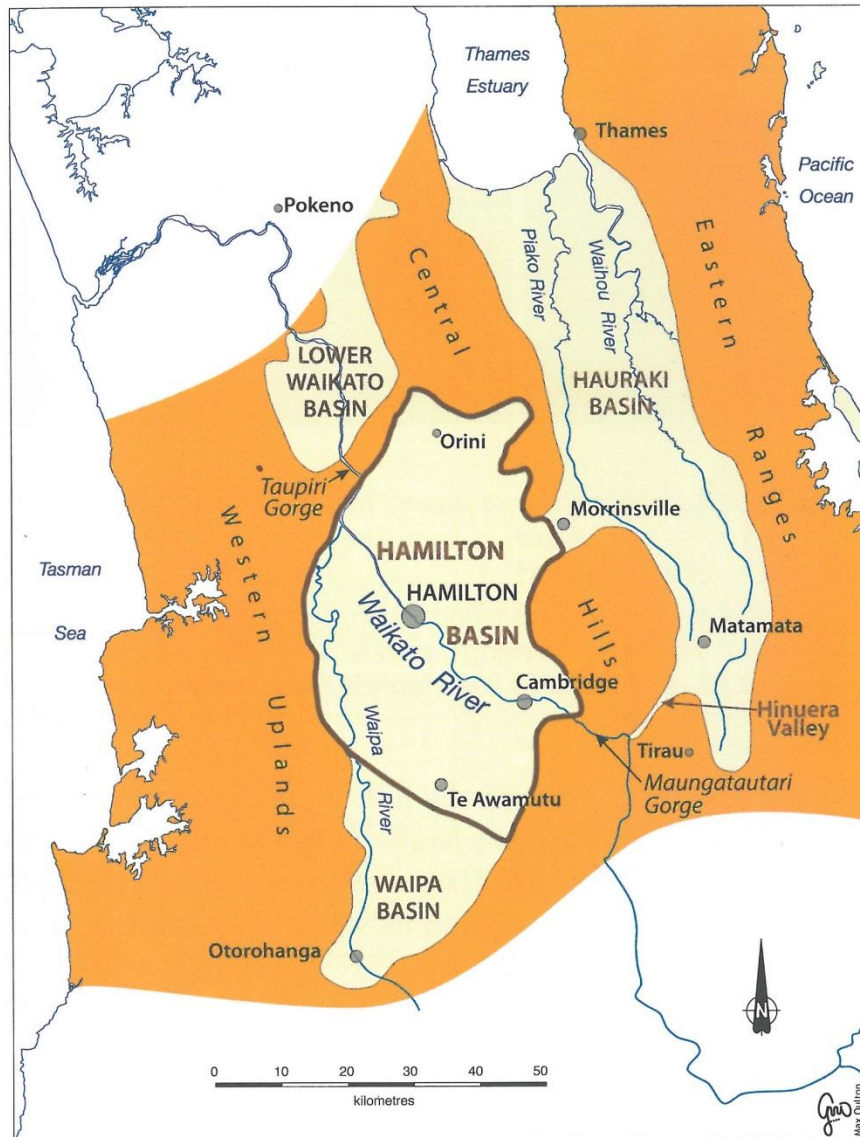


Figure 1.1: Location map highlighting the study area: Hamilton and Hauraki basins (McCraw, 2011).

1.2 Summary of existing research

Studies undertaken in the past on the sedimentology of the Hinuera Formation have recognised post-depositional structural features such as expulsion structures, flame structures and corrugated laminations (Hume *et al.*, 1975). These have largely been

interpreted as syn-depositional features representing modifications to the sedimentary structures as the freshly-deposited sediments are compacted and expel excess water. It is possible, however, that some or all of the features may be due to liquefaction caused by earthquake movement at a later time.

Simple screening and classification methods for assessing liquefaction potential of the Hinuera Formation suggest low susceptibility for these materials (Hodder & Moon, 2007; Moon & Stichbury, 2012; Clayton & Johnson, 2013). However, instrumental methods, typically Cone Penetration Test (CPT) or Standard Penetration Test (SPT) indicate much higher susceptibility (Clayton & Johnson, 2013). Screening tools (e.g. Youd and Perkins 1978) measure a low susceptibility of liquefaction in older sediments as exposure to previous liquefaction events, and sediment compaction during these events is perceived as reducing the future likelihood of liquefaction. However, events in Christchurch clearly indicate that repeated liquefaction events may occur at one site, suggesting that past liquefaction does not provide protection from future events. Instrumental methods have been questioned as a tool for assessing liquefaction in volcanic deposits containing crushable pumice grains (Orense & Pender, 2013; Orense *et al.*, 2014). In the Hauraki Basin pumice is a significant component of the Hinuera Formation (see chapter 2), suggesting that the instruments may be overestimating the likelihood of liquefaction in these materials. Likewise, it has also been suggested that cementation developed during “aging” of older deposits, such as cementation by iron or manganese oxides, may impart a greater resistance to liquefaction than the instruments suggest (Clayton & Johnson, 2013).

The Kerepehi Fault is recognised as an active fault with a clearly identifiable trace through the Hinuera Formation in the Hauraki Basin (Houghton & Cuthbertson, 1989; de Lange & Lowe, 1990; Edbrooke, 2005; Leonard *et al.*, 2010). This fault thus provides a potential source for past or future liquefaction within the Waikato Region.

Recognition of paleoliquefaction events is based on identifying earthquake-induced liquefaction structures in susceptible materials. Paleoliquefaction structures are

identified as injection structures in the form of clastic dikes or sills (e.g. Bastin *et al.*, 2013).

1.3 Aims and objectives

The aim of this study is to further understand the hazards associated with liquefaction within the Hinuera Formation. The four key objectives of this study are:

1. Identify paleoliquefaction features in the Hinuera Formation using geological methods. Liquefaction structures identified will be studied further to attempt to determine whether they are related to paleoseismicity or depositional processes. Such study will involve considering the grain size distribution of putative liquefaction structures, their position with respect to other sedimentary structures, and their shape.
2. Use radiocarbon dating techniques to determine ages of organic material so that a maximum age of occurrence of paleoliquefaction features can be established.
3. Perform a liquefaction assessment and determine if instrumental methods, such as piezocone penetration tests (CPTu), give a valid prediction of liquefaction potential.
4. Produce a soil-landscape model to predict areas of high liquefaction susceptibility according to the spatial distribution of modern surface soils and their position within the landscape.

Chapter 2

Literature Review

2.1 Introduction

Soil liquefaction is a complex process. Liquefaction potential assessments are therefore important contributors to hazard management. This chapter is separated into several sections. Firstly, soil liquefaction is defined, followed by descriptions of paleoliquefaction features and their different morphologies, as this helps to differentiate between seismic and non-seismic triggers. A widely used stress-based method for assessing liquefaction potential is then reviewed. This is followed by a summary of the Hinuera Formation within the Hamilton and Hauraki basins. Finally, a summary the 2010-2011 Canterbury earthquakes is given, as these events provide the perfect application of uniformitarianism, “the present is the key to the past” for this study.

2.2 Soil liquefaction

Liquefaction is a process in which saturated, loosely packed, cohesionless fine grained granular soils momentarily acts as a fluid (Lowe, 1975; Marcuson, 1978; Allen, 1982; Seed & Idriss, 1982). Two types of soil liquefaction can be identified: flow liquefaction and cyclic liquefaction.

2.2.1 *Flow (static) liquefaction*

Flow liquefaction occurs in strain softening soils where the initial void ratio is higher than its steady (or critical) state (Robertson & Wride, 1998). Strain softening is a soil behaviour where shear stresses decrease after the yield point with continuous loading. Flow liquefaction is induced by either monotonic or cyclic loading. Monotonic loading is increased tension or compression, whereas cyclic loading is applying an oscillation force where the material experiences both tension and compression. Soils susceptible to flow liquefaction include: saturated loose fine to coarse sands, and very sensitive clays and silts. Failure because of flow liquefaction is either through flowing or sliding and is a reflection of the material

type and ground geometry. For example, saturated, loosely packed sands beneath slopes may fail if there is a sufficient shear stress applied. Increased shear stresses can be achieved by: depositing sediment on the slope crest, by erosion at the base of the slope (slope toe), or by changing seepage forces—all of which are examples of monotonic loading. Seismic vibrations can also increase shear stresses and most commonly occur as a result of an earthquake. This is an example of cyclic loading (Robertson & Cabal, 2012).

2.2.2 Cyclic (softening) liquefaction

Cyclic liquefaction occurs in soils that experience shear reversal, where the effective stresses reach values of zero or near zero. This process is only induced by cyclic loading, typically from earthquakes (Robertson & Wride, 1998). Large deformations can occur during load cycles and cease directly after the earthquake ceases. Cyclic liquefaction typically occurs in saturated sands, if the cyclic energy is sufficient. Clays may also experience cyclic softening; however, deformation is minor due to cohesive soil characteristics. My study focusses only on cyclic liquefaction; and soil liquefaction or liquefaction will be used interchangeably to describe cyclic liquefaction.

The cyclic energy of an earthquake destroys the solid soil matrix, where shear strength or effective stresses of the soils are essentially zero. Before an earthquake, soils have strong grain-to-grain strength. The water located in voids is enclosed as the granular material attempts to compact down. Pore water pressure builds up as the water attempts to relieve increased pressures; but there is no time for the water pressure to reach equilibrium. As a result the water suspends the granular material. The water and soil mixture may be transported up to the surface. This mechanism is also defined as a fluidisation process, where moving water is able to transport sediments (Lowe, 1975). Compaction occurs in a later process and as a result causes settling.

Liquefaction susceptibility considers the material type and its relation to the water table level, whereas liquefaction potential is the probability of liquefaction occurring, involving both liquefaction susceptibility and the earthquake magnitude

(Obermeier *et al.*, 2005). Liquefaction susceptibility is highest in young sediments of less than 500 years (Youd & Perkins, 1978), and less common in Late Pleistocene deposits. Furthermore, liquefaction susceptibility can be high in loosely packed, poorly graded (well sorted) sands and silts. Saturated soils are a pre-requisite for liquefaction to occur, and therefore a high water table must also be present; this is most common in low-lying alluvial and coastal soils, or soils in foot-slope geomorphic positions. Loosely packed soils are a result of uniform grading, as this creates large void ratios so that large volumes of water may exist. The state of soil material before an earthquake event is important in order to identify liquefaction susceptibility.

The key trigger agent for cyclic liquefaction events are earthquakes, but more importantly earthquake magnitude, so that there is a sufficient build-up of pore water pressure. A commonly quoted earthquake magnitude threshold for liquefaction is at least M_w 5.5 (Ambraseys, 1988). However, liquefaction may also occur at magnitudes as low as M_w 5.0 (Obermeier, 1996).

2.3 Paleoliquefaction

Paleoliquefaction features are preserved within the geological record and indicate evidence of past liquefaction events. Earthquake-induced liquefaction structures have been identified as injection structures in the form of sand dikes or sills, bowl intrusions and sand boils/volcanoes (Sims & Garvin, 1995; Obermeier, 1996; Tuttle, 2001) (Figure 2.1). Liquefaction structures are classified as soft-sediment deformations, and can be formed due to either seismic or non-seismic triggers. Identifying the correct trigger agent is challenging as structures formed due to seismic or non-seismic triggers present similar morphologies.

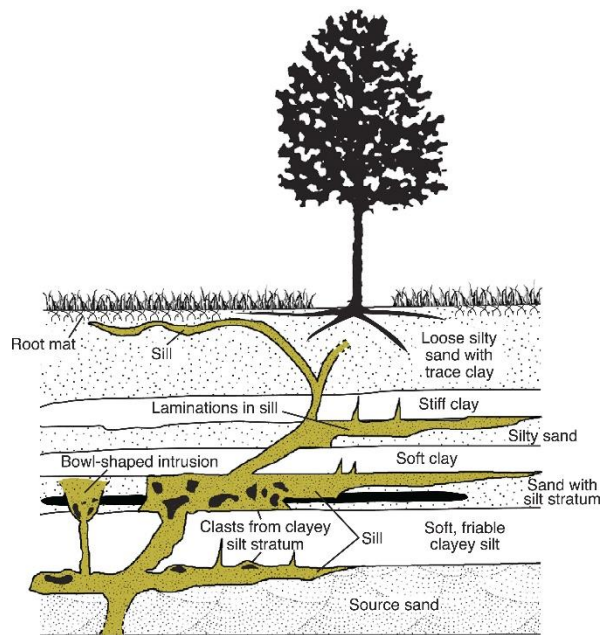


Figure 2.1: Typical morphology of paleoliquefaction features from Obermeier *et al.* (2005) modified after Obermeier (1996).

2.3.1 *Soft-sediment deformation*

Soft-sediment deformation develops from rapid dewatering, usually shortly after deposition, as there is little time for sediments to consolidate. Formation of these structures involves a deformation mechanism and a trigger agent. The deformation mechanism is the process that enables deformation to occur (Owen, 1987). Liquefaction and fluidisation are deformation mechanism for cohesionless soils, where cohesive soils deform under thixotropy, or due to high sensitivity. Thixotropic behaviour is the time-dependent, shear thinning of soils and sensitivity is the substantial loss of soil strength. The most common trigger agents for soft-sediment deformation are seismically induced. However, non-seismic triggers include: sudden loading due to syn-depositional processes, rapid sediment loading, pressure fluctuations caused by breaking water waves, storm waves and varying turbulence in water flow, tsunamis, floods, a fluctuating groundwater level, gravity on slopes, unequal loading due to changes in topography or dense sediments overlying less dense sediments, impacting wave motions and even the impact from meteorites (Owen & Moretti, 2011; Owen *et al.*, 2011). Soft-sediment deformation structures induced by earthquakes are referred to as “seismites” and structures caused by “shallow depth liquefaction” are a sub-category (Seilacher, 1969, 1984; Montenat *et al.*, 2007).

2.3.1.1 Seismites

Seismites display chaotic and diverse structures such as ball-and-pillow structures, pseudo-nodules, dish-and-pillar structures, flame structures, and clastic dikes and sills. Ball-and-pillow structures are rounded sediment masses that lie on top of one another (Figure 2.2a). If there is only a single row of rounded masses or an isolated individual mass, these are referred to as pseudo-nodules (Owen, 2003) (Figure 2.2b). Dish structures are flat to concaved horizontal features whereas pillar structures are vertical to sub-vertical columns (Sylvester & Lowe, 2003) (Figure 2.2c). Flame structures are crested and contain a sharp tip, and these have intruded irregularly into the overlying bed (Middleton, 2003) (Figure 2.2b). Clastic dikes and sills (also called injection structures) are sediments that rapidly fill fractures or intrude through overlying beds by injecting upwards. Dikes are vertical or near-vertical features that cross-cut bedding (Figure 2.2d), whereas sills occur essentially horizontally. Identifying the trigger agent is important as all structures mentioned can be formed under either seismic or syn-depositional processes. If the trigger agent is not from a seismic origin the structures are no longer identified as seismites.

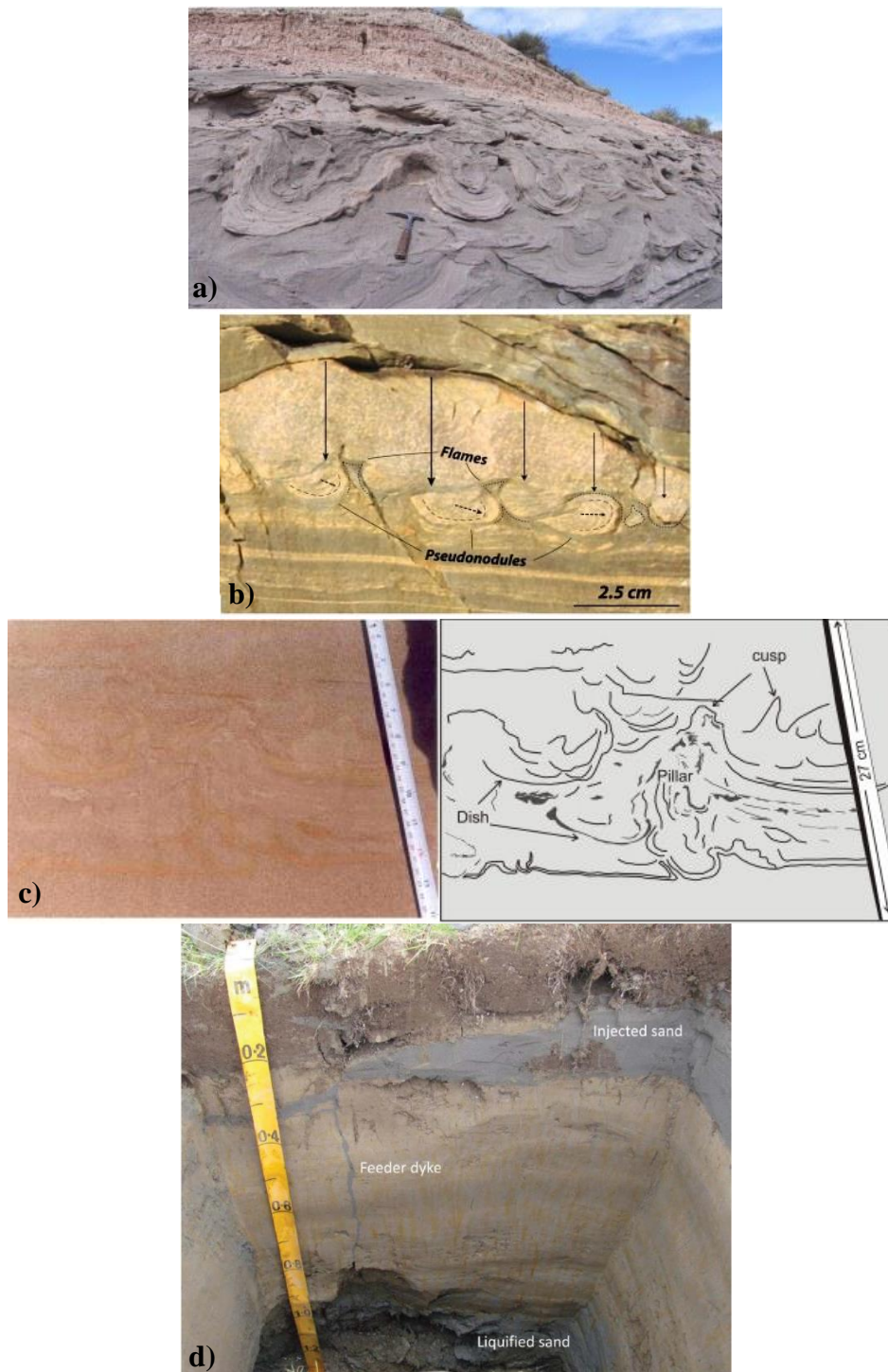


Figure 2.2: Structures of different seismites. (a) Ball-and-pillow structures (Moretti & Ronchi, 2011). (b) Individual pseudo-nodules and flame structures (Rana *et al.*, 2013). (c) Dish-and-pillar structures, field observation (left) and schematic diagram (right) (Ghosh *et al.*, 2012). (d) Clastic sand dike from the Darfield Earthquake (Almond *et al.*, 2010).

2.3.1.2 Trigger agent

Inferring the trigger of liquefaction structures is often very difficult due to inadequate knowledge, and most methods do not consider all seismic and non-seismic triggers (Owen *et al.*, 2011). There are two key approaches in identifying trigger agents: criteria-based and context-based (Owen & Moretti, 2011). Criteria-based, which is the most common method, considers characteristics that increase the outcome for a seismic trigger such as lateral extent, vertical continuity, morphology comparison to recent earthquake, proximity to faults and complexity of structures in relation to faults (Table 2-1).

Table 2-1: Criteria-based trigger identification for a seismic agent summarised from Owen and Moretti (2011).

Factor	Explanation for a seismic trigger
Lateral extent	Similar structures are found at multiple locations over a large area (kilometres in radius)
Vertical continuity	Structures are reproduced through a vertical section due to the recurrent nature of earthquakes
Morphology to recent earthquakes	Structures are similar to liquefaction structures produced by recent earthquakes
Proximity to faults	Liquefaction structures are more likely to occur near faults, although large earthquakes can effect an entire basin
Complexity of structures with distance to fault	Complexity and frequency of structures decrease with distance to fault

The context-based approach involves a full assessment of the sedimentology and paleoenvironment to infer deformation mechanisms and considers all possible trigger agents. Firstly, a facies analysis is conducted with a significant focus on erosional and depositional processes, which will aid the determination of a seismic or non-seismic trigger. Non-seismic triggers will show a reoccurring soft-sediment deformation structure in the particular facies at different locations, while a seismic trigger will not show this relationship. Secondly, a thorough description of the soft sediment deformation(s) incorporating the reconstructed pre-deformation structure and timing of deformation relative to deposition of surrounding layers is taken (Figure 2.3). This helps to infer the driving forces that lead to a liquefaction/fluidisation deformation mechanism.

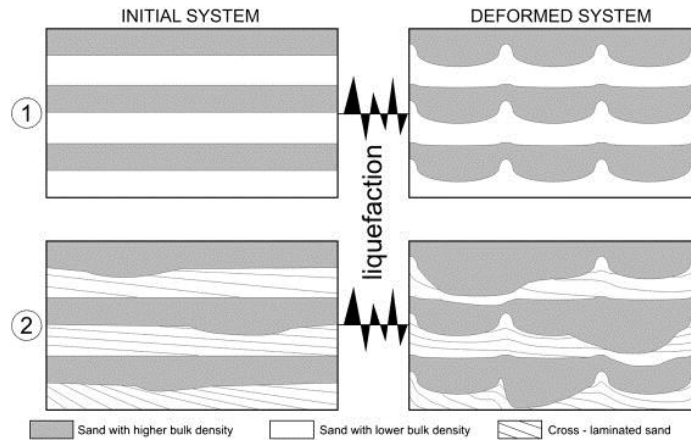


Figure 2.3: Reconstruction of pre-deformed stratigraphy (initial system) to the deformed system, showing regular and irregular deformations from massive (1) and cross-bedded (2) strata (Moretti & Ronchi, 2011).

Lastly, a comprehensive interpretation of the trigger agent can be achieved (Figure 2.4). Important indicators of a seismic trigger include: correct grain size (coarse silt to medium sand), saturated deposits, ductile characteristics, deformation increasing upwards and preserved stratification (Owen & Moretti, 2011) (Table 2-2).

Table 2-2: Summary of liquefaction indicators for a context-based approach modified from Owen and Moretti (2011).

Indicator	Explanation
Appropriate sediment characteristics	Liquefaction is optimal in saturated coarse silt to medium sand, however larger grain sizes could liquefy also
Ductile characteristics	The momentary change to liquid-like behaviour will exhibit ductile characteristics as opposed to brittle deformation, however material above the water table may experience brittle deformation forming lateral cracks
Increased deformation upwards	Liquefied state is prolonged in upper beds
Preserved stratification	Stratification will remain intact as displacement between grains are small during liquefaction
Morphology of deformed layer	Upper surface will be flat after liquefaction due to no shear strength in liquid state

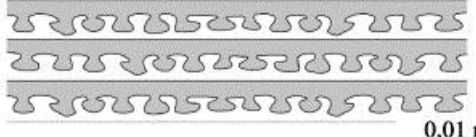
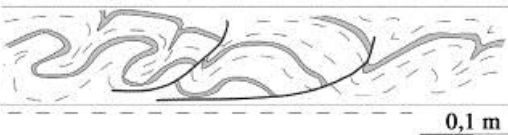
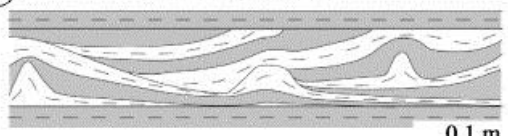
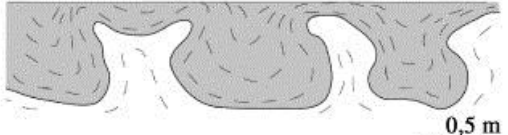
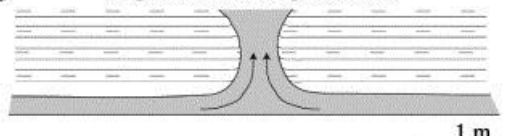
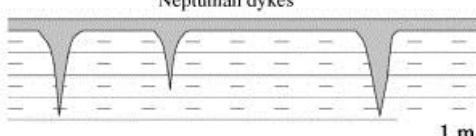
Soft-sediment deformation structures	Driving-force system	Trigger mechanism
<p>(A) Small-scale load-structures</p>  <p>0,01 m</p>	Gravitationally unstable density gradient	<p>Overloading</p> 
<p>(B) Small-scale slump structures</p>  <p>0,1 m</p>	Gravitational body force	<p>Earthquake</p> 
<p>(C) Deformed lamination</p>  <p>0,1 m</p>	Multiple driving-forces	<p>Overloading or Earthquake</p> 
<p>(D) Large-scale load-structures</p>  <p>0,5 m</p>	Gravitationally unstable density gradient	<p>Earthquake</p> 
<p>(E) Large-scale water escape structures</p>  <p>1 m</p>	Vertical shear stress	<p>Earthquake</p> 
<p>(F) Neptunian dykes</p>  <p>1 m</p>	Extension in cohesive sediments	<p>Extensional tectonics</p> 

Figure 2.4: Context-based analysis from lacustrine deposits in the Sant' Arcangelo Basin, Italy with sketches of the soft-sediment deformation and their associated driving forces and trigger agent (Moretti & Sabato, 2007).

2.4 Ground effects

Liquefaction causes permanent ground failures such as lateral spread and vertical settlement. Lateral spreading is the horizontal movement of a soil slab in gently to steeply sloping surfaces which usually occurs near riverbanks and streams. Slabs can result in subsidence, rotation, or flow. Liquefaction also causes slope failure in steeply sloping topography. However, most liquefaction assessments are based on near horizontal surfaces. Vertical settlement is the sinking of the land surface due

to compaction. Damage includes landslides, lateral movement on bridge supports, settling and tilting of buildings and failure of retaining wall structures.

Liquefaction ground failure forms clastic dikes and their widths provide evidence for the failure mechanism such as hydraulic fracturing, lateral spreading and surface oscillations. Hydraulic fracturing occurs in the overlying silt-rich or clay-rich layer to the liquefied sand layer, referred to as the cap layer. On receiving cyclic shear waves, pore water pressures are increased and are forced to escape along existing weak points forming cracks. Clastic dikes infill along the cracks and are usually thin (0.1 to 10 cm thick). Lateral spreading in gently sloping surfaces are translated horizontally due to little friction between the liquefied bed and the overlying deposits. Clastic dikes formed by lateral spread are usually very wide and can be up to 0.5 to 0.7 m thick. Surface oscillations are formed by back and forth movement of the overlying deposits, and can be amplified according to the bedrock material. The oscillations form cracks so that clastic dikes are injected upwards therefore infilling the crack. These dikes can be up to 15 cm thick (Obermeier *et al.*, 2005).

2.5 Liquefaction assessment

The “simplified approach” developed by Seed and Idriss (1971) is a widely used stress-based method that evaluates liquefaction potential. The concept compares the applied seismic energy against the capacity of soil layers to resist liquefaction, thus enabling a prediction of liquefaction susceptibility. The applied seismic energy is described in terms of Cyclic Stress Ratio (CSR) and the soil’s resistance to liquefaction as Cyclic Resistance Ratio (CRR) (Youd *et al.*, 2001). Liquefaction is predicted to occur if CSR exceeds CRR.

2.5.1 Cyclic Stress Ratio

CSR is the energy generated by an earthquake and is determined using equation (2-1):

$$CSR = \left(\frac{\tau_{av}}{\sigma'_{vo}} \right) = 0.65 \left(\frac{a_{max}}{g} \right) \left(\frac{\sigma_v}{\sigma'_v} \right) r_d \quad (2-1)$$

Where

τ_{av}	= average cyclic shear stress
σ_v	= total vertical stress
σ'_v	= effective vertical stress
a_{max}	= peak horizontal acceleration
g	= acceleration due to gravity (9.81 ms^{-1})
r_d	= stress reduction coefficient (dependent on depth)

CSR is primarily impacted by the earthquake's cyclic shear stress expressed on soils and is quantified as Peak Ground Acceleration ($PGA = a_{max}/g$) for a given site. Overburden vertical stress (σ_v/σ'_v) also has an effect on CSR but assumes deformation of a rigid body for the entire soil column. Soils near the surface are more susceptible to deformation and so express larger stresses compared to soils at greater depths; by applying the stress reduction coefficient (r_d), the soil's non-rigid body is accounted for.

2.5.2 Cyclic Resistance Ratio (CRR)

CRR is the capacity a soil has to resist liquefaction. Variables for CRR are derived from the soil's characteristics and extracted by *in situ* tests. Laboratory tests like triaxial shear of undisturbed soil samples would be ideal in determining CRR, however, collecting samples without destroying the soil's matrix is challenging. There are three *in situ* field techniques that resolve soil collection complications: Standard Penetration Test (SPT), Cone Penetration Test (CPT), and shear-wave velocity measurements (V_s) (Youd *et al.*, 2001). Field records of historical earthquake liquefaction and non-liquefaction events define curved boundaries to determine liquefaction resistance of soil layers. Empirical correlations that derived CRR equations are specific to each *in situ* test.

2.5.2.1 Standard Penetration Test (SPT)

Standard Penetration Test (SPT) is an *in situ* experiment that measures the relative density and consistency of granular soils, thereby estimating soil strength and liquefaction potential. The test involves driving a split-spoon sampler or half barrel into a pre-excavated borehole by repeatedly dropping a 63.5 kg hammer a distance of 760 mm (Figure 2.5). The N-value, or standard penetration resistance is recorded, which is the number of blows needed to penetrate 300 mm of subsurface soil (Clayton, 1995). Material is disturbed due to the borehole procedure and so for the first 150 mm the blow count is not recorded; this increment is known as “seating”. Large N-values indicate very dense sand (> 50 blows) or hard clays (> 30 blows) and low N-values indicate fine very loose sands (< 4 blows) and very soft clays (< 2 blows) (Price, 2008). SPTs can be implemented on a wide of variety soils and the method is also suitable for very soft clays and gravel materials. The split-spoon sampler is able to retrieve soil samples and record soil density simultaneously, but as a result the samples are disturbed and the N-values are crude (Mayne *et al.*, 2001). To overcome crude N-values and to maintain consistency between tests, the blow count must be normalised and energy efficiency of the dropping hammer is the most influential factor. N-values are corrected for 60% efficiency to reflect the loss in efficiency of a falling hammer that is affected by friction (Skempton, 1986). This correction is denoted N_{60} . Overburden pressure is also a common correction factor: as the depth of sand units with the same relative density, shows a constant increase of recorded blow count. Thus the N-value is determined for an effective overburden pressure of 100 kPa, denoted $(N_1)_{60}$ (Liao & Whitman, 1986).

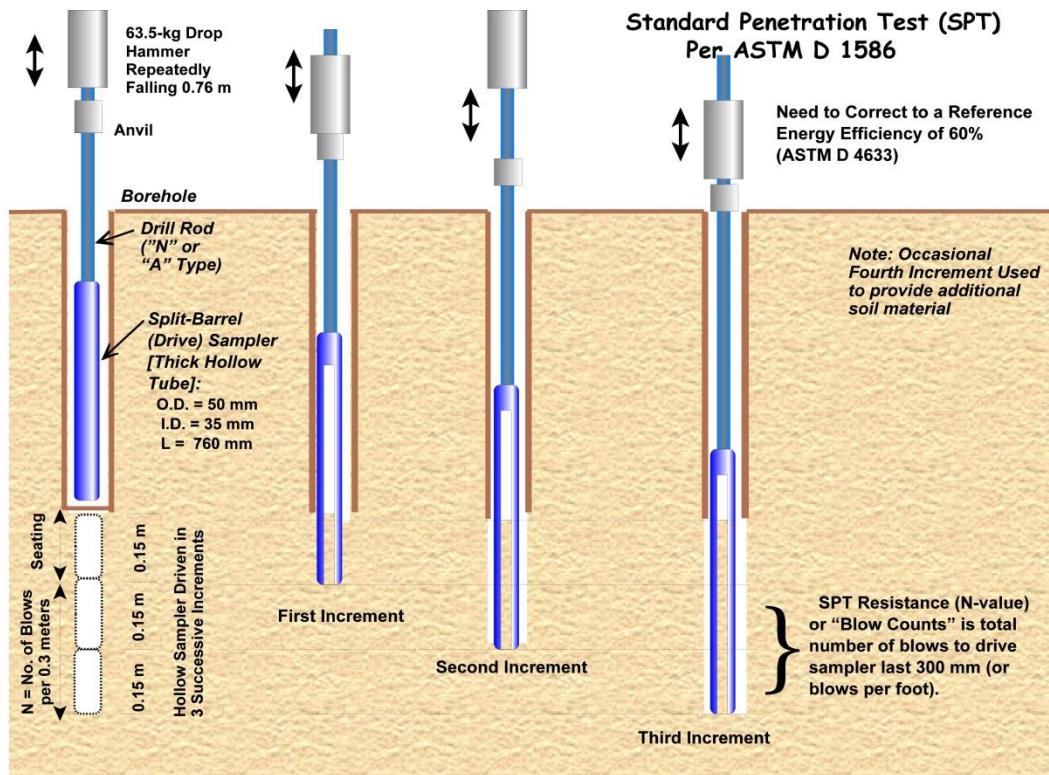


Figure 2.5 Standard Penetration Test (SPT) procedure based on the ASTM standard (Mayne *et al.*, 2001).

Threshold CRR for SPT data are derived from field observations at liquefied and non-liquefied sites (Seed *et al.*, 1985). Relationships of CSR and $(N_1)_{60}$ for historical liquefied and non-liquefied events have been graphed so that a curved boundary defining the level of a soil's resistance to liquefaction could be calculated. Generally, the SPT clean-sand base curve equation (2-2) from Youd *et al.* (2001) is used as it is standardised for an earthquake of magnitude 7.5 and for soils with $\leq 5\%$ fine grained sediments.

$$CRR_{7.5} = \frac{1}{34 - (N_1)_{60}} + \frac{(N_1)_{60}}{135} + \frac{50}{[10 \times (N_1)_{60} \times 24]^2} - \frac{1}{200} \quad (2-2)$$

2.5.2.2 Cone Penetration Test (CPT)

Cone Penetration Test (CPT) produces near continuous soil profiles by driving a cone penetrometer constantly into the subsurface to depths of typically 20 m (Lunne *et al.*, 1997). A commonly used international standard by The American Society for Testing and Materials (ASTM) established a detailed method for CPT,

and the following description is based on ASTM D5778 – 12 (ASTM International, 2012). Measurements are recorded using an electric cone penetrometer (Figure 2.6), which is a cylindrical steel probe containing a 60° angled cone with a 10 cm² surface area and a friction sleeve with a 150 cm² surface area (Mayne *et al.*, 2001; Mayne, 2014). There are varying cone sizes from 2 to 40 cm² probes. Cone size depends on the investigation; for shallow tests small probes are used whilst large probes are used for more gravelly material (Robertson & Cabal, 2012). The probe may also include a porous filter which measures the dynamic pore water pressure (u_2); these tests are known as piezocone penetration test (CPTu). Basic parameters obtained from CPT include: cone resistance (q_c), which is the force on the cone (Q_c) divided by surface area of the cone (A_c), and sleeve friction (f_s), which is the force acting on the sleeve (F_s) divided by the surface area of the sleeve (A_s) (Robertson & Cabal, 2012). The corrected cone resistance (q_t) accounts for water effects by incorporating the measured pore water pressures. In soft clays and silts, unequal end effects occur. This results when pore water pressure acts on the cone shoulder and friction sleeves that do not contain the same area. For sands, q_t equals q_c as the water effects are minimal. Large q_t values indicate sands and low q_t values indicate clays.

Readings are taken at 50 mm intervals or 20 mm intervals for high resolution data and is shown instantaneously on a computer—this presents a fast method for obtaining near continuous subsurface stratigraphy. A large range of soil types are optimal for CPTs, for example soft clays, firm silts, and dense sand, however gravels, cobbles and hard rock are not ideal as damage to the cone is likely (Mayne, 2007). Inclusions of large gravel or cobble in fine-grained soils causes a rapid increase in sleeve friction, which is caused by escalating local lateral stress as the inclusion moves away from the probe (Ramsey, 2010). This causes pore water pressure readings to rapidly decrease as a result of local suction, and, these may take meters to recover (Ramsey, 2010). Samples cannot be taken during the test as the procedure is continuous, however samples may be extracted afterwards by push-in soil samplers and laboratory experiments that enhance the quality of results obtained (Ramsey, 2010).

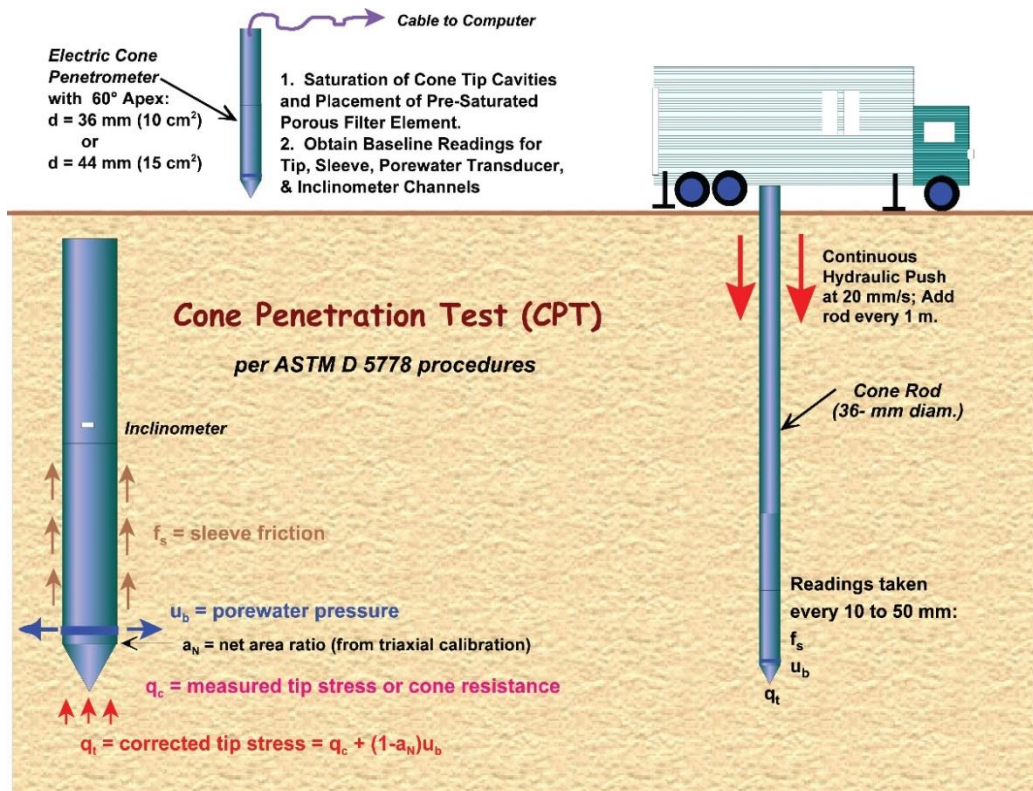


Figure 2.6: Cone Penetration Test (CPT) procedure with important measuring variables (Mayne *et al.*, 2001).

CPT data identify soil type based on mechanical behaviour such as soil strength, stiffness and compressibility rather than conventional laboratory methods that determine grain size distribution or Atterberg Limits. Soil behaviour type (SBT) is a classification system derived from cone resistance (q_c) versus friction ratio (R_f) charts (Robertson *et al.*, 1986). The friction ratio is given by equation (2-3).

$$R_f = \frac{f_s}{q_c} \times 100 \quad (2-3)$$

Where:

R_f	=	friction ratio as a %
F_s	=	sleeve friction
q_c	=	cone resistance

SBT charts developed by Robertson (1990) (Figure 2.7) use normalised parameters (Q_{tn} and F_r) that correct for overburden pressure and effective stress. Q_{tn} is the dimensionless normalised cone resistance with a variable stress factor (Robertson & Wride, 1998; Zhang *et al.*, 2002) and is calculated by equation (2-4).

$$Q_{tn} = \left[\frac{(q_t - \sigma_{vo})}{p_a} \right] \left(\frac{p_a}{\sigma'_{vo}} \right)^n \quad (2-4)$$

Where σ_{vo} and σ'_{vo} = vertical stress and effective vertical stress
 p_a = atmospheric pressure
 n = varying stress component

F_r is the dimensionless normalised friction ratio obtained by the following equation:

$$F_r = \frac{f_s}{q_t - \sigma_{vo}} \times 100 \quad (2-5)$$

Finally the soil behaviour type index (I_c) defines the boundaries for the differing soil types using equation (2-6).

$$I_c = [(3.47 - \log Q_{tn})^2 - (\log F + 1.22)^n]^{0.5} \quad (2-6)$$

Basic measurements of Robertson *et al.* (1986) non-normalised SBT charts may be used in situations where effective vertical stress is between 50 and 150 kPa as normalised and non-normalised SBT charts are almost identical (Robertson, 2009; Robertson, 2010b).

- | | |
|--|---------------------------------------|
| 1. Sensitive, fine grained | 6. Sands – clean sand to silty sand |
| 2. Organic soils – peats | 7. Gravelly sand to dense sand |
| 3. Clays – silty clay to clay | 8. Very stiff sand to clayey sand* |
| 4. Silt mixtures – clayey silt to silty clay | 9. Very stiff, fine grained* |
| 5. Sand mixtures – silty sand to sandy silt | *Heavily overconsolidated or cemented |

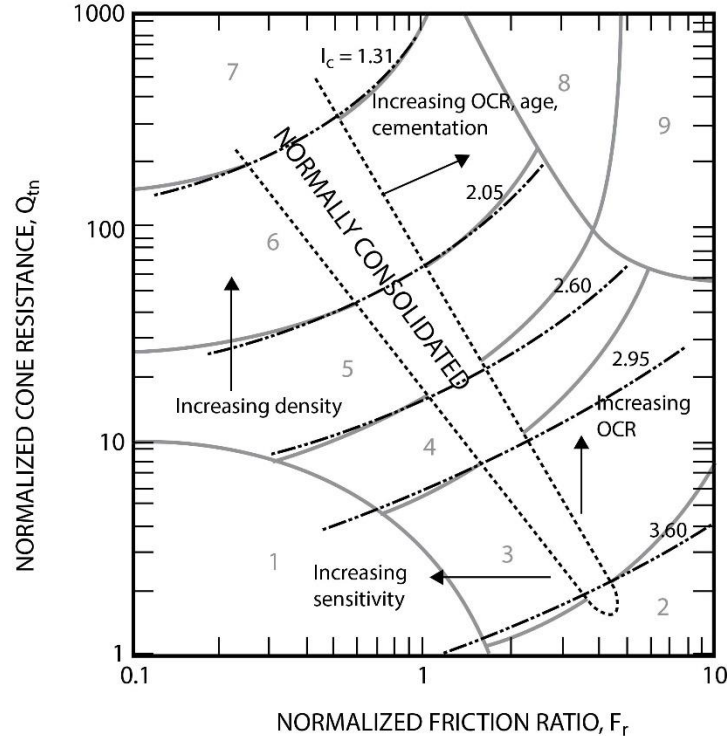


Figure 2.7: Soil Behaviour Type (SBT) chart for normalised cone resistance and friction ratio with the various soil types defined by SBT index (I_c). From Robertson (2010a), modified version of Robertson and Wride (1998).

CRR for CPT data is determined through empirical correlations of liquefaction and non-liquefaction earthquake events (Figure 2.8). Threshold CRR is calculated by the CPT clean-sand base curve: equation (2-7) or equation (2-8) (Robertson & Wride, 1998). Where the calculation is standardised for a 7.5 earthquake magnitude ($CRR_{7.5}$) and fine grained material are corrected for the equivalent clean sand penetration resistance ($Q_{tn, cs}$).

$$(Q_{tn})_{cs} = K_c Q_{tn} \quad (2-7)$$

Where K_c = correction factor dependent on fines content and plasticity

for $Q_{tn,cs} 50 - 160$

$$CRR_{7.5} = 93 \left[\frac{(Q_{tn,cs})}{1000} \right]^3 + 0.08 \quad (2-8)$$

or

for $Q_{tn,cs} < 50$

$$CRR_{7.5} = 0.833 \left[\frac{(Q_{tn,cs})}{1000} \right] + 0.05 \quad (2-9)$$

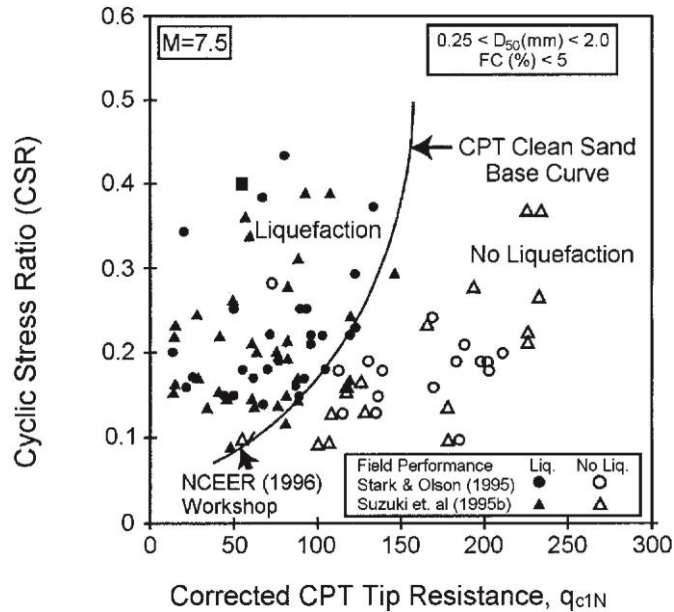


Figure 2.8: Relationship between CSR and q_{c1N} for historical earthquakes producing liquefaction and no liquefaction events to determine threshold CRR for CPT which is the CPT clean-sand base curve indicated on graph.

2.5.2.3 Shear-wave velocity (V_s)

Shear-waves travel through the Earth creating transverse movements of the subsurface soil material. Shear-wave velocity (V_s) provides important information about the *in situ* soil properties without sampling. There are various geophysical techniques that are able to record V_s , such as seismic cone penetration tests (SCPT), spectral analysis of surface waves (SASW), seismic refraction, and seismic reflection. Soil types are categorised according to the “Caltrans Seismic Design Criteria” which is derived from shear-wave velocity of the upper 30 m of the soil profile (V_{s30}) (Wair *et al.*, 2012). High velocities indicate hard rock and low velocities indicate soft soils (Table 2-2). V_s tests can be conducted in hard to reach places such as at contaminated sites because tests are performed on the surface.

They are also useful in gravelly material where CPTs or SPTs cannot penetrate. Thin layers cannot be detected if spacing of geophones is not small enough and samples cannot be collected to identify clay material which is non-liquefiable (Youd *et al.*, 2001).

Table 2-2: Soil profile name according to the V_s (Wair *et al.*, 2012).

Site Class	Soil Profile Name	V_{s30}
A	Hard Rock	> 5,000 ft/s >1,500 m/s
B	Rock	2,500 to 5,000 ft/s 760 to 1,500 m/s
C	Very Dense Soil and Soft Rock	1,200 to 2,500 ft/s 360 to 760 m/s
D	Stiff Soil	600 to 1,200 ft/s 180 to 360 m/s
E	Soft Soil ¹	< 600 ft/s < 180 m/s
F	Soils Requiring Site-Specific Evaluation ²	---

CRR using V_s was developed by Andrus and Stokoe (2000) using historical earthquake liquefaction and no-liquefaction events (Figure 2.9). Shear-wave measurements are firstly corrected for overburden pressure by the following equation:

$$V_{s1} = V_s \left(\frac{P_a}{\sigma'_{vo}} \right)^{0.25} \quad (2-10)$$

Where P_a = atmospheric pressure (estimated)
 σ'_{vo} = effective vertical stress

A critical CRR is then derived from equation (2-11) and is the boundary between liquefied soils and non-liquefied soils, standardised for earthquake's of magnitude is 7.5 and for soils with $\leq 5\%$ fines:

$$CRR_{7.5} = a \left(\frac{V_{s1}}{100} \right)^2 + b \left(\frac{1}{V_{s1}^* - V_{s1}} - \frac{1}{V_{s1}^*} \right) \quad (2-11)$$

Where

a and b = curve fitting variables

V_{s1}^* = limiting upper V_{s1} value influenced by fines content

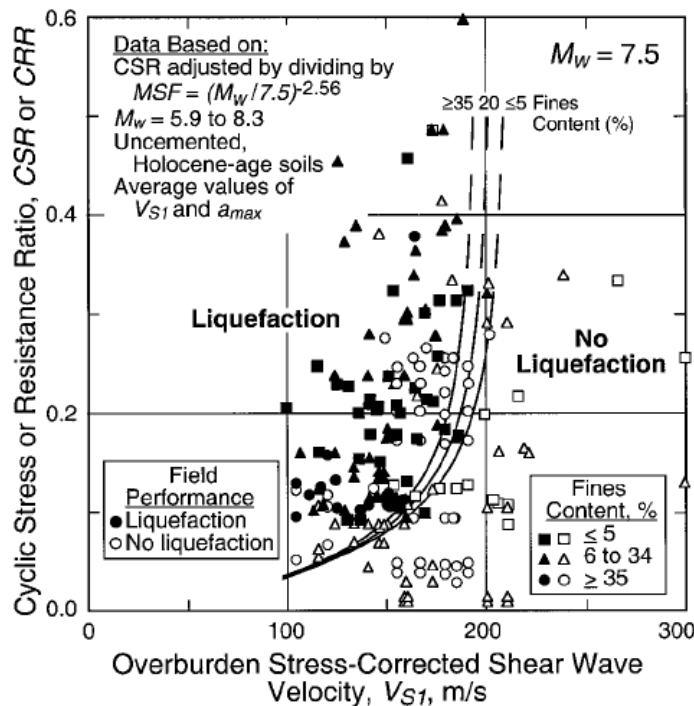


Figure 2.9: Correlation between CSR and V_{s1} for shear-wave measurements for historical liquefaction and non-liquefaction events. Curved boundary is defined as CRR for differing fine contents (Andrus & Stokoe, 2000).

2.6 Study area

2.6.1 Hinuera Formation

The Hinuera Formation, defined as part of the Piako Subgroup within the Tauranga Group (Kear & Schofield, 1978; Edbrooke, 2005), comprises volcanogenic alluvium deposited as large, very low-angle fans by a high-energy, braided ancestral Waikato River, firstly in the Hauraki Basin (prior to $\sim 22,000$ calendar [cal.] years ago) and then in the Hamilton Basin from $\sim 22,000$ to $\sim 18,000$ cal. years ago (McCraw, 2011). The Hinuera deposits are highly variable and complex and vary

both laterally and vertically in both basins, and hence no two sites are identical. Sediments accumulated rapidly, forming thick deposits of cross-bedded mainly gravelly or slightly gravelly sands, sandy gravels and silts, together with local interbedded peats (Schofield, 1965; Hume *et al.*, 1975; Kear & Schofield, 1978; McGlone *et al.*, 1978; Houghton & Cuthbertson, 1989; Edbrooke, 2005). Hume *et al.* (1975) described the gravel-sized material as dominated by fragments of rhyolitic breccia, rhyolite, pumice clasts, and ignimbrite, with sand and silt fractions predominantly volcanic quartz, plagioclase, pumice, and glass shards. Sedimentary structures are dominated by thick co-sets of cross-stratified gravelly sands and sandy gravels composed mainly of lithologically heterogeneous cross-strata (Hume *et al.*, 1975). Horizontally stratified and massive units are locally common, particularly in pumice silts and sands. Sedimentary structures in sands and gravels are the product of specific bed forms developed on longitudinal and transverse channel bars under both lower-flow and upper-flow regimes. A variety of post-depositional deformation structures in gravelly sands and silts was recognised by Hume *et al.* (1975).

The most active phase of deposition of the Hinuera Formation occurred after the eruption of the Kawakawa (Oruanui) tephra ~25,400 cal. years ago (Vandergoes *et al.*, 2013). Large volumes of loose pyroclastic material and break-out flood deposits from the eruption were reworked over several millennia at least. The ancestral Waikato River avulsed from its long-established route through the Hauraki Basin into the Hamilton Basin ~22,000 cal. years ago at the Hinuera Disjunction at Piarere (Manville & Wilson, 2004; Manville *et al.*, 2007). Ages used to help constrain the depositional history of the Hinuera Formation are summarised in Manville and Wilson (2004) and are based on radiocarbon dating and tephrochronology (Green & Lowe, 1985; Hogg *et al.*, 1987; McCraw, 2011).

Today 'Hinuera C' deposits—as describe by Manville and Wilson (2004)—underlie the very gently sloping to flat land surfaces of the alluvial fans over large areas of both the Hamilton and Hauraki basins and are referred to as the Hinuera Surface (Schofield, 1965; Kear & Schofield, 1978; Selby, 1992; Manville & Wilson, 2004).

Note that in many places the Hinuera Surface has a thin cover bed of intermixed tephra fall deposits younger than c. 20,000 cal. years and ~0.5 m in total thickness in the Hamilton Basin, and younger than c. 22,000 cal. years and ~0.8 m in total thickness in the Hauraki Basin (Lowe, 1986; Lowe, 1988; Lowe *et al.*, 2010). The tephras provide in part the parent materials for some of the modern pedological ‘two-storied’ (multisequal) soils including those of the Horotiu series in the Hamilton Basin and those of the Waihou series in the Hauraki Basin (Bruce, 1979; Singleton, 1991; McLeod, 1992; Selby, 1992). Extensive peat bogs and numerous small lakes occur on the Hinuera Surface as well (McCraw, 1967; Lowe & Green, 1992; McCraw, 2011).

An important feature throughout the Hinuera Formation is the presence of groundwater within the deposits (Schofield, 1972; Chapman, 2008). Groundwater levels occur between 2 m and 6 m below the ground surface in the Hamilton Basin. Because of the lithological variability of the Hinuera Formation (relating to its modes of deposition, noted above), the deposits are characterised through its lack of lithological continuity. Changes in lithology occur in both vertical and horizontal directions over short distances, and this spatial variability in turn influences the behaviour of groundwater and causes changes in the water table level and storage capacity over relatively short distances. Consequently, there are numerous small zones of higher permeability rather than single, well defined aquifers (Chapman, 2008).

2.6.2 Hauraki Basin

The Hauraki Basin, infilled in part by the Hinuera Formation, extends from Tirau to the Firth of Thames (Houghton & Cuthbertson, 1989). The basin is bounded by the Firth of Thames Fault in the west, the Hauraki Fault in the east, and the Kerepehi Fault runs through the central part of the basin (Hochstein & Nixon, 1979; Beanland *et al.*, 1996; Leonard *et al.*, 2010).

2.6.2.1 Kerepehi Fault

The active Kerepehi Fault has moved at least four times in the Holocene, c. 10,000, c. 7600, c. 6400, and c. 1300 cal. years ago (de Lange & Lowe, 1990). According

to Hochstein and Nixon (1979) and Beanland *et al.* (2006), transverse faults cross the Hauraki Basin causing horizontal offsets of the main faults noted above. The full extent of Kerepehi Fault traces from approximately 2 km north of Okoroire in the south, northward through the Koupouatai bog, to approximately 5 km north of Kerepehi. The fault possibly extends further offshore through the Firth of Thames. The normal fault trends in a NNW direction, dipping towards the west with a vertical displacement ranging from 2 to 8 m (Beanland & Berryman, 1986). The Kerepehi Fault includes three fault segments south of the Koupouatai bog, from Elstow to Te Poi (Figure 2.10). The fault traces include Elstow, Waitoa and Te Poi segments (Beanland *et al.*, 1996). The Elstow segment is located from Elstow to 2 km south; the Waitoa segment extends from Elstow to Hungahunga, and the Te Poi segment traces from Te Poi to Hungahunga (Persaud *et al.*, 2003). These segments are separated by 3 km steps towards the east. Lateral displacement is rare, although Beanland and Berryman (1986) did identify a channel bar that was offset by 22 m, located 70 m north of Tower Road. This feature, however, is not representative of the entire fault. The average recurrence interval for significant movement on the Kerepehi Fault was estimated to be c. 2500 years by de Lange and Lowe (1990).

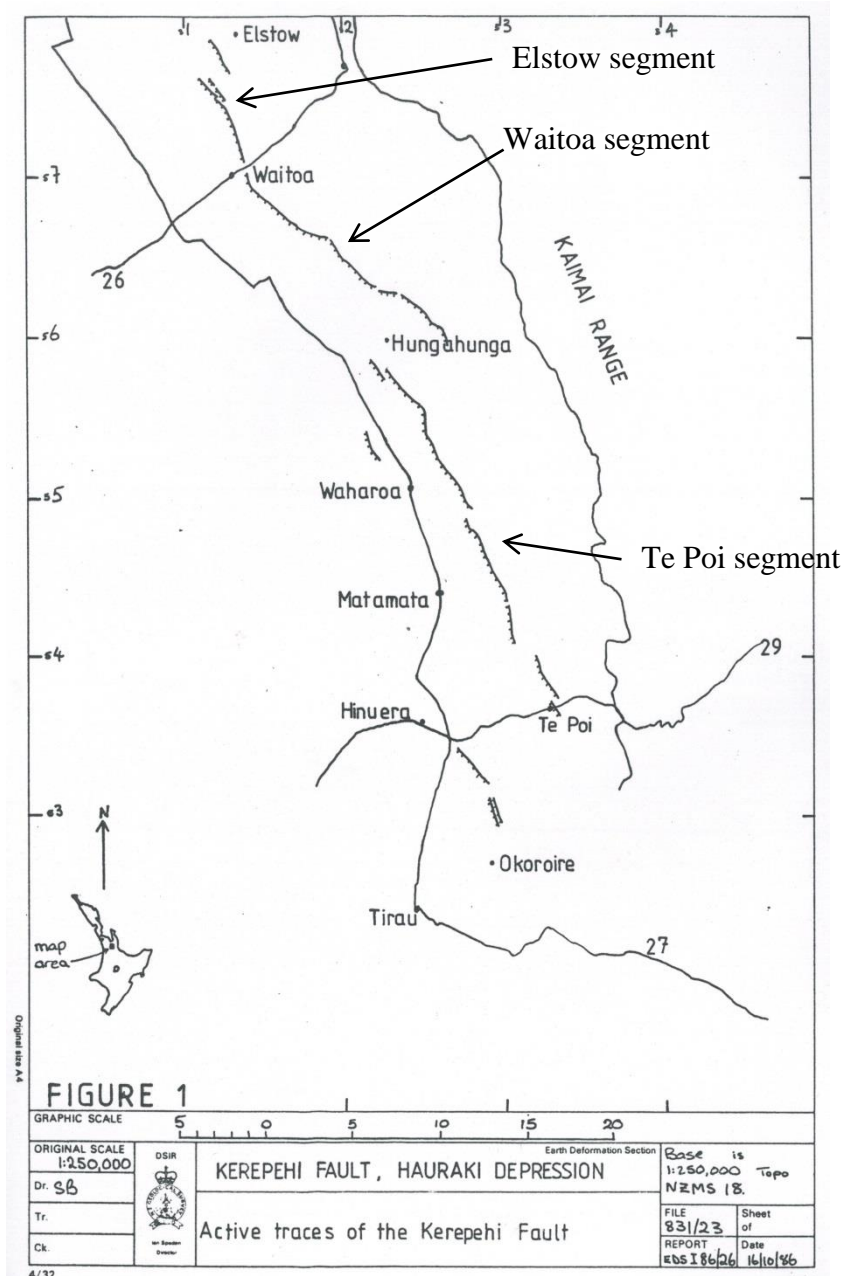


Figure 2.10: Location of the Kerepehi Fault and sections (Beanland & Berryman, 1986).

2.6.3 Hamilton Basin

The Hamilton Basin, infilled partly by the Hinuera Formation, is an oval-shaped depression that extends from near Te Awamutu to Taupiri (Fig. 2.11). The basin is bounded by the Waipa Fault to the west but no faults are known within the Hamilton Basin, other than old faults inferred in underlying basement rocks (Edbrooke, 2005).

2.6.4 Historical Earthquakes

Waikato historical earthquakes with moment magnitudes greater than 5.0 are summarised in Table 2-3. This table was compiled from a range of earthquake catalogues (Eiby, 1968; GeoNet, 2014; Downes & Dowrick, 2014) and magnitudes are derived through a multitude of methods. Local magnitudes (M_L) were derived from LOCAL software packages before 1987; surface wave magnitudes (M_S) are sourced from Dowrick and Rhoades (1998) and moment magnitudes (M_W) are determined using New Zealand seismographs stations sourced from GeoNet (2014). According to historical records, the 1976 Waikato Earthquake, previously known as the Korakonui earthquake, obtained the most severe intensities (MM8) within this study area. Damage from the Waikato Earthquake was dispersed from Hamilton to Te Kuiti, with intensities greatest in the township Korakonui, where some houses losing their chimneys (Eiby, 1977). Energy from large earthquakes at distal sources may also have an effect on the Hamilton and Hauraki basins. In particular, the Bay of Plenty 1987 Edgecumbe Earthquake producing recorded magnitudes M_L 6.1 and M_S 6.6 and intensities of MM9 in Edgecumbe, Matata, Thorton, Kawerau and Te Teko. The earthquake was also felt in Hamilton, Taupo, Napier and Gisborne, where Hamilton recorded intensities of MM3 (Lowry *et al.*, 1989).

Records of pre-historical and historical liquefaction earthquake events are scarce within the Waikato Region. Pre-historic liquefaction earthquake-induced events were interpreted from the deformation of clayey material in near-basal parts of the Hamilton Ash Formation (Tonkin, 1970) (stratigraphically referred to as Rangitawa tephra, c. 340,000 years old: Lowe *et al.*, 2001). In several tephra-bearing lake cores from the Hamilton Basin, deformations of the Rotorua Tephra in particular, and several other tephras, were possibly earthquake induced but were interpreted at the time as “ash-filled burrows” (i.e. caused by bioturbation rather than seismoturbation) (Lowe, 1988).

Table 2-3: Historical Earthquakes within the Waikato Area.

Earthquake	Date	Magnitude	Maximum intensity	Epicentre	Depth
25 km north-east of Pukekohe	1835 Jan-01	M _w 7.0	≥MM7	5903258, 1777962	25 km
Waikato Heads	1891 Jun-23	M _{wI} 6.2	MM6	5859833, 1723914	12 km
Waikato	1912 May-26	M _s 5.5 M _w [^] 5.7	MM6	5792298, 1775603	12 km
Morrinsville	1926 Nov-11	M _{wI} 4.6	MM7	5829958, 1824962	5 km
20 km west of Te Aroha	1927 Nov-07	M _w 6.0	≥MM7	5846723, 1820994	25 km
West Bay of Plenty	1937 Jun-03	M _w 6.0	≥MM7	5901462, 1849161	25 km
15 km south-west of Tokoroa	1947 Apr-16	M _w 5.0	MM6	5751586, 1846430	12 km
Te Aroha	1972 Jan-08	M _L 5.3 M _s 4.9	MM6	5837484, 1834005	12 km
Waikato (formerly Korakonui)	1976 Dec-05	M _w [^] 5.3 M _L 5.1	MM8	5778933, 1822689	12 km

M_L: local magnitude, determined from seismic data

M_s: surface wave magnitude; source from Dowrick and Rhoades (1998)

M_{wI}: moment magnitude estimated from intensity data and isoseismal pattern, using the attenuation relationships in Dowrick and Rhoades (2005)

M_w[^]: moment magnitude based on Dowrick and Rhoades, (1998) regression with M_s

MM: modified Mercalli scale (Dowrick, 1996)

Seismic hazard assessments incorporate likely predicted earthquakes sourced from the National Seismic Hazard Model (NSHM) and are most abundantly used in New Zealand loading standards (Stirling *et al.*, 2012). The NSHM uses methodologies of a probabilistic seismic hazard analysis (PSHA) which integrates recorded historical earthquake spatial data and fault source data. This then provides estimated frequency and magnitudes of predicted earthquakes for different areas within New Zealand. The Hamilton and Hauraki basins within the “extensional western North Island faults” defined in Stirling *et al.* (2012) which includes the Kerepehi Fault (north to northwest striking faults) and contains predicted magnitudes of M_w 6.8 (Kerepehi North), M_w 6.9 (Kerepehi Central) M_w 6.6 (Kerepehi South). Ground-motion equations are used to predict peak ground acceleration (PGA), based on site subsoil class from McVerry *et al.* (2006). New Zealand loading standard NZS1170.5 (Standards New Zealand, 2004) and Bridge Manual section 6 (NZTA, 2014) adopt this seismic hazard analysis methodology.

2.7 Canterbury Earthquake Sequence 2010-2012

Liquefaction events during the Canterbury Earthquake Sequence (CES) from 2010 to 2012 have emphasised the severity of liquefaction as a hazard. The four most severe liquefaction events originated from the 2010 Darfield Earthquake, the 2011 Christchurch Earthquake and the two largest subsequent aftershocks.

The Darfield Earthquake in 2010 was the first of the CES, caused by the rupturing of the Greendale Fault. The earthquake occurred at 4.35 am NZST on 4 September, with a magnitude of M_w 7.1 and intensity of MM9 (GeoNet, 2014). The formerly untraceable Greendale Fault, located in Darfield 40 km west of Christchurch, became exposed, producing large and complex surface deformations. The Greendale Fault in the Canterbury Plains was part of an active deformation system of strike-slip and reverse faults associated with the Australian and Pacific Plate convergence. During the last glacial maximum c. 32,000 to 18,000 cal. years ago (Forsyth *et al.*, 2008; Newnham *et al.*, 2013), three river channels (Rakaia, Selwyn and Waimakariri) joined, depositing thick alluvial sediments tens to hundreds of metres thick, whilst burying strike-slip faults like the Greendale Fault. Slow slip rates of less than 2 mm yr^{-1} (Pettinga *et al.*, 2001) also added to the difficulty of identifying buried faults in geophysical assessments. Surface rupture of the Greendale Fault is separated into three segments: western, central and eastern (Villamor *et al.*, 2012; Duffy *et al.*, 2013). The western segment is 7 km long and is identified as a releasing bend. The complex central segment contains push up structures, Riedel shears, P thrusts, normal/reverse faults and folds; and the eastern segment is a broad horizontal flexure portraying a monocline.

Fortunately there was no loss of life, but the earthquake was responsible for severe structural damage. Areas most severely damaged were eastern Christchurch—in particular the suburb Avonside which is adjacent to the Avon River—and Kaiapoi, located north of Christchurch (Cubrinovski, 2010).

The Christchurch Earthquake occurred 5 months after the Darfield Earthquake on 22 February 2011 at 12.51 pm NZST. Despite the Christchurch Earthquake being

of smaller magnitude (M_w 6.3), it was by far the most devastating with 185 fatalities, severe structural damage, and a maximum intensity of MM8 (GeoNet, 2014). The epicentre was located 5 km southeast of Christchurch City; due to the proximity of the Banks Peninsula volcanic complex in the same area, the surface waves were amplified (Cubrinovski *et al.*, 2011). Liquefaction was most prominent in the suburbs east of the Avon River (Avonside, Dallington, Avondale, Burwood and Bexley). PGA measured in the Christchurch City ranged from 0.37 to 0.52 g, which is approximately 1.6 times larger than the PGA for the previous Darfield Earthquake (Cubrinovski *et al.*, 2011)(Figure 2.11).

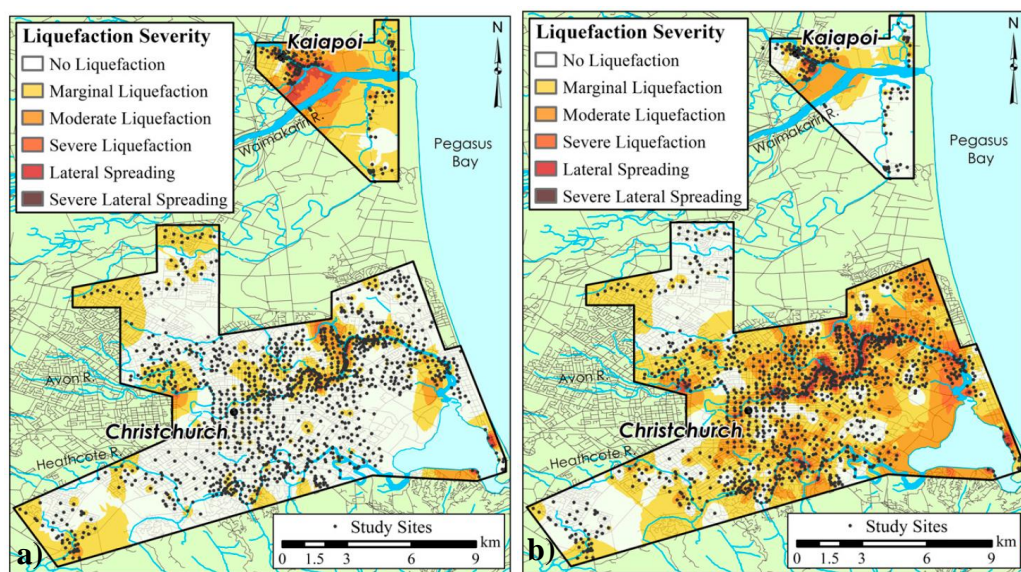


Figure 2.11: Comparison of liquefaction severity between the (a) Darfield earthquake and the (b) Christchurch earthquake (Maurer *et al.*, 2014).

Aftershocks occurred on 13 June 2011 with M_w 6.4 and 23 December 2011 with M_w 6.0. Liquefaction was reactivated multiple times thereafter, but more vigorously during these earthquake aftershock events.

A paleoliquefaction study was conducted in Avonside to determine whether severely liquefied areas also showed evidence of liquefaction events in the past. Two sites were studied in detail, 11 Bracken Street and Sullivan Park, which are both located near an inner bend of the meandering Avon River. During the CES, the site on Bracken Street experienced multiple reactivating liquefaction events (Quigley *et al.*, 2013) and Sullivan Park experienced severe lateral spreading (Bastin *et al.*, 2013). Trenches were excavated at both sites, perpendicular to the

sand blow orientation at the site on Bracken Street, and perpendicular to the lateral spreading at Sullivan Park. CPT and liquefaction analyses were also conducted at Sullivan Park. Trench mapping at the Bracken Street site showed evidence of both modern feeder dikes originating from the CES and paleoliquefaction feeder dikes. The modern dikes were distinguished as bluish grey, fine to medium sands while the paleoliquefaction dikes showed evidence of orange mottling and oxidation (Bastin *et al.*, 2013). Overall, the trench portrayed only two major generations of feeder dikes. However, it was recorded that at least 11 liquefaction events occurred during the CES (Quigley *et al.*, 2013). This information implies that the observable feeder dike generations only provide a minimum account of liquefaction events (Bastin *et al.*, 2013). At Sullivan Park both modern and paleoliquefaction dikes were identified and were distinguished from the same colour and grain sizes as at Bracken Street. The CPT data also confirmed that the PGAs recorded from the Darfield Earthquake and the Christchurch Earthquake would undeniably liquefy the source bed. Minimum PGAs were also determined, giving values of 0.15 g (Darfield Earthquake), 0.19 g (Christchurch Earthquake) and ~0.2 g (June and December 2011 aftershocks) (Bastin *et al.*, 2013).

2.8 Summary

Soil liquefaction, morphologies of paleoliquefaction features, the simplified procedure liquefaction assessment, the Hinuera Formation within the Hamilton and Hauraki Basins, and the 2010-2011 Canterbury earthquakes are reviewed. There is controversy over the potential risk the Hinuera Formation poses within the Hamilton and Hauraki basins, mainly as it is considered as a minor potential hazard due the age of the deposit (late Pleistocene). Therefore few studies have been conducted and hence there is little literature on liquefaction within the Waikato Region. However, the potential hazard within the Hamilton and Hauraki basins are high, as engineers have designed for liquefaction according to CPT-based liquefaction assessments for a long time. It is this hazard that motivates this study.

Chapter 3

Methods

3.1 Introduction

Identification of paleoliquefaction requires detailed stratigraphic description. Assessment of liquefaction susceptibility involves laboratory testing of samples, and *in situ* field testing. This chapter describes methods of site selection, facies analysis, laboratory methods, and susceptibility assessment using CPTu data.

3.2 Site selection

Site investigations took place throughout the Hamilton and southern Hauraki basins. A total of 17 sites are visited, six in the Hauraki Basin and 11 in the Hamilton Basin (Figure 3.1). Almost any excavation into the Hinuera Surface would provide information relevant to this study as these late Quaternary alluvial geological deposits of the Hauraki and Hamilton basins are generally flat-lying, therefore exposures are limited. Liquefaction usually occurs within the top 10 to 16 m, as deeper deposits are more likely to be subjected to diagenesis and below this, overburden stress becomes so high that generating pore water pressures high enough for zero effective stress is too difficult. Therefore, pre-excavated surfaces such as sand quarries, sandpits on private properties, road cuttings and construction sites are selected. Sand quarries are initially sourced from the Waikato Regional Council database, although many quarries listed are no longer operating. For larger commercial quarries, contact information is generally available online. The majority of sites are obtained from local knowledge by word-of-mouth communication. All sites identified are visited; however, many are discarded due to poor or minimal exposure.

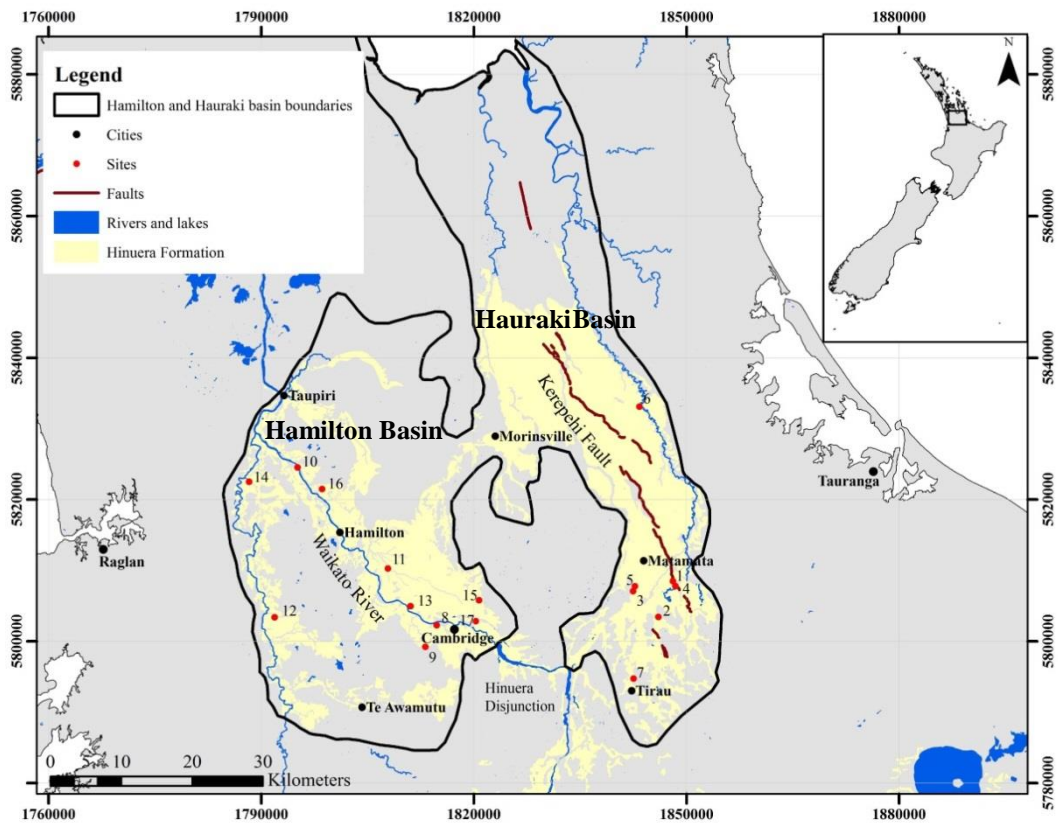


Figure 3.1: Locality map of sites visited in the Hamilton and Hauraki basins. Site numbering defined in chapter 4.

3.3 Facies analysis

A facies analysis is conducted at all sites, accompanied by detailed stratigraphic logs and geological descriptions. A lithofacies analysis is a geological technique that groups lithological units, defined by a combination of primary physical appearances, in order to interpret a paleoenvironment (Dalrymple & James, 2010). Stratigraphic logs are firstly drawn in the field and a final copy is prepared in Adobe Illustrator (see appendix 1). Geological descriptions followed a mixture of sedimentological and engineering geology guidelines—the latter are based on New Zealand Geotechnical Society (NZGS), (2005) .

3.3.1 Site descriptions

A preliminary visual assessment (walk over) of each site is undertaken with a lookout for any indication of a water table, through evidence of small pools or ponds, seepage, iron (Fe) staining and manganese (Mn) coating. A high water table is an important pre-requisite for liquefaction to occur. Once this initial evaluation

is completed, several sections are logged and described to provide a good representation of the lithologies and their stratigraphic relationships for the whole site.

3.3.2 Geological description

Geological descriptions generally follow methods in accordance with the NZGS (2005) guidelines. However, adjustments are made to incorporate aspects following sedimentological methods and in particular, identifying primary structures (such as bedding) to aid a paleoenvironment interpretation. Grain size descriptions also followed sedimentological methods which uses the Udden-Wentworth scale. This scale generally follows main grain boundaries (silt, sand and gravels) which are the same as NZGS (2005) grain size criteria. However, sub-categories (e.g. fine sand, medium sand and coarse sand) differ between the two classification systems. The most important difference between grain size scales is the clay-silt boundary. Udden-Wentworth scale positions the clay-silt boundary at 0.004 mm where NZGS (2005) is 0.002 mm (Figure 3.2). Each lithological unit is systematically described in detail and follows this order: colour; weathering; primary sedimentary structures or bedding; consolidation; material sizes and proportions; sorting; and moisture. Sediment texture such as roundness and clast shape are described if clasts are gravels or larger. Plasticity is also noted for fine grained material (i.e. silts and clays).

Phi	Millimeters	Wentworth size class		Millimeters	NZGS (2005) grain size
-12.0	4096	Boulder	Gravel	200	Boulder
-8.0	256	Cobble		60	Cobble
-6.0	64	Pebble		20	Coarse gravel
-2.0	4	Granule		6	Medium gravel
-1.0	2.00	Very coarse sand		2	Fine gravel
0.0	1.00	Coarse sand	Sand	0.6	Coarse sand
1.0	0.50	Medium sand		0.2	Medium sand
2.0	0.25	Fine sand		0.06	Fine sand
3.0	0.125	Very fine sand			
4.0	0.0625	Coarse silt	Silt		
5.0	0.031	Medium silt			
6.0	0.0156	Fine silt			
7.0	0.0078	Very fine silt			
8.0	0.0039	Clay	Mud	0.002	Silt
14.0	0.00006				

Figure 3.2: Comparison between Udden-Wentworth scale and NZGS (2005) grain size criteria. Arrows show similarities.

3.3.3 Lithofacies and paleoenvironment interpretation

Progression into assigning facies to lithological units can only be accomplished once all units have been described from all sites because the purpose of a facies analysis is to incorporate the whole array of deposits present. This study developed a new local classification of lithofacies following standardised facies schemes for fluvial environments. Hume *et al.* (1975) lithofacies are correlated to the 14 lithofacies identified in this study (see chapter 4). Numerous geological characteristics indicate that the Hinuera Formation was deposited by a high-energy, braided ancestral river system, and the deposits form a series of very low-angle alluvial fans which, because of their low slopes, resemble floodplains. Therefore the paleoenvironment of a particular site would include geomorphic units of a braided river system such as channels, levees, and floodplains. Paleoenvironment interpretations are based on the physiographic model developed by Hume *et al.* (1975) (see chapter 4). Other expected depositional environments include tephra-fall deposition and lake or peat sedimentation.

3.4 Soft sediment deformation

All soft sediment deformations identified are described as ball-and-pillow structures, pseudo-nodules, dish-and-pillar structures, flame structures, or clastic dikes and sills, focussing particularly on any observations of injection structures (sand dikes). Secondary sedimentary structures are usually minor compared to the rest of the deposit, and therefore a thorough search of any vertical structures must be completed. Targeted areas include proximity to a water table or deposits that contain characteristics which impede drainage. Injection structures of a vertical nature are the principal means of identification, as they would be highlighted against the horizontal nature of the deposits. There are difficulties in preservation of these structures, as not only are they are small, they are also prone to erosion. Frequently, the sand volcano produced on a pre-earthquake surface is eroded off, while the injection structure remains. Once secondary structures are recognised, their deformation mechanism and seismic or non-seismic trigger agent are derived through context-based approaches suggested by Owen & Moretti (2011) and Owen *et al.* (2011) (see chapter 2).

3.5 Particle size analysis

A particle size analysis is conducted using the Malvern Mastersizer 2000 to obtain percentages of differing particle size within a sample. Samples are collected from the injection structures and the enclosing deposits in order to compare results. Preparation included sieving material at 2 mm to remove any large clasts which the laser sizer would be unable to measure. Approximately 5 g of each sample is placed into small glass jars, which are then immersed in a 10% hydrogen peroxide (H_2O_2) solution to remove organic material. Digestion took over three weeks, as most samples are heavily iron stained. The reaction between H_2O_2 and possibly MnO_2 associated with the iron staining is vigorous and constant refilling of H_2O_2 is required. Finally, the samples are placed on a hot plate with 10 % sodium hexametaphosphate (Calgon). Heat acts as a catalyst to further remove any residual carbonaceous material and to dry the sample while Calgon acts as a chemical deflocculant to separate the fine grained material. The laser sizer uses a scattering of blue light and red light to measure particle size using the Mie theory. For each sample, a laser sizer analysis is replicated three times to achieve an average result from the tests. Particle size diameters are determined using the Udden-Wentworth scale (Figure 3.2).

Statistical measures are key to inferring transporting agents and depositional settings. Measured particle sizes are converted into phi (ϕ) units before statistical measures (mean, sorting, skewness and kurtosis) are calculated (Folk, 1968). The mean is average grain size, sorting calculated as standard deviation, skewness (symmetry of the distribution curve) is a comparison between coarse and fine sorting; and kurtosis or peakedness is sorting efficiency of the most frequently occurring grain size (Folk, 1968).

3.6 Liquefaction assessment

Data collected from the piezocone penetration test (CPTu) at sites that showed definitive evidence of cyclic induced paleoliquefaction features are used for the liquefaction assessment. Opus Hamilton are contracted to perform the CPTu tests. The interpretation of the CPTu data is conducted in the software packages CPeT-IT and CLiq software (GeoLogismiki, 2006). CPeT-IT provides the soil

behaviour type interpretations and estimations of other important geotechnical parameters such as shear strength, whereas CLiq performs liquefaction susceptibility calculations.

3.7 Radiocarbon dating

The estimated age of deposition is obtained from the soil component of organic silt and peat deposits from sites where liquefaction structures are found. Through cross-cutting relationships, depositional ages would suggest a maximum occurrence age, as the injection structures would post-date the time of deposition. Conventional radiometric dating using liquid scintillation spectrometry is conducted at the University of Waikato Radiocarbon Dating Laboratory. Soil and peat pre-treatments involved removing any visible wood fragments from the samples followed by an acid-base-acid wash using HCl and NaOH. After each wash, the samples are rinsed and dried. Radiocarbon ages (C^{14} yr BP) are calibrated based on OxCal v.4.2.4 (Bronk Ramsey, 2001) and SHCal13 (Hogg *et al.*, 2013).

3.7.1 *CPTu-based soil analysis*

3.7.1.1 Basic CPTu plots

Raw CPTu data are firstly imported into CPeT-IT and basic calculations of corrected cone resistance (q_t), friction ratio (R_f), and pore water pressure (u_2) are described. Furthermore, estimated parameter plots of cohesive soil shear strengths are used to help determine the site subsoil class.

3.7.1.2 Site subsoil class

Building structures are designed according to site subsoil class which are based on the response of soil or rock material to earthquake loadings. Determining site subsoil class is important as calculations for design Peak Ground Acceleration (PGA) incorporates site “Class”. PGA is the maximum acceleration measured at sites from seismic energy and is roughly the acceleration a building will experience. A combination of surface geology and geotechnical characteristics are used to derive site subsoil class. The classification scheme is summarised in Table 3-1 and Table 3-2. In this study, the site subsoil class is determined using

surface geology and the approximated depth of the Hinuera Formation to underlying rock (Standards New Zealand, 2004).

Table 3-1: Site subsoil classification scheme (McVerry *et al.*, 2006; Standards New Zealand, 2004).

Class	Definition
Class A – Strong Rock	Strong to extremely-strong rock with: (a) Unconfined compressive strength greater than 50 MPa; and (b) An average shear-wave velocity over the top 30 m greater than 1500 m/s; and (c) Not underlain by materials having a compressive strength less than 18 MPa or a shear-wave velocity less than 600 m/s.
Class B – Rock	Rock with: (a) A compressive strength between 1 and 50 MPa; and (b) An average shear-wave velocity over the top 30 m greater than 360 m/s; and (c) Not underlain by materials having a compressive strength less than 0.8 MPa or a shear-wave velocity less than 300 m/s. A surface layer of no more than 3 m depth of highly-weathered or completely-weathered rock or soil (a material with a compressive strength less than 1 MPa) may be present.
Class C – Shallow Soil Site	Sites where: (a) They are not class A , class B or class E sites; and (b) The low amplitude natural period is less than or equal to 0.6 s; or (c) Depths of soil do not exceed those listed in Table 3.2.
Class D – Deep or Soft Soil Sites	(a) That are not class A , class B or class E sites; and (b) Where low-amplitude natural period is greater than 0.6 s; or (c) With depths of soils exceeding those listed in Table 3.2; or (d) Underlain by less than 10 m of soils with an undrained shear-strength less than 12.5 kPa or soils with SPT N-values less than 6.
Class E – Very Soft Soil Sites	(a) More than 10 m of very soft soils with undrained shear strength less than 12.5 kPa; or (b) More than 10 m of soils with SPT N-values less than 6; or (c) More than 10 m depth of soils with shear-wave velocities of 150 m/s or less; or (d) More than 10 m combined depth of soils with properties as described in (a), (b) and (c) above.

Table 3-2: Maximum depth limits: Table 3.2 from NZS1170.5: 2004 (Standards New Zealand, 2004).

Soil type and description	Maximum depth of soil
----------------------------------	------------------------------

Cohesive soil	Representative undrained shear strengths (kPa)	(m)
Very soft	< 12.5	0
Soft	12.5 – 25	20
Firm	25 – 50	25
Stiff	50 – 100	40
Very stiff or hard	100 – 200	60

Cohesionless soil	Representative SPT N values	
Very loose	< 6	0
Loose dry	6 – 10	40
Medium dense	10 – 30	45
Dense	30 – 50	55
Very dense	> 50	60
Gravels	> 30	100

3.7.1.3 Soil behaviour type (SBT)

CPTu derives soil behaviour type according to calculations from Robertson *et al.* (1986) for non-normalised SBT plots and from Robertson (1990) for normalised SBT plots (SBTn). Identifying the critical layer in field observations, defined as the source bed or liquefied layer (Green *et al.*, 2014), is key to the liquefaction assessment. As these depths are then used to approximate the critical layer on the SBT plots.

3.7.2 CPTu cyclic liquefaction analysis

Loading Standards require building designs to: firstly, remain fully operational during frequent and moderate intensity earthquakes; and secondly, to remain stable in rare, high intensity earthquakes (Standards New Zealand, 2004). Therefore, the probability of exceedance for Serviceability Limit State (SLS), a 1 in 25 year return period, corresponds to frequent, moderate earthquake intensities. The Ultimate Limit State (ULS), a 1 in 500 year return period, is associated with rare, high earthquake intensities. Maximum Considered Earthquake (MCE), a 1 in 2500 year return period, is also analysed as this return period is the recurrence interval of the Kerepehi Fault.

The liquefaction assessment is performed in CLiq using a modification of the “simplified procedure” suggested in Youd *et al.* (2001). Refined calculation

methods for the empirical CRR curves are derived from Idriss and Boulanger (2008) and Boulanger and Idriss (2014). Liquefaction assessments require a combination of effective magnitude (M_{eff}) and unweighted PGA and are summarised in the following sections.

3.7.2.1 Effective magnitude

Effective magnitudes are based on the national seismic hazard model (Standards New Zealand, 2004; Stirling *et al.*, 2012). The Bridge Manual (New Zealand Transport Agency (NZTA), 2014) provides maps in which M_{eff} can be estimated and a table corresponding to main cities in which M_{eff} is calculated. The Bridge Manual suggests using M_{eff} values from (Table 3-3) they provide the more conservative results. These conservative results are used in this study.

Table 3-3: Peak ground coefficients for a 1000 year return period ($C_{0,1000}$) and effective magnitudes (M_{eff}) for towns and cities in the Hamilton and Hauraki basins (from Table 6A.1: NZTA, 2014).

Town/City	$C_{0,1000}$		Effective magnitudes (M_{eff}) for design return period (years)	
	Class A/B rock	Class D&E deep/ soft soil	500 – 2500	50 – 100
Ngaruawahia	0.23	0.27	5.8	
Morrinsville	0.27	0.32	5.9	
Te Aroha	0.29	0.34	5.9	
Hamilton	0.24	0.28	5.9	
Cambridge	0.26	0.32	5.9	
Te Awamutu	0.24	0.29	5.9	
Matamata	0.27	0.34	5.9	

3.7.2.2 Peak ground acceleration (PGA)

Unweighted peak ground accelerations derived from the Bridge Manual (NZTA, 2014) are used as opposed to magnitude weighted PGAs in NZS1170.5 (Standards New Zealand, 2004). Unweighted PGA provides an accurate site specific PGA and is derived from equation (3-1).

$$PGA = C_{0,1000} \times \frac{R_u}{1.3} \times f \times g \quad (3-1)$$

Where

- $C_{0,1000}$ = PGA coefficient for a 1000 year return period (see Table 3-3)
- R_u = return period factor (=1, see NZS1170.5)
- f = subsoil class factor (=1 for Class D and E)
- g = acceleration due to gravity

3.7.2.3 CLiq inputs

CLiq then requires parameters such as a calculation method, PGA, M_{eff} and water table height to predict liquefaction susceptibility. Calculation methods from both Idriss and Boulanger (2008) and Boulanger and Idriss (2014) are implemented. Table 3-4 contains calculated PGA and M_{eff} . The water table height is set to zero depth to assume a worst case scenario (all soils saturated). Predicted liquefaction is calculated by the factor of safety (FS), which is a ratio of CSR and CRR measurements. FS values ≥ 1 are safe and liquefaction is predicted to not occur, FS values < 1 are considered unsafe and liquefaction is predicted to occur.

Table 3-4: Summary of liquefaction parameters, used in CLiq for Hamilton and Cambridge.

Town/City	Parameter	SLS (1/25)	ULS (1/500)	MLS (1/2500)
Hamilton	M_{eff}	5.9	5.9	5.9
	PGA	0.05	0.22	0.39
	$C_{0,1000}$	0.28	0.28	0.28
	R_u	0.25	1.0	1.8
	f	1.0	1.0	1.0
Cambridge	M_{eff}	5.9	5.9	5.9
	PGA	0.06	0.25	0.44
	$C_{0,1000}$	0.32	0.32	0.32
	R_u	0.25	1.0	1.8
	f	1.0	1.0	1.0

3.7.3 Minimum PGA

Minimum PGA is an estimation of the earthquake size needed to trigger liquefaction. The method suggested by Andrew Holland (personal communication, 2014) is conducted by trial-and-error. This method is where PGA is systematically altered until the CSR curve and CRR curve are on top of on each other, essentially estimating a FS value of 1 for the critical layer. PGA is compared to settlements,

Liquefaction Potential Index (LPI) and Liquefaction Severity Number (LSN). Settlements are calculated according to methods by Zhang *et al.* (2002). LPI is a measure of the vulnerability to liquefaction calculated by equation (3-2) (Juang *et al.*, 2005; Iwasaki *et al.*, 1982). LPI values 0 to 5 are low risk, 5 to 15 as high risk, and >15 for very high risk

$$LPI = \int_0^{20} F_1 W(z) dz \quad (3-2)$$

Where z = depth below the ground surface
 $W(z)$ = $10 - 0.5z$
 F_1 = $1 - FS$ for $FS < 1.0$ or
 F_1 = 0 for $FS > 1.0$

LSN also expresses liquefaction vulnerability and incorporates deep liquefied layers that are less damaging compared to shallow layers (Tonkin and Taylor, 2013). LSN values 0 to 10 show little to no expression of liquefaction, 10 to 20: minor expression of liquefaction, 20 to 30: moderate expression of liquefaction, 30 to 40: moderate to severe expression of liquefaction, 40 to 50: major expression of liquefaction, > 50: severe expression of liquefaction.

$$LSN = \int \frac{\varepsilon_v}{z} dz \quad (3-3)$$

ε_v = volumetric consolidation strain
 z = depth below ground

Chapter 4

Lithofacies analysis of the Hinuera Formation

4.1 Introduction

At all sites a sedimentary facies analysis is performed. A list of the lithofacies present (facies hereafter), their inferred paleoenvironment, the water table location, and any secondary sedimentary structures have been noted for each site. A total of 14 facies are defined, based primarily on dominant grain size but also composition and sedimentary structures. These are shown in Table 4-1 along with their code notation and inferred paleoenvironments. Hume *et al.* (1975) devised lithofacies for the Hinuera Formation (Figure 4.1). My facies analysis is more detailed and the correlation is shown in Table 4-1. Full facies descriptions, stratigraphic logs and their associated field photos are presented in appendix 1.

Table 4-1: Lithofacies identified and their interpreted paleoenvironment.

Facies	Code	H*	Geological name	Interpreted paleoenvironment
Gravel	G1	C1	Pumiceous sandy gravel	Levee
	XBG1	A1	Rhyolitic sandy gravel Cross-bedded pumiceous sandy gravel Cross-bedded rhyolitic sandy gravel	Paleochannel
Sand	S1	A2	Pumiceous gravelly sand	Levee
	XBS1	A1	Cross-bedded pumiceous gravelly sand Cross-bedded rhyolitic gravelly sand	Paleochannel
	XBS1a	A1	Manganese-oxidized coated cross-bedded pumiceous gravelly sand (blackish staining)	Paleochannel
	XBS1b	A1	Profusely iron-oxide stained cross-bedded pumiceous gravelly sand (reddish staining)	Paleochannel
	S2	C	Pumiceous coarse sand	Levee
Silt	S3	C	Pumiceous medium sand	Levee
	S4	C	Pumiceous fine sand	Levee
	Z1	D	Pumiceous sandy silt	Overbank silt
	Z2	-	Pumiceous clayey silt	Tephra-fall deposits or loess [§]
	Z2a	-	Clayey silt with pumice clasts	Reworked pyroclastic flow or fall deposits
	Z3	E	Organic silt	Swamp
Peat	P1	E	Peat	Swamp or lake

*Lithofacies of Hume *et al.* (1975) (see Figure 4.1).

[§] Deposited over sediments of Hinuera Formation (i.e. post-Hinuera)

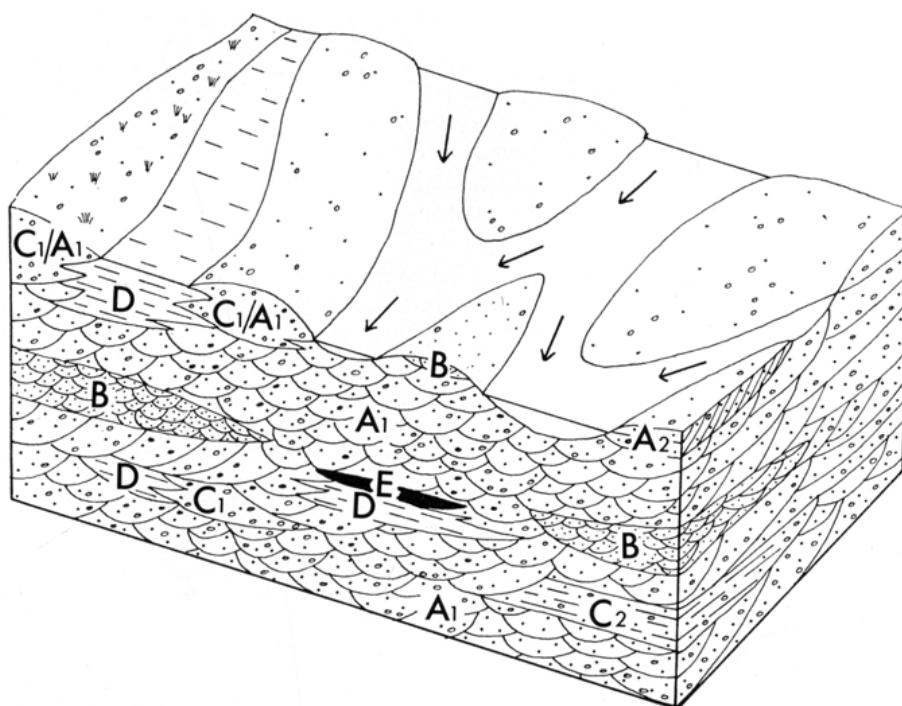


Figure 4.1: Physiographic and lithofacies model for Hinuera Formation from Hume *et al.*, (1975). A1: Large trough cross-bedded, rhyolitic and pumiceous gravelly and slightly gravelly quartzofeldspathic sands. A2: Planar cross-bedded, gravelly sands (same texture as A1). B: Fine trough cross-bedded sands. C1: Poorly defined horizontally stratified (often appears structureless), rhyolitic sandy gravels. C2: Horizontal to gently dipping laminae, gravelly sands. D: Horizontal laminae pumiceous silts. E: Horizontal laminae to massive peats and peaty pumiceous silts.

4.2 Hauraki Basin

4.2.1 Site 1 – Private property (Kevin Nola’s Sandpit)

Kevin Nola’s Sandpit is located on Tauranga Road, Matamata, at the southern end of the Kerepehi Fault (1848089, 5808490). Two facies are identified: pumiceous sandy gravel (G1) and a pumiceous gravelly sand (S1) (Figure 4.2a). The pumiceous sandy gravel is overlain by a pumiceous gravelly sand, and the inferred paleoenvironments for both facies are river levees. Pumiceous sandy gravel involves a massive deposit with horizontal bedding near its upper boundary transitioning into pumiceous gravelly sand. The horizontal bedding is an indication of increased depositional energy. Throughout the pumiceous gravelly sand facies, micro-faulting is evident, probably a consequence of proximity to the Kerepehi Fault. Also evident are soft sediment deformations of vertical, elongated pseudo-nodules (Figure 4.2b), interpreted as syn-depositional features because of their

discontinuous nature. There is no evidence of a water table, although, at the top of the pumiceous gravelly sand facies, finer grained beds showed slightly impermeable properties and a dark grey colour in comparison to the rest of the deposit.

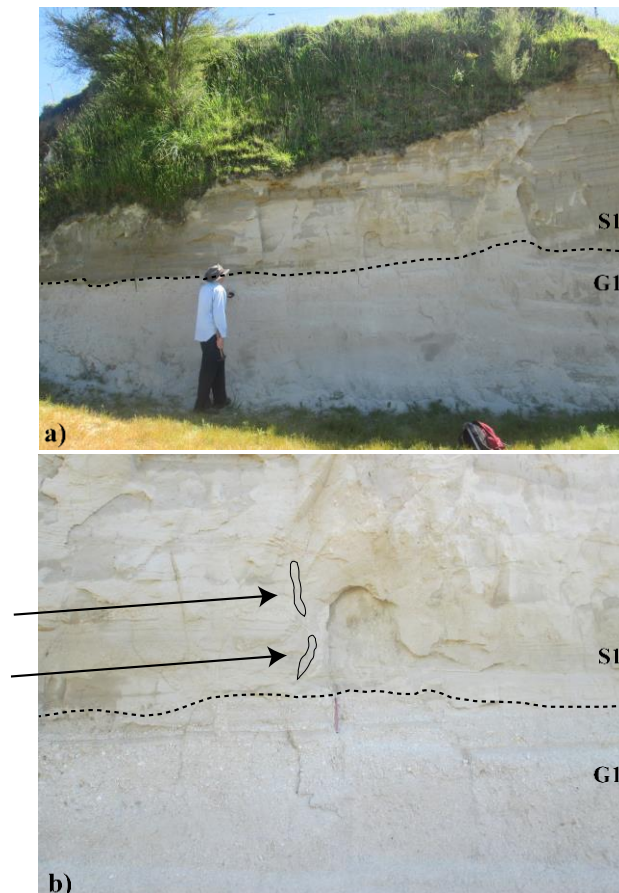


Figure 4.2: (a) Stratigraphic section at Kevin Nola's Sandpit showing horizontal bedding near upper boundary in S1. Person is 1.8 m tall. (b) Contact between G1 and S1. Arrows point to pseudo-nodules. Scale pencil 14 cm long.

4.2.2 Site 2 – McPhersons Sand Supply

Site 2 is located on State Highway 29 near the small township of Te Poi (1846039, 5803451). McPhersons Sand Supply is an active sand quarry with quarry faces up to 15 m high. Three facies are recognised within the quarry face: a pumiceous sandy silt (Z1), cross-bedded pumiceous sandy gravel (XBG1) and a pumiceous clayey silt (Z2). The pumiceous sandy silt is overlain by a cross-bedded pumiceous sandy gravel and a pumiceous clayey silt. Their paleoenvironments are interpreted to be a low energy environment overbank or an abandoned channel setting for the silt deposit, followed by an active, high energy channel migrating over the silt for the

gravel deposit. The pumiceous sandy silt showed evidence of wavy soft sediment deformation structures, most likely directly related to the large influx of sediment causing rapid loading. Although one deformation structure showed continuous, injection-like characteristics (Figure 4.3), there is no connection to its source bed. The pumiceous clayey silt is interpreted as a capping of tephra-fall deposits (post-Hinuera) in the Hamilton-southern Hauraki basins, which are documented by Lowe (1988). Adjacent to the quarry, towards the northwest and approximately 6 m below the main quarry floor, is a small pond with peat at the bottom which is evidence of the present day water table.

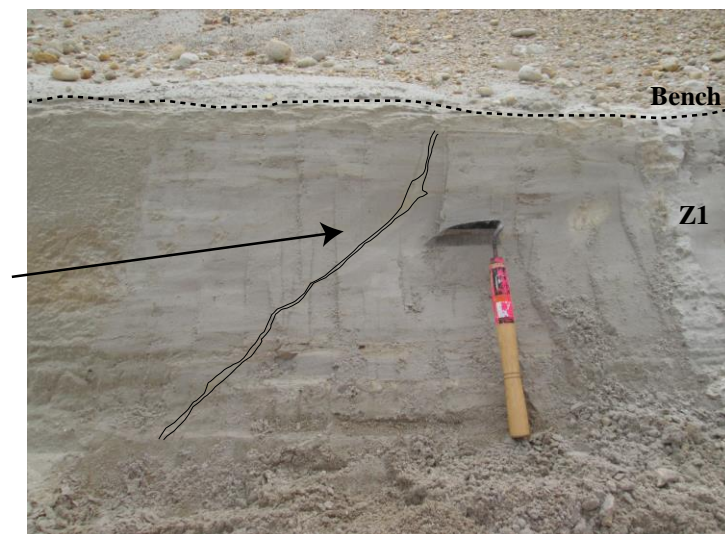


Figure 4.3: Light grey, soft sediment deformation (arrow) intruding through Z1 at section at McPhersons Sand Supply. Cutting tool 30 cm long.

4.2.3 Site 3 – Daltons Sand Ltd

Daltons Sand is a well-established sand supplier and manufacture of potting mixes located at 266 Hinuera Road, Matamata (1842467, 5807094). Constantly quarried throughout the year, the site contains quarry faces up to 10 m high. Three facies are identified. The first consists of cross-bedded gravelly sand (XBS1) and within this, two further facies are scattered: a fine sand (S4) and a pumiceous sandy silt (Z1). A paleochannel once existed here, later becoming abandoned. The decrease in depositional energy is indicated by the finer sands (S4) and thin cross-beds until eventually the area is completely abandoned, allowing silts to be deposited (Figure 4.4). A younger channel then passed through Site 3 again. Within the deposits in this younger paleochannel are large rip-up clasts, which are characteristic of an active channel rapidly eroding the underlying silt deposit. No

evidence of liquefaction structures or of a water table are identified. The pumiceous sandy silts exhibit properties that would impede drainage, but at Site 3 this bed is only 20 cm thick and would not contain enough moisture to enable a liquefaction event to be recorded.

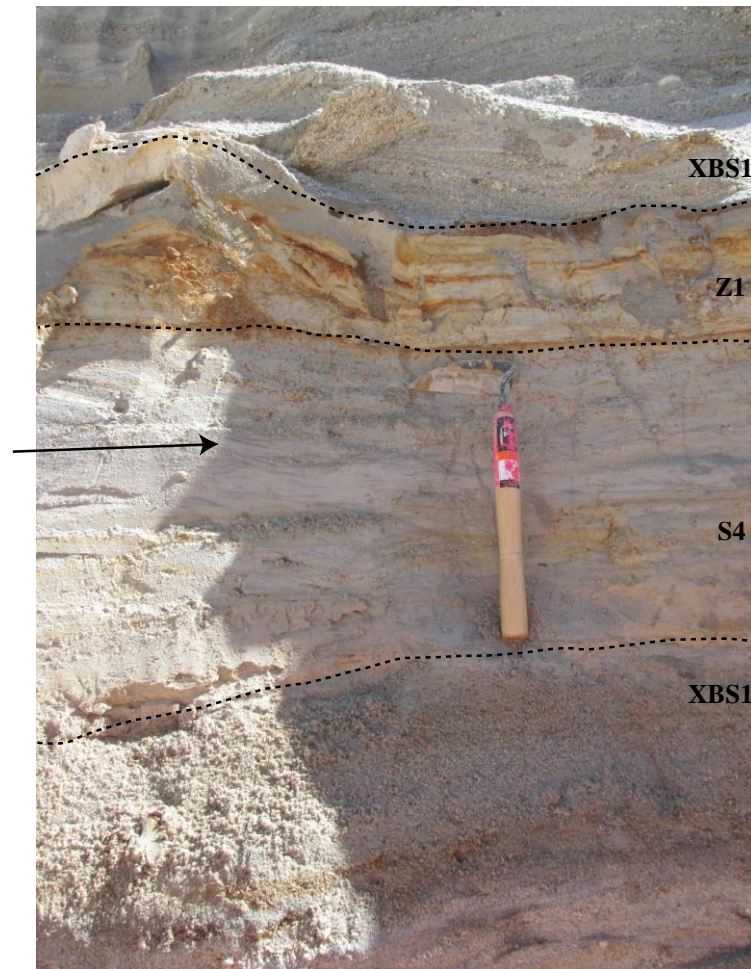


Figure 4.4: S4 overlain by Z1 at Daltons Sand quarry. S4 contains fine cross-beds (arrow) and is interpreted as a minor channel. Cutting tool 30 cm long.

4.2.4 Site 4 – Private property (Ian Settle’s Sandpit)

The sandpit on Ian Settle’s farm is located south of Matamata (1848444, 5807808) and is no longer in use. As a result the deposits are covered in a weakly cemented sand wash and are sporadically covered in vegetation (Figure 4.5). Three facies are present: a pumiceous medium sand (S3) overlain by a cross-bedded gravelly sand (XBS1), and a pumiceous clayey silt (Z2). The recorded depositional environment is inferred to have changed from a levee to a paleochannel and finally to tephra-fall. A water table is not located, and the entire quarry area is very dry.



Figure 4.5: The inactive sandpit at site 4 contains weakly cemented surficial sand wash and vegetation cover on facies XBS1 and Z2. Person 1.6 m tall.

4.2.5 Site 5 – Wilsons Sand

Wilsons Sand is a large sand quarry adjacent to Site 3 at 196 Hinuera Road, Matamata (1842718, 5807793). There are two operating sand quarries at this site, a larger one that is parallel to Hinuera Road with slope faces up to 18 m high and a smaller quarry near the back of the site, 1.5 km west of the road. Two facies are present at the larger quarry: a very thick (15 m) deposit of pumiceous cross-bedded gravelly sand (XBS1), overlain by a light brown pumiceous clayey silt (Z2) deposit (Figure 4.6a). These facies correlate to a long-lived paleochannel followed by a tephra blanket. Within the smaller quarry several facies are identified: pumiceous cross-bedded gravelly sand (XBS1), pumiceous sandy silt (Z1), interbedded pumiceous gravelly sand and sandy silt (S1 & Z1) and a capping white pumiceous sandy silt (Z2). The inferred paleoenvironment began as a high energy braided channel (XBS1) that reduced to a lower energy, overbank deposit (Z1). This sequence is repeated but the second silt deposit is much thinner, at only 5 cm, and shows evidence of wavy deformation induced by the overlying paleochannel facies (XBS1). In the subsequent beds are interbedded gravelly sands and sandy silts with horizontal bedding (S1 & Z1) (Figure 4.6b), corresponding to the waning stage of the river flow. These deposits are followed by a white cap of tephra. No evidence of a water table or paleoliquefaction features are observed.

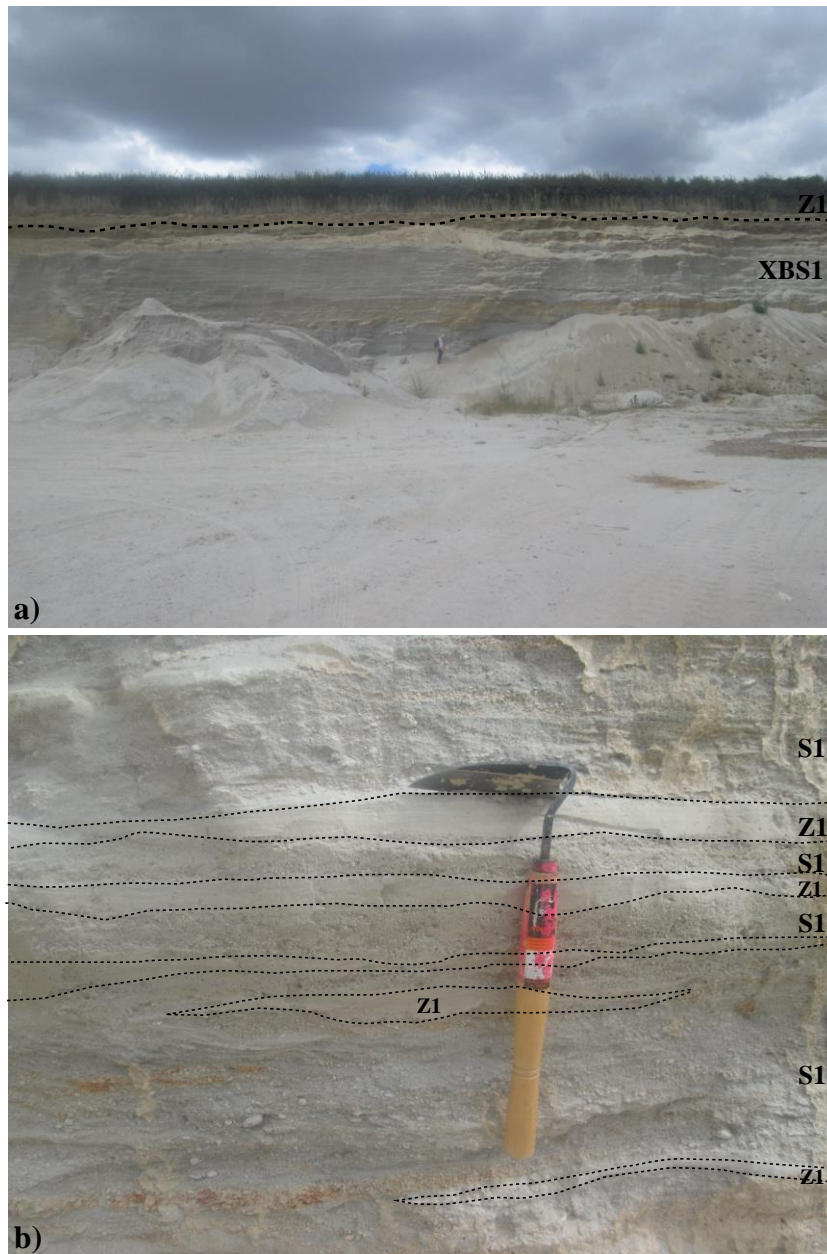


Figure 4.6: (a) Large quarry: facies XBS1 and Z1 at Wilson Sand, XBS1 contains a thick orange iron stained bed. Person 1.8m tall. (b) Small quarry: interbedded gravelly sands and sandy silt (S1 & Z1). Cutting tool 30 cm long.

4.2.6 Site 6 – Manawaru Sandfill and Livestock Ltd

The Manawaru Sandfill is the most northern site in the Hauraki Basin, located at 234 Manawaru Road, Te Aroha (1843367, 5833143). Four facies are identified: pumiceous cross-bedded gravelly sand (XBS1), manganese-oxide coated cross-bedded pumiceous gravelly sand (XBS1a), profusely iron stained cross-bedded pumiceous gravelly sand (XBS1b) and pumiceous clayey silt (Z2). Pumiceous cross-bedded gravelly sand (XBS1) contains heavily weathered XBS1a and XBS1b facies near the quarry floor (Figure 4.7). The black (manganese) and dark orange (iron) staining represents the prolonged existence of a previous water table that has fluctuated so that wetting and drying occurred. Site 6 paleoenvironments are interpreted as an ancient braided channel overlain by a tephra cap. The present water table is not evident and no secondary sedimentary structures are identified.

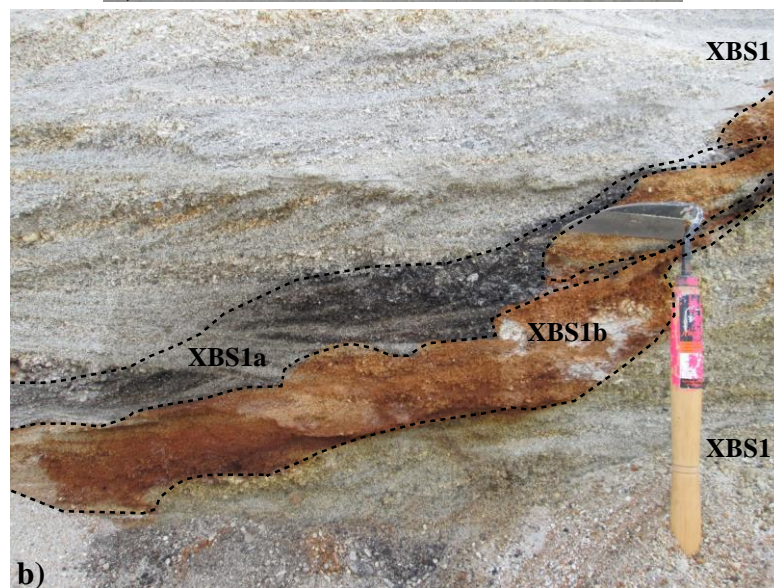
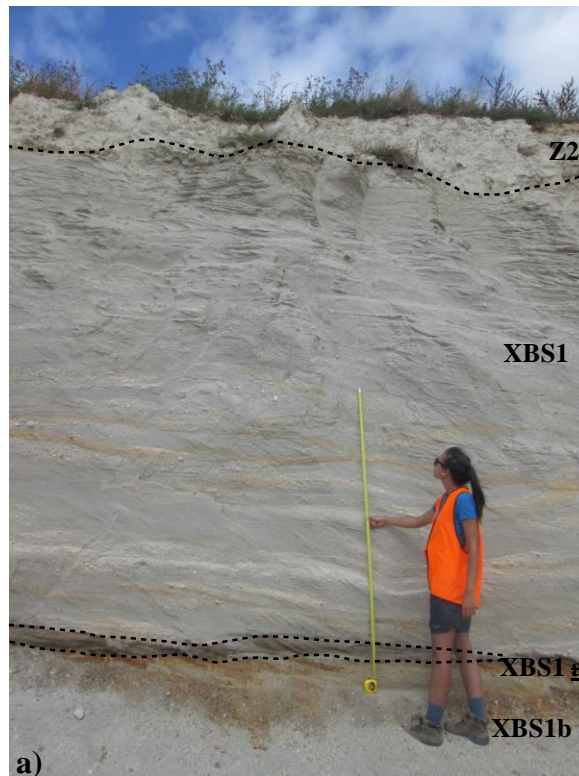


Figure 4.7: (a) Stratigraphic section of Manawaru Sandfill deposits. Person 1.7 m tall, tape measure 2 m long. (b) Heavily stained and consolidated XBS1a (manganese) and XBS1b (iron) facies. Cutting tool 30 cm long.

4.2.7 Site 7 – Tirau Sand Quarry

Tirau Sand Quarry is the most southern site in the Hauraki Basin (1842541, 5794762). It is a sand supplier for construction, farming, drainage and landscaping, located at 148 State Highway 27, Tirau. The six facies identified are pumiceous sandy silt (Z1), rhyolitic sandy gravel (XBG1), pumiceous clayey silt (Z2),

pumiceous cross-bedded gravelly sand (XBS1), rhyolitic sandy gravel (G1) and a clayey silt with pumice clasts (Z2a). For the majority of Site 7, the stratigraphic sequence upwards comprises pumiceous sandy silt (Z1) to rhyolitic cross-bedded sandy gravel (XBG1) to a light brown pumiceous clayey silt (Z2). This sequence corresponds to paleoenvironmental change from overbank silts to high energy paleochannel deposits to a tephra cap. Within the pumiceous sandy silt bed (Z1) there is evidence of a possible small-scale injection structure, but its source bed could not be located and not pursued further (Figure 4.8a). The water table is evident at the lower boundary of the pumiceous sandy silt (Z1). A rare stratigraphic sequence is recognised at Site 7 consisting of pumiceous cross-bedded gravelly sand (XBS1), rhyolitic sandy gravel (G1), clayey silt with pumice clasts (Z2a), and pumiceous clayey silt (Z2). The first two facies are interpreted as paleochannel sediments followed by a gravel levee. Facies Z2a is inferred to be a pyroclastic material of uncertain origin (possibly reworked flow material or distal tephra fallout) (Figure 4.8b). It is overlain by the same tephra cap observed in the previous sequence.

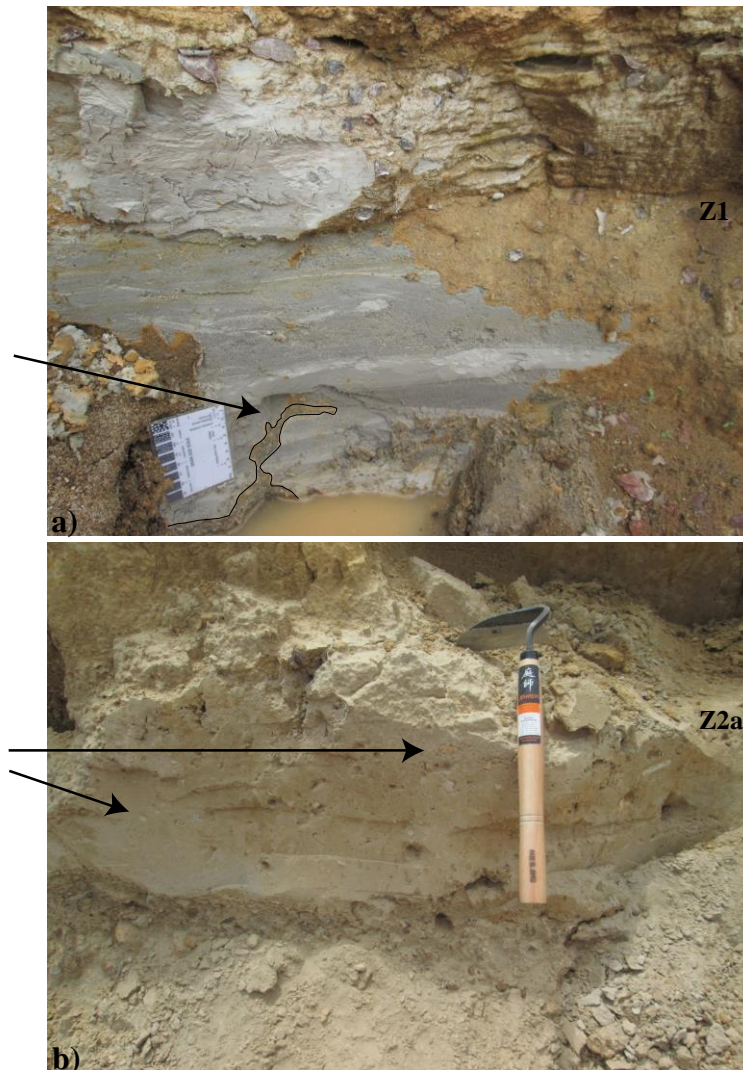


Figure 4.8: (a) Small possible liquefaction structure (arrow) in facies Z1 at Tirau Sand Quarry. Also note evidence of a water table. Scale 8 cm long. (b) Inferred pyroclastic deposit with pumice clasts (arrows) at Tirau Sand Quarry. Cutting tool 30 cm.

4.3 Hamilton Basin

4.3.1 Site 8 – Landcycle

Landcycle is an operating quarry, providing concrete sand, equestrian sand, pit sand, unscreened topsoil and landscaping stone. It is located at 3807 Cambridge–Te Awamutu Road, Cambridge (1814766, 5802279). The quarry visited contained two sections, an active quarry area and an inactive quarry part. Rhyolitic cross-bedded sandy gravel (XBG1) and pumiceous clayey silt (Z2) are identified at the active quarry face with paleoenvironment interpretations of a paleochannel covered by a light brown tephra cap (Figure 4.9a). The inactive quarry face consisted of pumiceous sandy silt (Z1), rhyolitic cross-bedded sandy gravel (XBG1) and a white

pumiceous clayey silt (Z2). This sequence indicates a past depositional environment of overbank silts and active braided channels, overlain by a white tephra cap (Figure 4.9b). No water table or injection structures are located at Site 8.

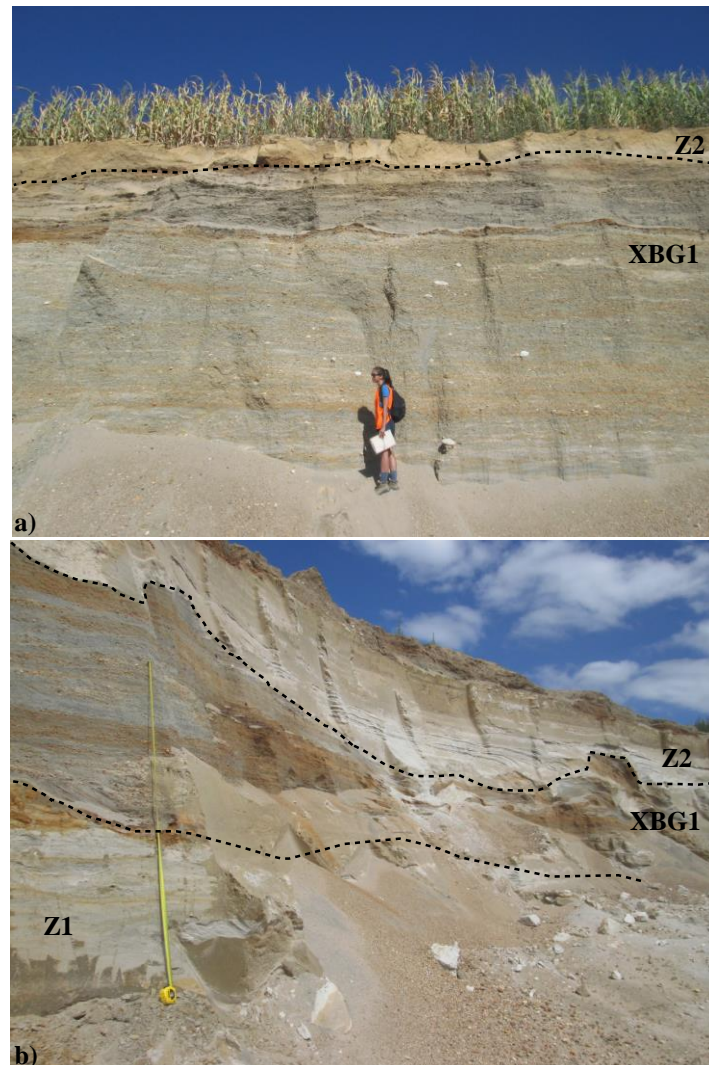


Figure 4.9: (a) Stratigraphic sequence of the active quarry section at Landcycle. Person 1.7 m tall. (b) Stratigraphic sequence of the inactive quarry section at Landcycle with a thick white tephra deposit (Z2). Tape measure 2 m long.

4.3.2 Site 9 – Monavale Sand Quarry

Monavale Sand Quarry is the most southern site for the Hamilton Basin, located at 75 Parallel Road, Cambridge (1813165, 5799227). The stratigraphic sequence consists of several different facies: pumiceous sandy silt (Z1), organic silt (Z3), interbedded coarse sand and sandy silt (S2 & Z1), pumiceous cross-bedded gravelly sand (XBS1), pumiceous gravelly sand (S1), pumiceous sandy gravel (G1) and a

light brown pumiceous clayey silt (Z2). Depositional environments are interpreted to have been low energy overbank silts that transitioned to a swamp. The facies change from silt deposits to organic material further supports a decrease in depositional energy. An increase in energy is signified by the interbedded coarse sand and sandy silt (S2 & Z1) facies followed by high energy channel deposition. These sediments are overlain by a silt deposit indicating a shift towards a floodplain environment. The upper boundary contains a very dark brown band representing the development of a soil horizon (paleosol). This sequence shows the depositional environment finally became a levee that involves a sand-dominated deposit followed by a gravel-dominated deposit, which is subsequently covered by tephra deposits. There is no water table recognised at site 9, nor are secondary sedimentary structures observed, apart from some possible rotated blocks adjacent to the section (Figure 4.10).

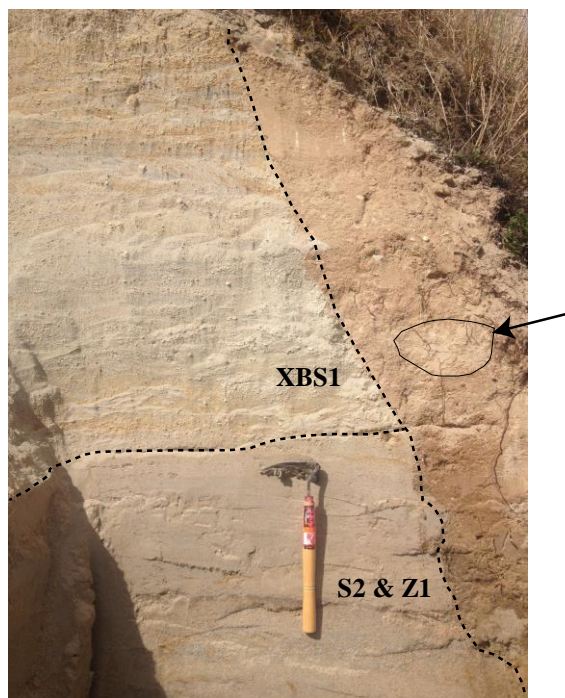


Figure 4.10: A section of the Monavale Sand Quarry stratigraphic sequence containing the interbedded S2 and Z1 overlain by XBS1. Colluvium to the left of the sequence contains possible rotated blocks (see arrow, faint light brown material) that may have resulted from quarrying. Cutting tool 30 cm long.

4.3.3 Site 10 – Perry Resources

The most northern site of the Hamilton Basin is Perry Resources situated at 21 Hutchinson Road, Horotiu (1795115, 5824566). This site contains quarry faces up to 20 m high. Facies identified are: pumiceous cross-bedded gravelly sand (XBS1), pumiceous sandy silt (Z1) and pumiceous clayey silt (Z2). These facies relate to paleochannel environments with two occurrences of overbank silts. A water table is recognised at the lower boundary of XBS1 (Figure 4.11), but due to the instability and height of the quarry faces, searching for injection structures is not permitted.



Figure 4.11: Section through the Perry Resources quarry face, encompassing all facies identified (XBS1, Z1 and Z2). Water table is evident as the pond.

4.3.4 Site 11 – Waikato Aggregates

Waikato Aggregates is a large sand quarry located at 34A Tauware Road, Tamahere (south Hamilton) (1807873, 5810298). The quarry started operations in October 2013 and within 6 months the quarry face reached over 20 m high. Three facies are identified at Site 11: pumiceous cross-bedded gravelly sand (XBS1), pumiceous sandy silt (Z1) and pumiceous clayey silt (Z2) (Figure 4.12a). This sequence involves a paleochannel transitioning into a floodplain (overbank silts) with two

paleosols, covered then by a tephra blanket (Figure 4.12b). A water table is identified at the lowest exposure of facies XBS1, but no injection structures are seen.

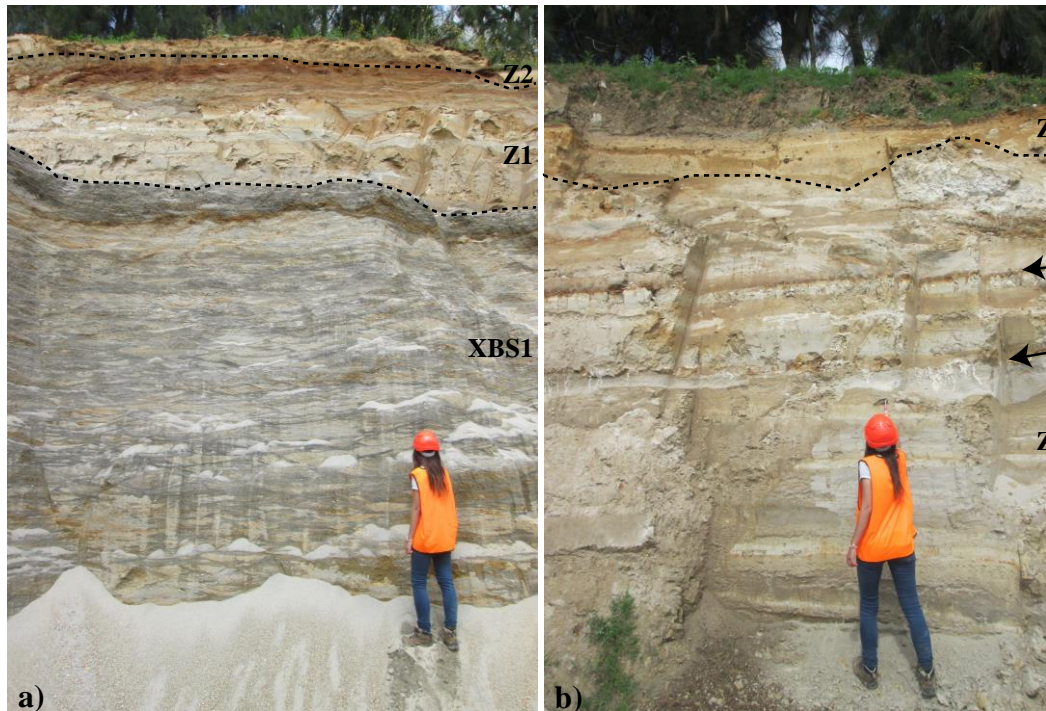


Figure 4.12: (a) Quarry face at Waikato Aggregates including all facies (XBS1, Z1 and Z2) noted. Person 1.7 m tall. (b) Upper part of the section seen in (a) showing Z1 and two paleosol beds (arrowed). Person 1.7 m tall.

4.3.5 Site 12 – Coombes Sand

Coombes Sand is located at 195 Old School Road, Ngahinapouri (1791890, 5803412) and is the closest site to the present day Waipa River. The facies present are cross-bedded gravelly sand (XBS1) and pumiceous sandy silt (Z1), which represent deposition in paleochannels followed by deposition of overbank silts. Cross-bedded gravelly sand (XBS1) comprises a thick orange iron stained bed located at its lower boundary (Figure 4.13a). The contact between facies XBS1 and Z1 is irregular, exhibiting a large sag structure of the silts that could correlate to a complex waning stage of the ancient river (Figure 4.13b). No evidence of paleoliquefaction features or of a shallow water table are found.

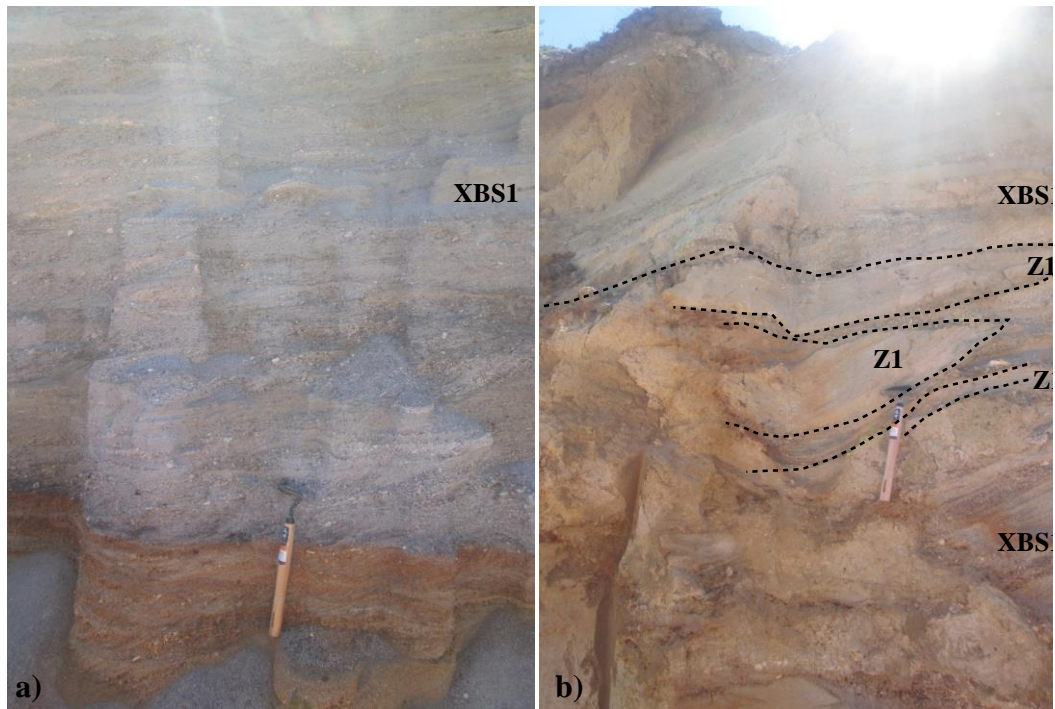


Figure 4.13: (a) Facies XBS1 at Coombes Sand with thick iron stained bed. (b) Facies Z1 irregular contact to XBS1 and depression structure due to eroded out material. Cutting tool 30 cm long.

4.3.6 Site 13 – Porritts Sand Quarry

Porritts Sand is an active sand and gravel quarry on 256A Hooker Road, Tamahere (1811054, 5804979). The two facies identified as cross-bedded rhyolitic sandy gravel (XBG1) and pumiceous clayey silt (Z2) correspond to ancient river channels overlain by the recurring tephra blanket. Facies XBG1 contains large rhyolitic gravel clasts (Figure 4.14) and horizontal bedding is evident near the upper boundary suggesting a decrease in depositional energy before the tephra blanket. No water table depth or liquefaction structures are encountered.



Figure 4.14: Rhyolitic XBG1 facies with large gravel clasts at Porritts Sand. Cutting tool 30 cm long.

4.3.7 Site 14 – IH Wedding and Sons Waikato Ltd

The sand quarry IH Wedding and Sons Waikato is situated at 53 Bedford Road, Te Kowhai (1788293, 5822524). Only a rhyolitic cross-bedded sandy gravel (XBG1) facies is identified and relates to active braided channels (Figure 4.15). A water table is recognised at the lower boundary of facies XBG1 within a pond at the entrance of the quarry. However, no paleoliquefaction features are observed.

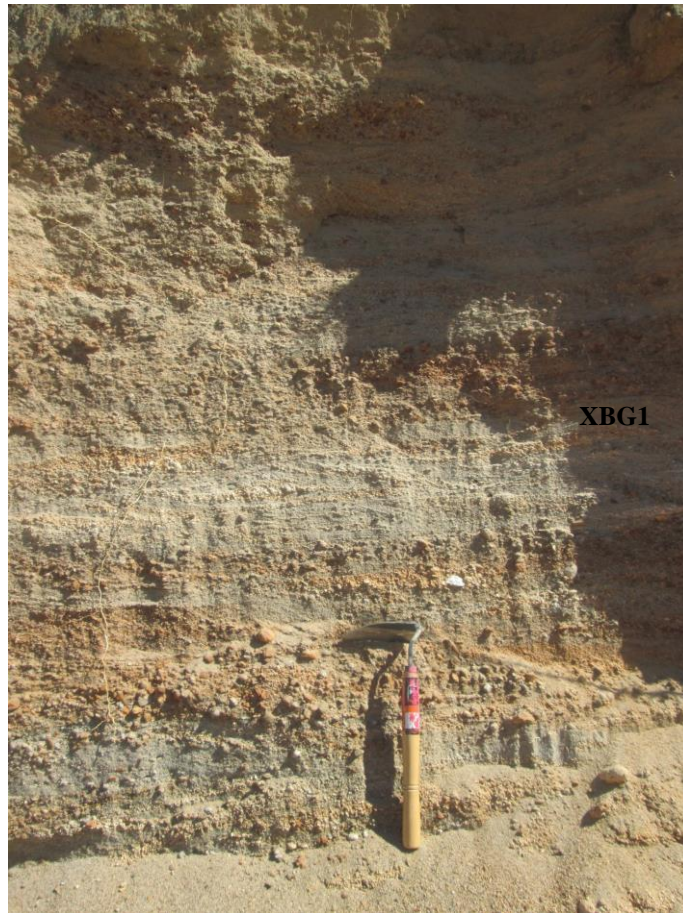


Figure 4.15: Trough cross-bedding of facies XBG1 at IH Wedding and Sons Waikato quarry. Cutting tool 30 cm long.

4.3.8 Site 15 – Quarry on Aspin Road

An active sand quarry is located on 72 Aspin Road, Cambridge (1820745, 5805814). A total of six facies are identified: pumiceous fine sand (S4), pumiceous sandy silt (Z1), organic silt (Z4), pumiceous coarse sand (S2), cross-bedded pumiceous gravelly sand (XBS1) and pumiceous clayey silt (Z2). The fluvial paleoenvironment at this site involved levees (S4) transitioning into low energy floodplains (Z1) followed by a swamp environment (Z4) which is overlain by a second Z1 deposit. Subsequent deposits showed an increase in depositional energy, evident from the shift towards a fine grained (S4) and coarse grained levee (S2) and eventually into an active paleochannel (XBS1). This entire sequence is all overlain by a tephra blanket (Z2). Injection structures are present intruding through facies: pumiceous sandy silt, organic silt and pumiceous coarse sand. A pond is observed adjacent to the section indicating a shallow water table.

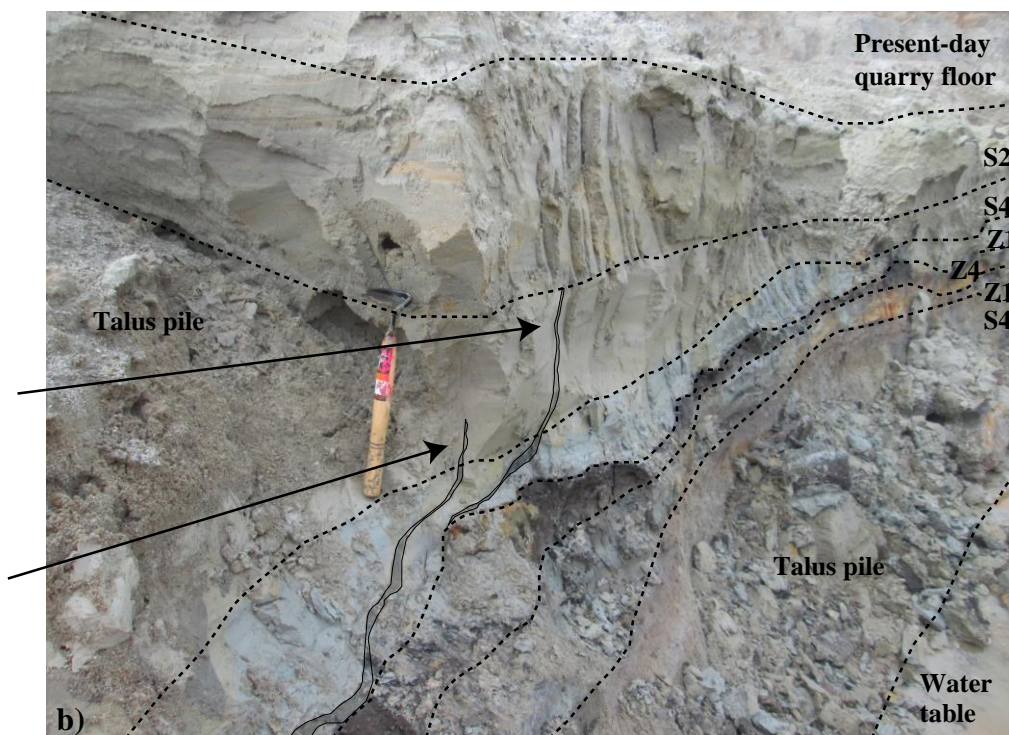
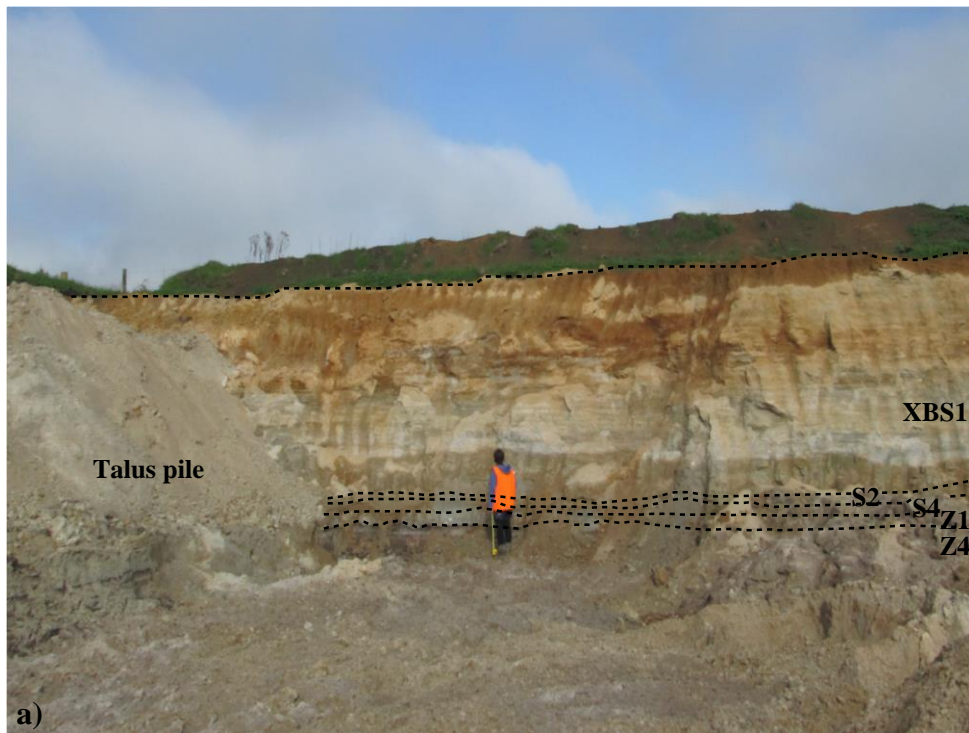


Figure 4.16: Sections at the Quarry on Aspin Road. (a) Quarry face. Niwashi cutting tool 30 cm long. (b) Injection structures (arrows). Water table adjacent to section indicating shallow water table. Cutting tool 30 cm long.

4.3.9 Site 16 – Endeavour Primary School

Endeavour Primary School is located on Endeavour Avenue, Flagstaff (1798577, 5821506). The foundation design required deep excavations (3 to 4 m) of site 16. Five facies are identified: pumiceous fine sand (S4), peat (P1), pumiceous sandy silt (Z1), gravelly sand (S1) and pumiceous clayey silt (Z2). The facies paleoenvironments are inferred as levee deposits (S4) overlain by swamp (P1), and overbank silts (Z1), followed by another levee environment and finally to a tephra cap (Z2). Multiple sand dikes are present in plan-view on the excavated floor at two localities: locality i (1798577, 5821506) and locality ii (1798645, 5821508) (Figure 4.17). After pit excavations, which revealed the sand dikes cross-section, they are interpreted as injection structures as a source bed was identified at locality i (Figure 4.17a). A water table was also positioned at the lowest boundary of the pumiceous sandy silt at locality i.



Figure 4.17: Injection structures at site 16. (a) Source bed and water table at locality i. (b) Injection structure across excavated floor. Cutting tool 30 cm long.

4.3.10 Site 17 – Waikato Expressway (Cambridge section)

The Waikato Expressway is a project to reduce congestion on State Highway 1 from small towns such as Huntly, Ngaruawahia and Cambridge. The Cambridge section

extends from Tamahere to south of Cambridge and the site investigated was located at the Cambridge off ramp adjacent to Tirau Road (1820267, 5802862). Thick deposits of organic silt (Z4) and pumiceous cross-bedded gravelly sand (XBS1) that relate to swamp and channel sediments are recognised. The lowest bed in facies Z4 showed water flowing out of it, indicating a perched water table. However, there was no evidence of paleoliquefaction features, only large-scale load structures that are inferred as seismic or syn-depositional deformation in facies Z4 (Figure 4.18).



Figure 4.18: Facies Z4 and XBS1 at the Waikato Expressway, Cambridge section showing deformation structure (arrow) from syn-depositional processes. Cutting tool 30 cm long.

4.4 Summary

Table 4-2 provides a summary of all sites investigated showing the facies present and their interpreted paleoenvironment, any indication of a water table and any secondary sedimentary structures. There are two sites that possibly had seismic induced features, small scaled injection structures at site 7 and lateral spread cracks at site 9. The two sites that showed definite evidence of past liquefaction are site 15 and 16, these will be analysed in chapter 5

Table 4-2: Summary table of sites with no definite evidence of paleoliquefaction

Site	Facies	Paleoenvironment	Water table location	Sedimentary structures
1	S1	Levee	None	Pseudo-nodules deformations, micro-faulting
	G1	Levee		
2	White Z2	Tephra cap	Pond	Syn-depositional sand dike
	Pumiceous XBG1	Paleochannel		
3	Z1	Overbank silts	None	-
	Pumiceous XBS1	Paleochannel		
4	S4 with cross-beds	Minor channel	None	-
	Z1	Overbank silts		
5	Z2	Tephra cap	Thick Fe stained bed in XBS1	-
	Pumiceous XBS1	Paleochannel		
6	S3	Levee	Mn-Fe staining	-
	Light brown and white Z2	Tephra cap		
7	Pumiceous XBS1	Paleochannel	Lower boundary of Z1 (perched water table)	Small possible injection structure
	Interbedded S1 and Z1	Waning stage of a river		
8	Z1	Overbank silts	None	-
	White Z2	Tephra cap		
9	XBS1a	Iron stained paleochannel	None	-
	XBS1b	Manganese stained paleochannel		
10	Z2a	Pyroclastic deposit	None	-
	Light brown Z2	Tephra cap		
11	G1	Levee	None	-
	XBS1	Paleochannel		
12	XBG1	Paleochannel	None	-
	Z1	Overbank silts		
13	White Z2	Tephra cap	None	-
	Z1	Overbank silts		
14	XBG1	Paleochannel	None	-

9	Light brown Z2 G1 S1 XBS1 Interbedded S2 and Z1 Z3 Z1	Tephra cap Levee Levee Paleochannel Waning river Swamp Overbank silts	None	Possible lateral spread cracks and rotated blocks
10	Light brown Z2 XBS1	Tephra cap Paleochannel	Pond	Not permitted to view quarry face close up
11	Z2 Z1 XBS1	Tephra cap Overbank silts Paleochannel	None	-
12	Z1 XBS1	Overbank silts Paleochannel	None	-
13	Light brown Z2 Rhyolitic XBG1	Tephra cap Paleochannel	None	-
14	Rhyolitic XBG1	Paleochannel	None	-
15	Z2 Pumiceous XBS1 S2 Z4 Z1 S4	Tephra cap Paleochannel Levee Swamp Overbank silts Levee	Pond	Injection structures
16	Z2 S1 Z1 P1 S4	Tephra cap Levee Overbank silts Swamp, paleolake Levee	Perched water table in Z1	Injection structures
17	XBS1 Z4	Paleochannel Swamp	Perched in Z4	Large-scale load structures

Chapter 5

Paleoliquefaction

5.1 Introduction

Only two sites from the 17 sites investigated contained definitive evidence of paleoliquefaction. These are located within the Hamilton Basin at Site 15 (Quarry on Aspin Road) and Site 16 (Endeavour Primary School). In this chapter I present detailed descriptions of the injection structures at both sites, a particle size analysis of the material making up the injection structures and surrounding lithologies, and the results of radiocarbon dating of organic beds present. These findings are then followed by a liquefaction assessment performed on CLiq (GeoLogismiki, 2006). The assessment uses two calculation methods: Idriss and Boulanger (2008) and Boulanger and Idriss (2014).

5.2 Site 15 – Quarry on Aspin Road

5.2.1 Injection structures

A prominent injection structure occurs intruding through four sedimentary units on an excavated quarry wall in the sand Quarry on Aspin Road near Cambridge (Figure 5.1). The quarry wall exposes an *in situ* natural sequence adjacent to a flocculation pond. The injection structures start at a depth of 1.5 m below the present quarry floor, which is approximately 3.5 m below the pre-excavated land surface. The stratigraphy identified in the field shows the source material for the injection structure at the base (Sand-1). This is overlain by these stratigraphic units: Silt-1, Organic silt, Silt-2, Sand-2, and Sand-3 (Figure 5.2). These six units correlate to lithofacies identified in chapter 4 as Sand-1 (pumiceous fine sand, S4), Silt-1 (pumiceous sandy silt, Z1), Organic silt (Z4), Silt-1 (pumiceous sandy silt, Z1), Sand-2 (pumiceous fine sand, S4) and Sand-3 (pumiceous coarse sand, S2). The injection structures intrude through the silts and organic material where they eventually splay into two different directions (Injection-1 and Injection-2a) in the overlying sand layer (Sand-2). Injection structure-1 is a dark grey colour intruding through Silt-2 and Sand-2, with a width of 3 cm, a vertical height of 30 cm and

horizontal length of 48 cm from where it tapers upwards (Figure 5.1). Injection structure-2 is also a dark grey colour that intrudes through Silt-1, Organic silt, Silt-2, and Sand-2, with a width of 2 cm, a vertical height 10 cm and a horizontal length of 1.20 m (Figure 5.3). Injection structure-2 cross-cuts the organic silt layer and connects to Sand-1 identified in field observations as the source bed (Figure 5.4).

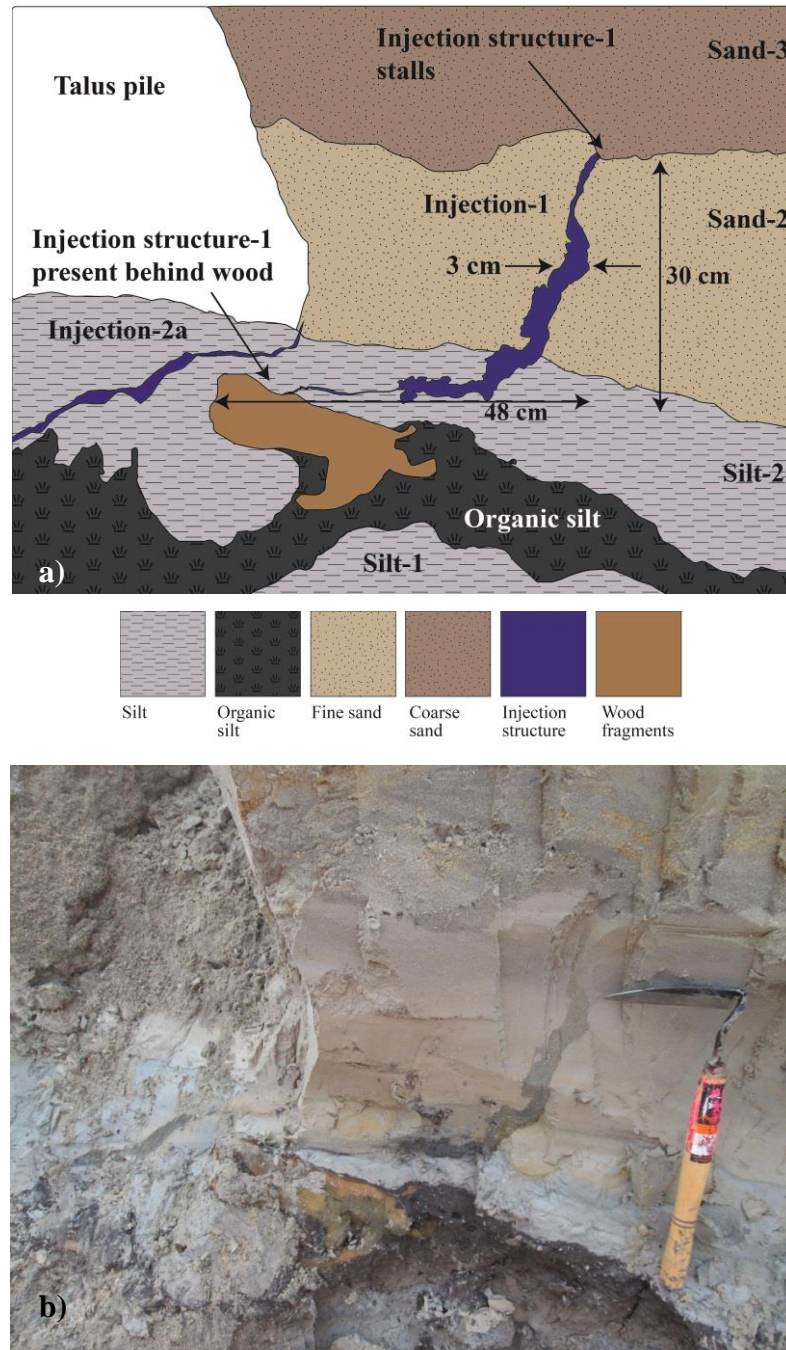


Figure 5.1: Cross-sectional view of injection structures found at the Quarry on Aspin Road, Cambridge. (a) Schematic diagram of injection structures and surrounding stratigraphic units, refer to key. Injection-1 stalls at the Sand-2 and Sand-3 boundary. (b) Field observations, cutting tool 30 cm.

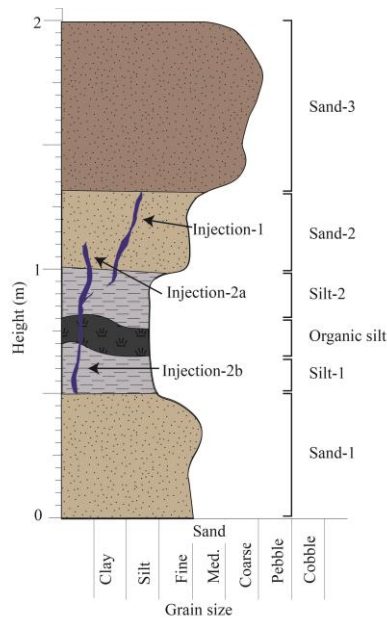


Figure 5.2: Stratigraphy at Quarry on Aspin Road, Cambridge, emphasising the stratigraphic units the injection structures intrude through (refer to key in Figure 5.1). Injection structure-1 tapers from injection structure-2 and intrudes through Silt-1 and Sand-2. Injection structure-2 intrudes through Silt-1, Organic silt, Silt-2 and stalls halfway in Sand-2.

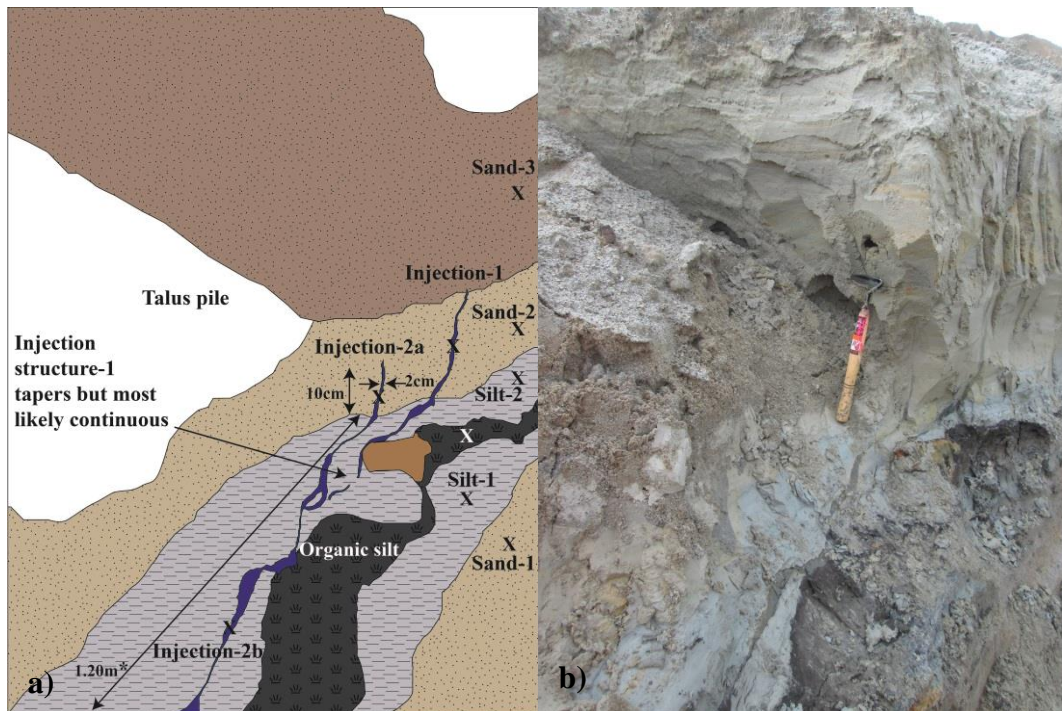


Figure 5.3: Longitudinal view of injection structures including all units in previous stratigraphic column (Figure 5.2) at Quarry on Aspin Road. Injection structure-2 dimensions: width 2 cm, vertical height 10 cm and horizontal length of 1.20 m (*total length of injection structure; this is not captured in image) (a) Schematic diagram, “X” defines sample locations (refer to key in Figure 5.1). (b) Field observations, cutting tool ~ 30 cm.

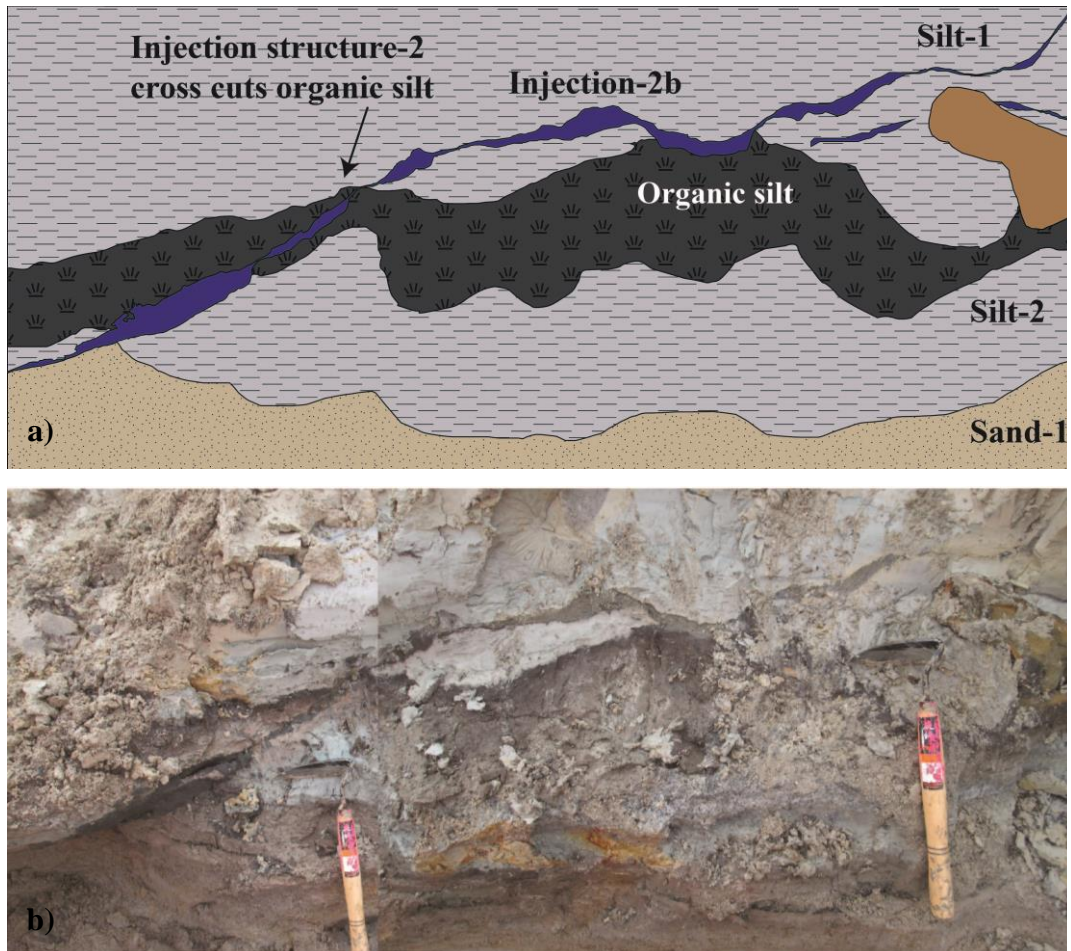


Figure 5.4: Cross-sectional view of injection structure-2 cross-cutting the organic silt layer and indicating its connection to Sand-1, providing field evidence as the source bed. (a) Schematic diagram (refer to key in Figure 5.1). (b) Field observation, cutting tool ~ 30 cm in length.

5.2.2 Particle size analysis

The deposits surrounding the injection structures, and the latter, are sampled for particle size analysis. A total of six layers are sampled (Sand-1, Silt-1, Organic silt, Silt-2, Sand-2, and Sand-3) for characterising the surrounding lithologies, whereas the injection structure is sampled in three places: one at its lateral position (Injection-2b), and two at its vertical position (Injection-1 and Injection-2a) (Figure 5.3). Cumulative grain size curves are produced to compare the injection structures and stratigraphic units (Figure 5.5). The grain size characterisation is important too, as this helps to determine the liquefaction susceptibility based on grain size compositional criteria (NZGS, 2010) and grain size regions as defined by the Ministry of Transport, Japan (MTJ, 1999).

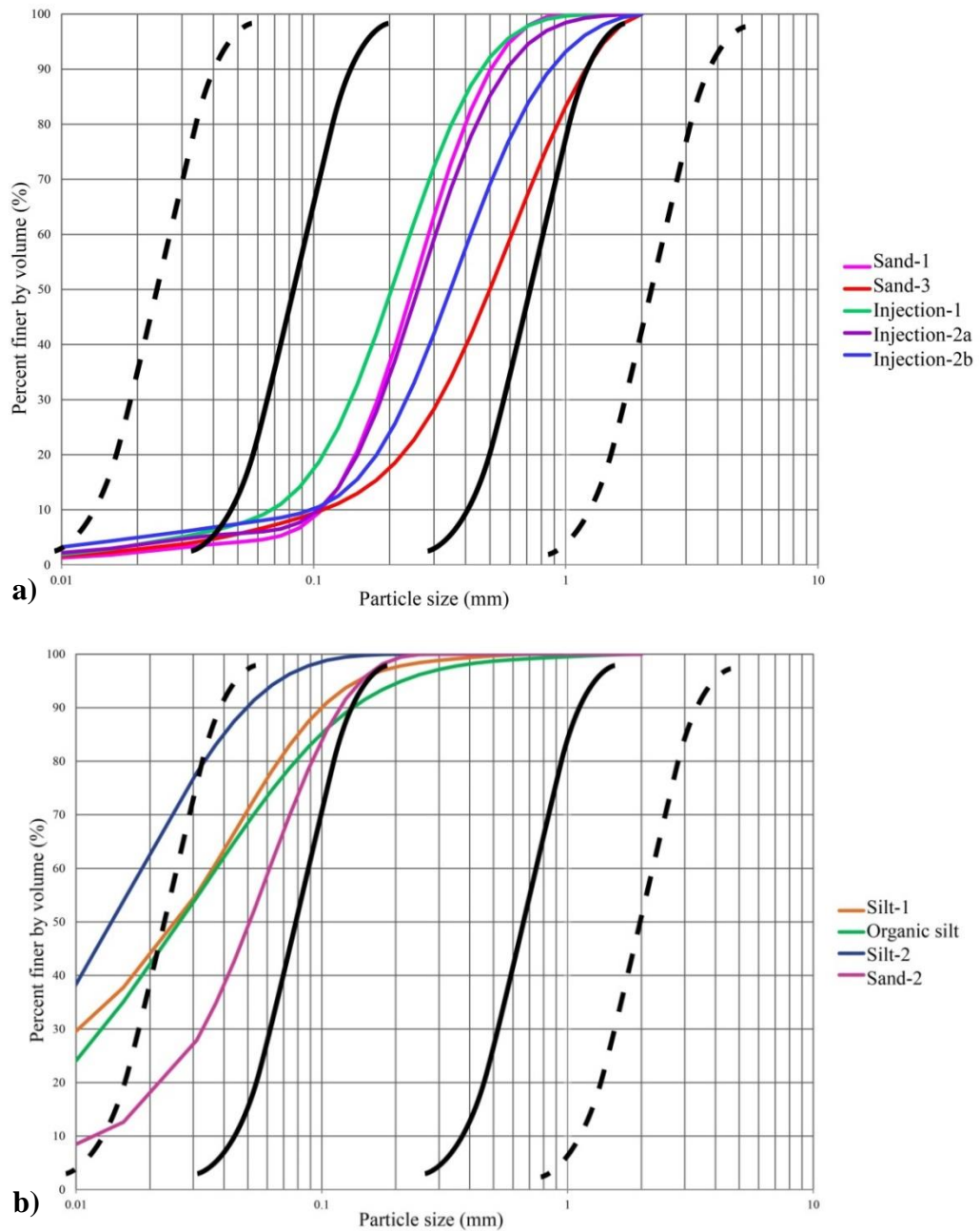


Figure 5.5: Cumulative plots of particle size at Quarry on Aspin Road for (a) stratigraphic units: Sand-1, Sand-3, Injection-1, Injection-2a and Injection-2b; and (b) stratigraphic units: Silt-1, Organic silt, Silt-2 and Sand-2. Bold inner boundaries define a high possibility of liquefaction occurring and outer dotted boundary define a possibility of liquefaction occurring (boundaries reproduced by NZGS (2010) modified from MTJ (1999)).

5.2.2.1 Statistical parameters

Statistical measures of mode, mean, sorting, skewness and kurtosis are presented in Table 5-1. In general, the most frequently occurring particle size (mode) and the average particle size (mean) are very similar, except for Sand-3, Silt-1 and Injection-2b where the mode is more than 10% less than the mean. (Note samples names in Table 5-1 are given during field observations and particle sizes determined by the laser sizer provides a more accurate measurement, therefore, sample name and laser sizer results may not be identical.) The sorting class for all lithological units is poorly sorted, and skewness shows results of mostly fine-skewed particle size distribution (finer sediments dominant over coarser sediments), except for Organic silt and Silt-2, which present near-symmetrical distributions (equal amounts of fine and coarse sediments). A mixture of kurtosis results is evident for the surrounding lithologies. For instance, Sand-3 and Sand-2 are leptokurtic (excessively peaked), Silt-2, Organic silt and Sand-1 are mesokurtic (normally peaked), and Silt-1 is platykurtic (deficiently peaked, flat distribution curve). The injection structures all show leptokurtic characteristics. Transportation is evident in field observations from Sand-1 (source) to Injection-2b, Injection-2a and furthest from the source at Injection-1. The mean grain size and kurtosis characteristics of this pathway indicate that the injection structures have selectively deposited coarser materials (at Injection-2b location) and finer grains are transported further within the sequence (finest at Injection-1).

Table 5-1: Mode, mean, sorting, skewness and kurtosis of the lithologies surrounding the injection structures (organised according to stratigraphic sequence) and of the injection structures (samples organised from source bed to loss in sequence) at Quarry on Aspin Road. Measurements of particle size are determined using Udden-Wentworth scale, values in phi units (ϕ) unless stated.

Sample	Mode (ϕ)	Mean (ϕ)	Sorting (ϕ)	Skewness (ϕ)	Kurtosis (ϕ)
Sand-3	0.63	1.14 (0.45mm)	1.38	0.28	1.27
	Coarse sand	Medium sand	Poorly sorted	Fine-skewed	Leptokurtic
Sand-2	4.36	4.43 (0.05mm)	1.29	0.25	1.22
	Coarse silt	Coarse silt	Poorly sorted	Fine-skewed	Leptokurtic
Silt-2	6.13	6.19 (0.01mm)	1.5	0.07	0.92
	Fine silt	Fine silt	Poorly sorted	Near-symmetrical	Mesokurtic
Organic silt	5.13	5.25 (0.03mm)	1.87	0.05	0.99
	Coarse silt	Medium silt	Poorly sorted	Near-symmetrical	Mesokurtic
Silt-1	4.36	5.53 (0.02mm)	1.91	0.22	0.86
	Coarse silt	Medium silt	Poorly sorted	Fine-skewed	Platykurtic
Sand-1	1.88	2.05 (0.24mm)	0.9	0.11	1.09
	Medium sand	Fine to medium sand	Moderately to poorly sorted	Fine-skewed	Mesokurtic*
Injection-2b	1.38	1.56 (0.34mm)	1.42	0.26	1.58
	Medium sand	Medium sand	Poorly sorted	Fine-skewed	Very leptokurtic
Injection-2a	1.88	1.97 (0.26mm)	1.14	0.18	1.43
	Medium sand	Fine to medium sand	Poorly sorted	Fine-skewed	Leptokurtic
Injection-1	2.13	2.35 (0.20mm)	1.16	0.19	1.31
	Fine sand	Fine sand	Poorly sorted	Fine-skewed	Leptokurtic

5.2.3 Radiocarbon dating

The ages obtained at site 15 (Quarry on Aspin Road) provide an estimated age of deposition of the materials, and hence pre-date the liquefaction structures through the principle of cross-cutting relationships. Samples of the organic silt bed are collected at three locations (NZTM2000: 5805808, 1820765; 5805822, 1820754; 5805825, 1820746) as quarry works progressed, and the injection structures are excavated out. However, the same organic silt layer is identified as an essentially continuous unit (consistent with findings of Pryce, (1997)). The silt proportion is therefore dated as large wood fragments and are no longer evident. Ages from the three samples are identical (Table 5-2), and thus a seismic event occurred sometime after c. $20,749 \pm 204$ calendar yr BP, the mean age (± 2 sd, $n = 3$) of the three Quarry on Aspin Road samples. The three ages (Wk39953 to Wk39955) are combined using the R_combine function of OxCal v4.2.4 (Bronk Ramsey, 2001), and the SHCal13 calibration dataset (Hogg *et al.*, 2013).

Table 5-2: Radiocarbon dates for organic silt at site 15.

Lab sample number*	Material type	Radiocarbon age [§] (¹⁴ C yr BP \pm 1 sd)	Calibrated age (calendar yr BP, 94.5 % probability range)
Wk39953	Organic silt	17,278 \pm 105	20,801 \pm 301
Wk39954	Organic silt	17,294 \pm 85	20,813 \pm 258
Wk39955	Organic silt	17,158 \pm 94	20,655 \pm 280

*Wk, University of Waikato Radiocarbon Dating Laboratory number

§ Conventional radiocarbon age (uncalibrated)

5.2.4 Liquefaction assessment

Two piezocone penetration tests (CPTu) are conducted at site 15 (Quarry on Aspin Road). The first containing the same stratigraphic sequence to where the injection structures had been located (CPTu-1). At the time of *in situ* testing active quarry works had excavated the section out. This test is below the present-day quarry floor. While the second is located on an upper bench attempting to incorporate the stratigraphic units below the pre-excavated surface (CPTu-2) (Figure 5.6).

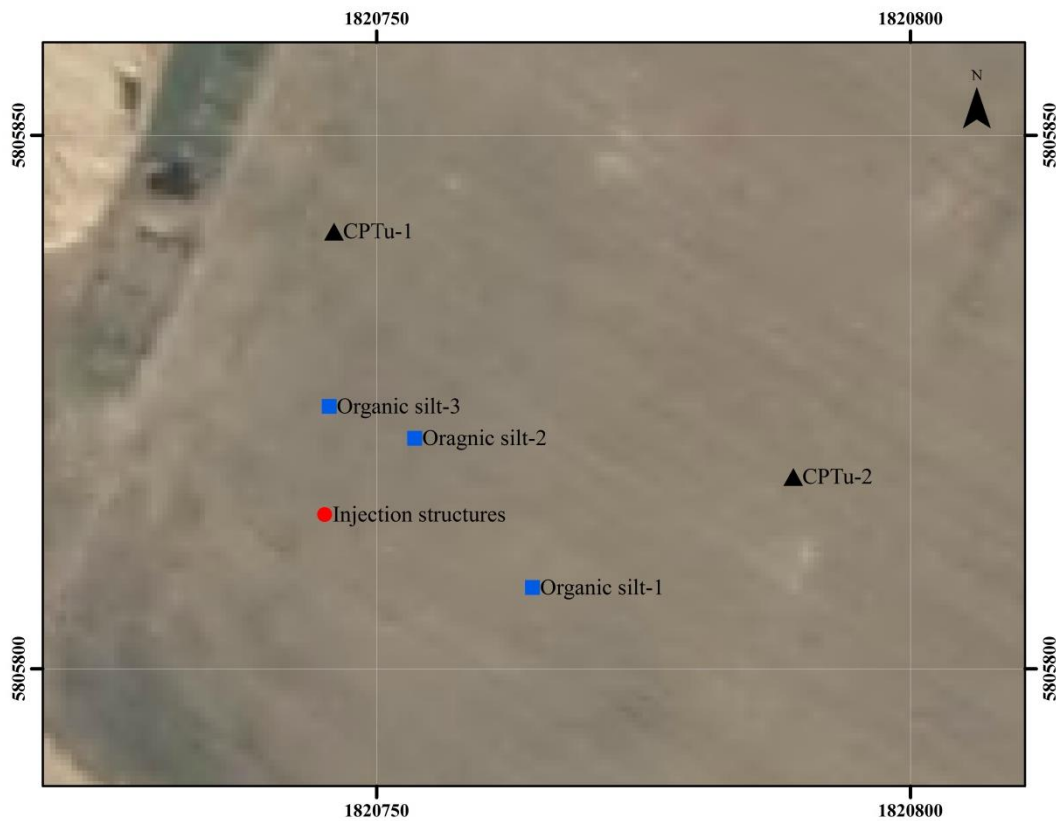


Figure 5.6: Site location of injection structures, CPTus, and radiocarbon samples of organic silt location for Quarry on Aspin Road.

Basic plots for CPTu-1 present mostly high cone resistances, low friction ratio percentages and pore water pressures that follow hydrostatic conditions (Figure 5.7a). High cone resistance values of 8 to 14 MPa are at depths 0 to 0.5 m, 1.8 to 5.7 m, 5.9 to 11.3 m and 11.9 to 15.4 m. Friction ratio plots display low percentages throughout, except for depths at 1.5 m, 5.7 m and from 15.5 m. This is because measurements increase to 3%. Generally, pore water pressures follow hydrostatic conditions, but peak at depths identical to friction ratio results, namely at 1.5 m, 5.7 m and after 15.5 m. CPTu-2 basic plots in general also show high cone resistance, low friction ratios and hydrostatic pore water pressures (Figure 5.7b) High cone resistance values are located in three sections: 1.7 to 2.5 m at approximately 4 MPa; 3.6 to 6.0 m at 8 to 12 MPa; and 7.5 to 13 m at 10 to 14 MPa. Friction ratio is usually low but peaks at depths 1.2 m, 3.0 m, 6.9 m and rapidly increases beyond 13.5 m. Pore water pressure only increases above hydrostatic values at 3 m and below 13.5 m.

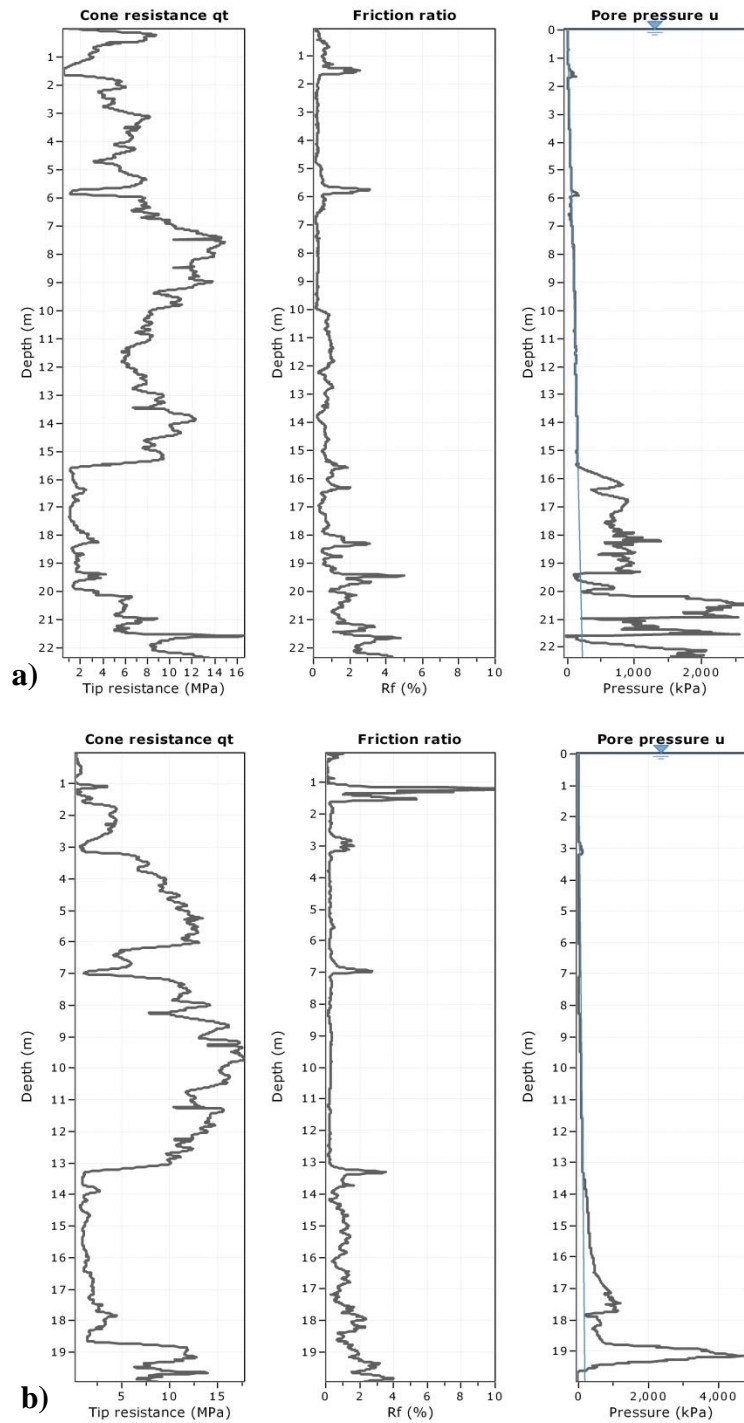


Figure 5.7: Plots exported from CPeT-IT presenting corrected cone resistance (q_t), friction ratio (R_f) and pore water pressure (u_2) at the Quarry on Aspin Road. (a) CPTu-1. (b) CPTu-2.

Site subsoil class for the Quarry on Aspin Road is determined as “Class D” according to NZS1170.5 (Standards New Zealand, 2004). Estimated parameter plots of shear strength exclude cohesionless soils and, where there are cohesive soils, shear strength is generally less than 200 kPa (Figure 5.8). From field observation the material at site 15 is classed as loose dry. Both soils are inferred to exceed depths

of 60 m or more for stiff to very stiff cohesive soils and 40 m for loose dry cohesionless soils (see Table 3-2 from NZS1170.5: Standards New Zealand, 2004); consistent with the Hinuera Formation containing a thickness of up to 90 m (Edbrooke, 2005). Where thicknesses are less than 90 m, the underlying soils consist of the Walton subgroup which is an older, more weathered fluvial deposit.

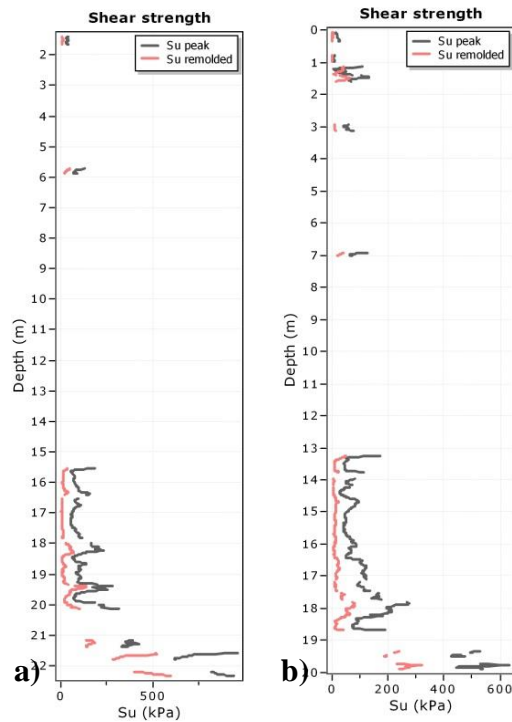


Figure 5.8: Depth versus shear strength plots exported from CPeT-IT for a) CPTu-1 and b) CPTu-2 at the Quarry on Aspin Road.

5.2.4.1 Soil behaviour type (SBT) plots

Stratigraphic unit Sand-1 is identified as the liquefied bed in field observations, and occurs approximately 1.5 m below the present quarry floor. The non-normalised SBT plot for CPTu-1 (Figure 5.9a) classes Sand-1 as “Sand and silty sand” at depths between of 1.73 to 5.64 m (3.91 m thick). CPTu-2 also classes Sand-1 as “Sand and silty sand” between depths of 3.19 to 6.81 m (3.62 m) (Figure 5.9b) and there are also many similar units below Sand-1. In the uppermost metre a “sensitive fine grained” material is recognised for CPTu-2, but this class relates to artificial reworked material that is used to construct a temporary path. See appendix 3 for normalised soil behaviour (SBTn) plots.

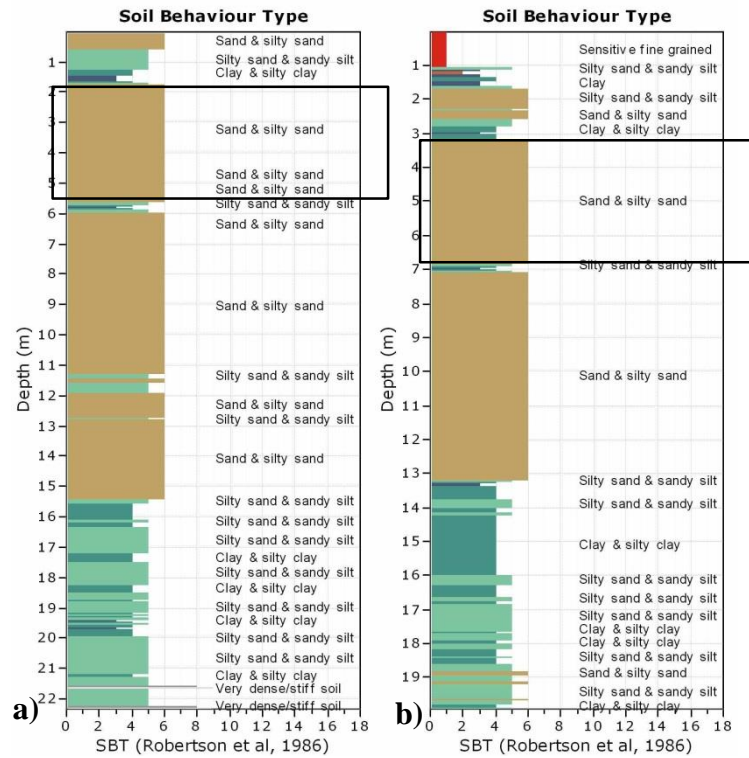


Figure 5.9: Non-normalised soil behaviour type plots for a) CPTu-1 and b) CPTu-2 at the Quarry on Aspin Road. Bold black box indicates critical layers for each CPTu test. Depths defining critical layer for CPTu-1: 1.73 to 5.64 m and CPTu-2: 3.19 to 6.81m.

5.2.4.2 Cyclic liquefaction plots

CSR and CRR plots are conducted and analysed for each annual probability of exceedance (SLS, ULS and MCE). See appendix 3b for all cyclic liquefaction plots. The liquefaction assessment primarily focusses on graphs produced from the predicted ULS (1 in 500 year return period), as no liquefaction is predicted to occur for a SLS earthquake event (appendix 3bi) and for MCE almost all soils are predicted to liquefy (appendix 3biii). MCE is clearly a much bigger earthquake event in comparison to ULS. Hence I came to the conclusion of focussing on the ULS, as a substantial amount of the liquefaction is already predicted to occur on a 1 in 500 year return period event.

5.2.4.2.1 Idriss and Boulanger (2008)

Applying the Idriss and Boulanger (2008) calculation method to a ULS event presents a factor of safety less than 1 at depths from 1.66 to 5.73 m for CPTu-1 and

3.13 to 3.84 m for CPTu-2 (Figure 5.10). Both are unsafe (i.e., liquefaction will occur) in terms of factor of safety, starting slightly above the defined critical layer, meaning layers above the defined critical are predicted to liquefy. For CPTu-1 liquefaction of the entire sand bed is predicted, but for CPTu-2 only the top 66 cm and the bottom 65 cm are predicted to liquefy. At the depth of the critical layer, LPI is located in the high risk zone for both CPTu-1 and CPTu-2. LPI is constantly increasing with depth for CPTu-1, while for the majority of CPTu-2, LPI values are not increasing with depth, thus predicting no liquefaction.

5.2.4.2.2 Boulanger and Idriss (2014)

Implementing calculation methods by Boulanger and Idriss (2014) increases the CSR, therefore increasing liquefaction susceptibility. The depths at which liquefaction is predicted to occur are nearly identical for both CPTu-1 and CPTu-2, but there is a noticeable shift towards the red zone for the factor of safety and LPI plots (Figure 5.11).

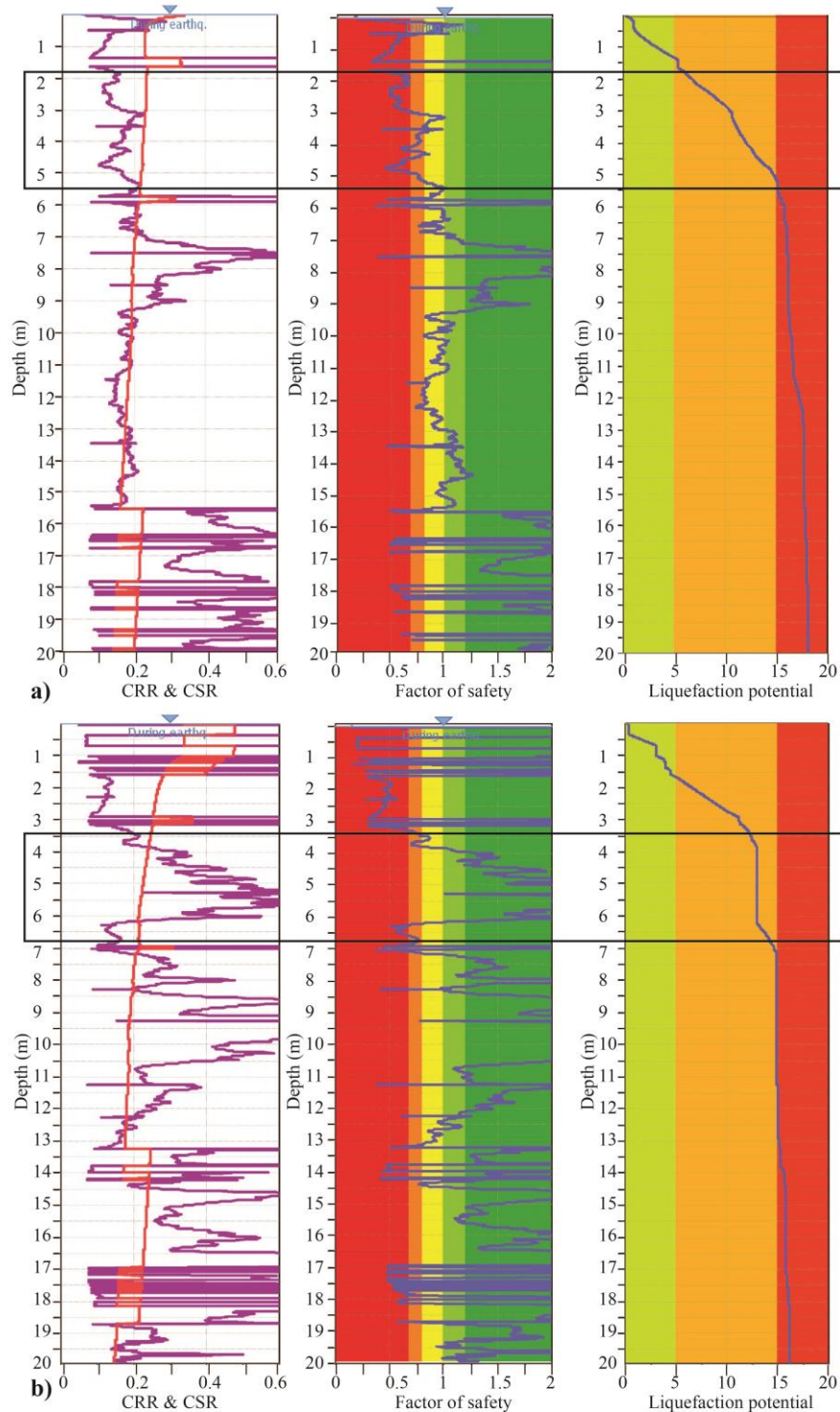


Figure 5.10: ULS (1 in 500 year return period) cyclic liquefaction plots at the Quarry on Aspin Road, imported from CLiq (GeoLogismiki, 2006). (a) CPTu-1 and (b) CPTu-2. Liquefaction parameters: M_{eff} 5.9, ground water table 0 m and PGA 0.25, calculation method Idriss and Boulanger (2008), bold black box defining critical layer. CRR and CSR plot: red line is the CSR, purple line is CRR. LPI plot: green zone is “low risk”, orange zone is “high risk” and red zone is “very high risk” of liquefaction occurring.

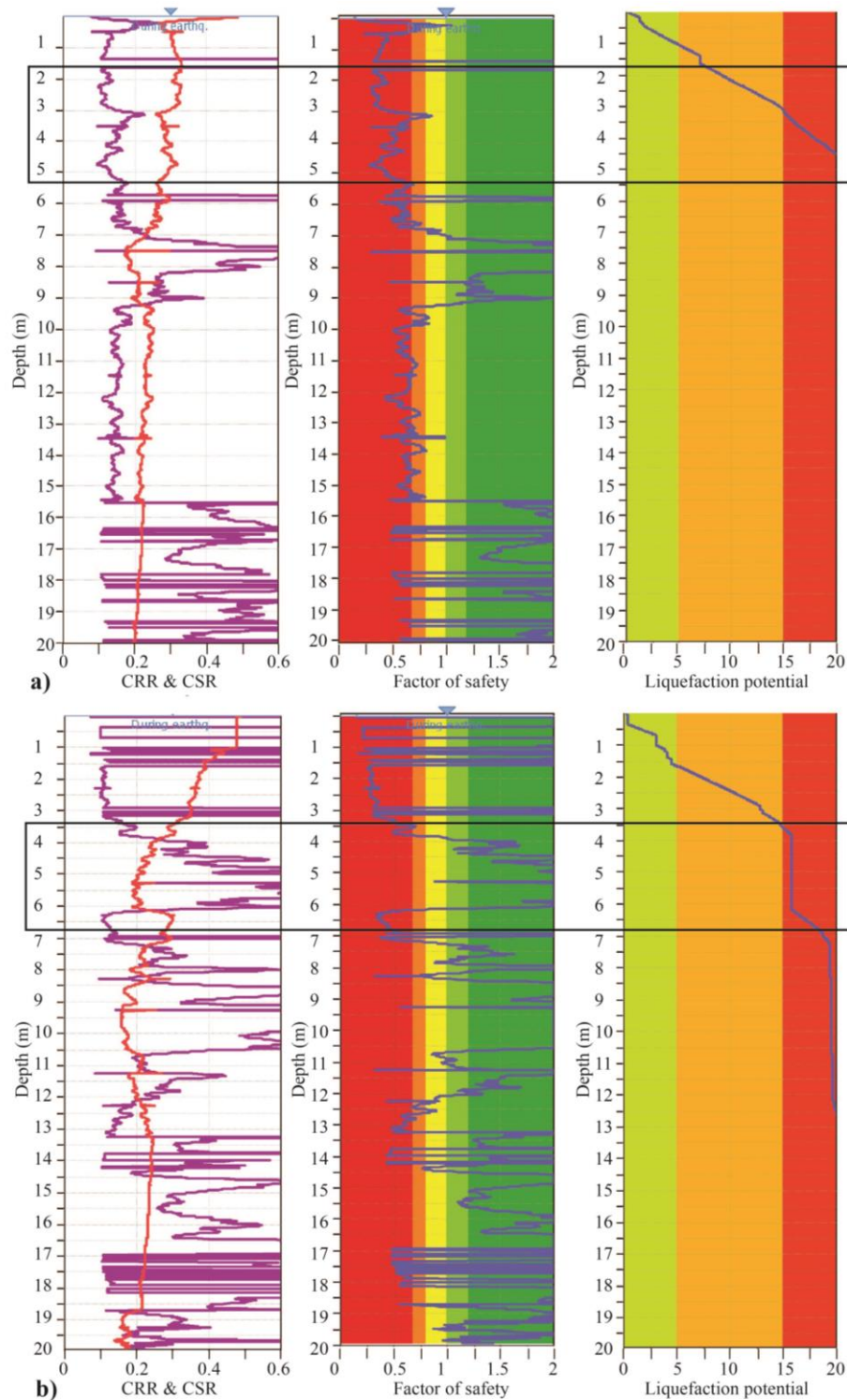


Figure 5.11: ULS (1 in 500 year return period) cyclic liquefaction plots at the Quarry on Aspin Road, imported from CLiq (GeoLogismiki, 2006). a) CPTu-1 and b) CPTu-2. Liquefaction parameters: M_{eff} 5.9, ground water table 0 m and PGA 0.25, calculation method Boulanger and Idriss (2014), bold black box defining critical layer. CRR plot: red line is the CSR, purple line is CRR. LPI plot: green zone is “low risk”, orange zone is “high risk” and red zone is “very high risk” of liquefaction occurring.

5.2.4.3 Triggering earthquake (minimum PGA)

The minimum PGA required to liquefy soils within the critical layer is approximated by inspection and summarised in Table 5-3. Parametric graphs portray calculated PGA for settlements, LPI and LSN using both calculation methods (Idriss & Boulanger 2008; Boulanger & Idriss 2014). Values of settlements, LPI and LSN for CPTu-1 and CPTu-2 are averaged for each probability of exceedance of the design earthquake SLS, ULS and MCE and for minimum PGA (M. PGA). See appendix 3 for how M. PGA is derived.

Table 5-3: Summary of minimum PGA results for site 15.

Calculation method	CPT	Minimum PGA (g)
Idriss and Boulanger (2008)	CPTu-1	0.16
	CPTu-2	0.21
	Average	0.19
Boulanger and Idriss (2014)	CPTu-1	0.06
	CPTu-2	0.10
	Average	0.13

5.2.4.3.1 Idriss and Boulanger (2008)

Parametric graphs for calculation method Idriss and Boulanger (2008) are presented in Figure 5.12. The data for CPTu-2 predicts more settlement below the threshold PGA, and beyond 0.19 g, CPTu-1 predicts considerably greater settlement. Liquefaction parameters for both CPTu are presented in (Table 5-4). Average predicted settlements become for the estimated minimum PGA. LPI is high for CPTu-2 until PGA reaches 0.23 g, where CPTu-1 has a much greater liquefaction potential. Overall, LPI presents low risk values for SLS, high risk for minimum PGA and very high risk for ULS and MCE. LSN values predicted by CLiq are all greater than 140 for the SLS earthquake event or greater (Figure 5.12c) indicating severe expression of liquefaction. This is not consistent with observation. Recalculating the LSN value using equation (3-3) gives the values shown in Table 5-4. These indicate minor expression for SLS and M.PGA and moderate expression of liquefaction for ULS and MCE earthquake events. It would appear that the algorithm in CLiq is producing a result one order of magnitude above those defined by Tonkin and Taylor (2013).

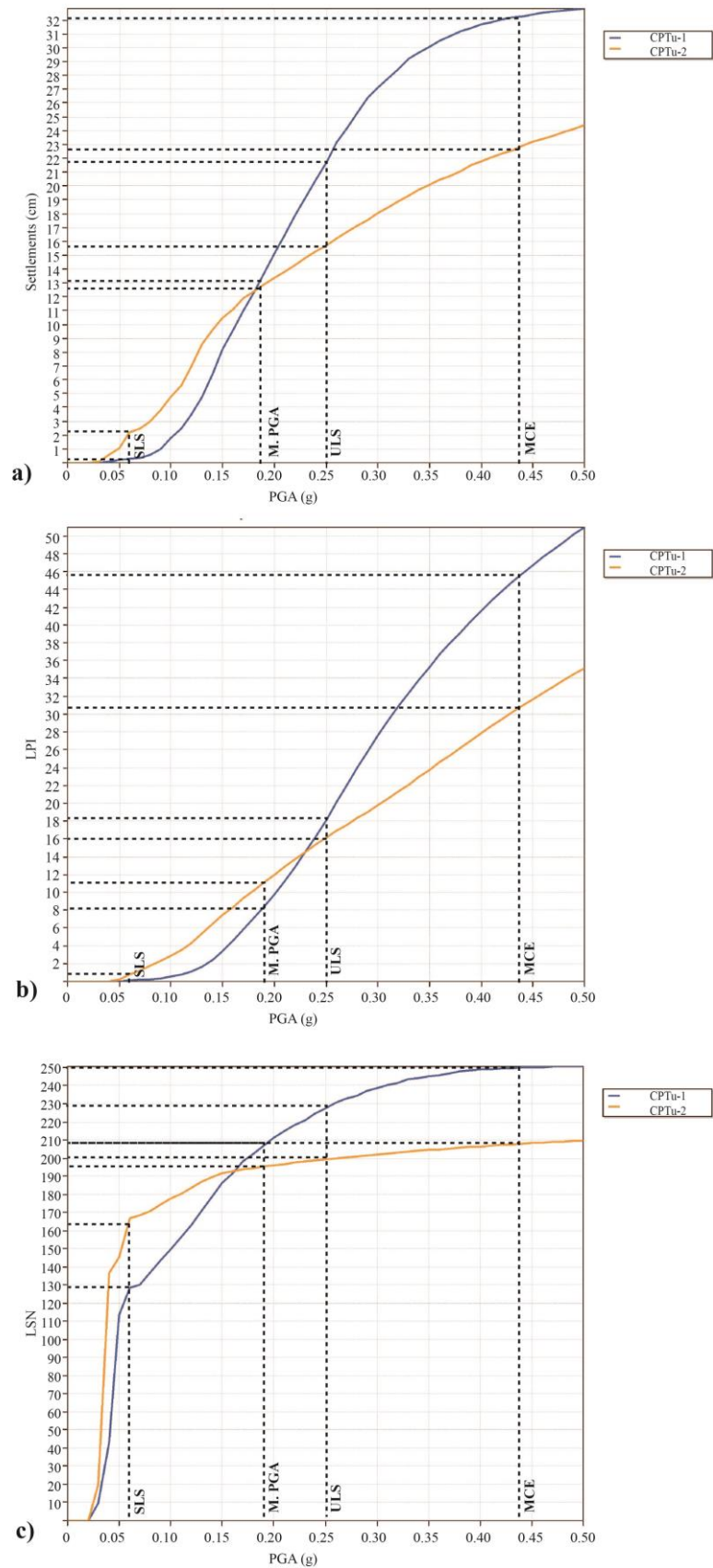


Figure 5.12: Parametric graphs of PGA calculated for (a) settlement, (b) LPI and (c) LSN using calculation method Idriss and Boulanger (2008) for site 15.

Table 5-4: Calculated liquefaction parameters for site 15 using Idriss and Boulanger (2008).

Liquefaction parameters	Earthquake event	CPTu-1	CPTu-2	Average	Interpretation
Settlements (cm)	SLS	0.1	2.4	1.25	Minimal
	M.PGA	13.1	12.5	12.8	Significant
	ULS	21.9	15.8	18.85	Significant
	MCE	23.8	32.1	27.95	Significant
LPI	SLS	0.0	1.0	0.5	Low risk
	M.PGA	8.0	13	10.5	High risk
	ULS	18.2	16	17.1	Very high risk
	MCE	45.8	31	38.4	Very high risk
LSN	SLS	12.8	16.7	14.8	Minor
	M.PGA	20.5	18.5	19.5	Minor
	ULS	22.7	19.9	21.3	Moderate
	MCE	25.0	20.8	22.9	Moderate

5.2.4.3.2 Boulanger and Idriss (2014)

Parametric graphs for the method of calculation Boulanger and Idriss (2014) are presented in (Figure 5.13). High predicted settlement is evident for CPTu-2 until calculated PGA of 0.08 g, where CPTu-1 predicts a much higher settlement. Liquefaction parameters for both CPTu are also presented in Table 5-5. Averaged settlement values become significant after triggering earthquake (M.PGA). This calculation method shows LPI values identical to levels of risk of those from Idriss and Boulanger (2008)—that is, low risk values for SLS, high risk for minimum PGA and very high risk for ULS and MCE. All LSN values predicted by CLiq also exceed 50 (Figure 5.13), which is the boundary for severe expression of liquefaction. These values are not reasonable as liquefaction for a SLS earthquake event is not expected to occur according to the CSR and CRR plots. Manually calculated LSN results in Table 5-5, show minor expression for SLS earthquake event and moderate expression for M.PGA, ULS and MCE— these results are sensible.

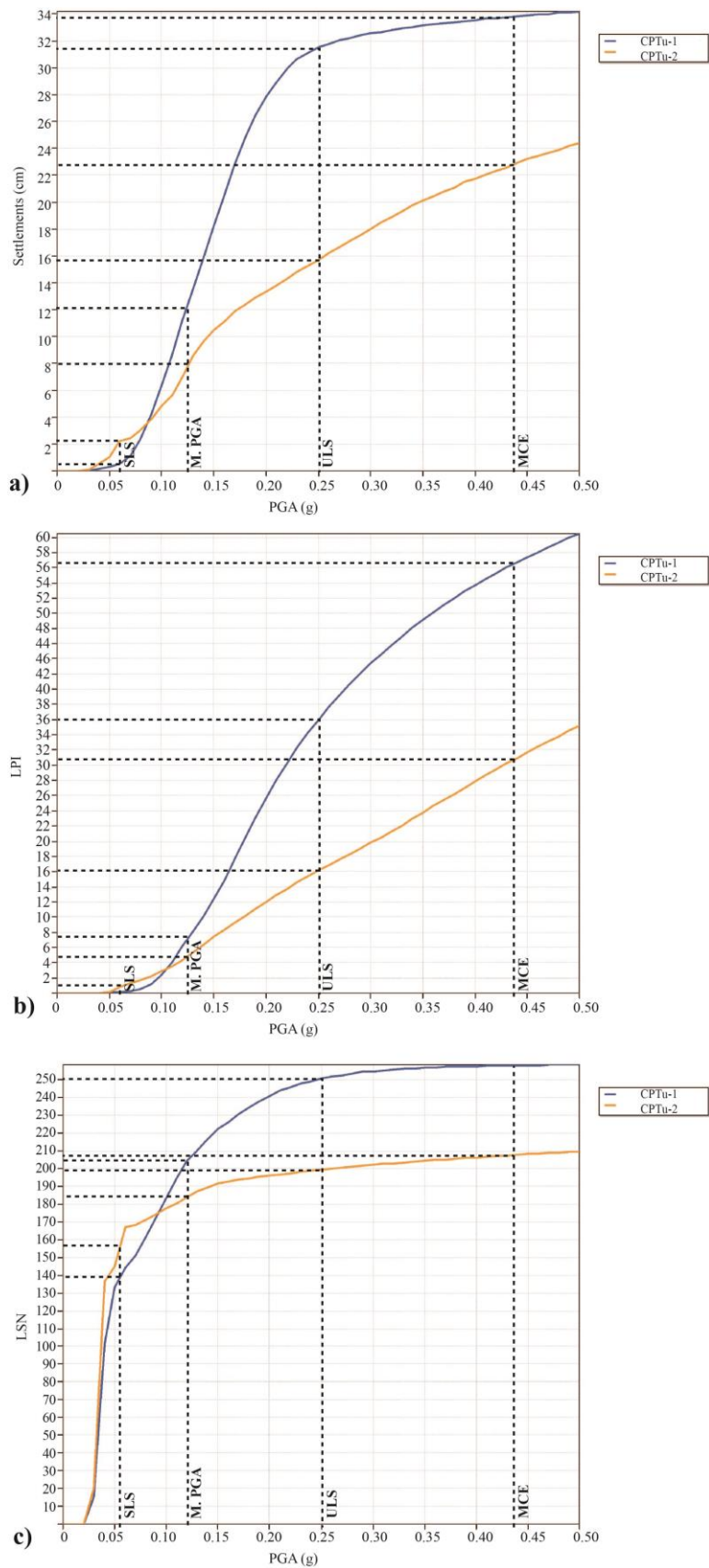


Figure 5.13: Parametric graphs of PGA verses (a) settlement, (b) LPI and (c) LSN using calculation method Boulanger and Idriss (2014) for site 15.

Table 5-5: Calculated liquefaction parameters for site 15 using Boulanger and Idriss (2014).

Liquefaction parameters	Earthquake event	CPTu-1	CPTu-2	Average	Interpretation
Settlements (cm)	SLS	0.5	2.1	1.3	Minimal
	M.PGA	12.0	8.0	10.0	Significant
	ULS	31.0	15.8	23.4	Significant
	MCE	33.8	23.0	28.4	Significant
LPI	SLS	0.0	1.0	0.5	Low risk
	M.PGA	7.5	5.0	6.3	High risk
	ULS	36.0	16.0	26.0	Very high risk
	MCE	56.8	31.0	43.9	Very high risk
LSN	SLS	14.4	15.9	15.2	Minor
	M.PGA	20.9	19.5	20.2	Moderate
	ULS	25.1	19.4	22.3	Moderate
	MCE	25.8	20.0	22.9	Moderate

5.3 Site 16 – Endeavour Primary School

5.3.1 Injection structures

Multiple liquefaction features are recognised in plan-view across the Endeavour Primary School site. Two localities containing swarms of paleoliquefaction features have been identified (localities i and ii). At both localities, a pit is excavated bisecting a paleoliquefaction feature to provide a cross-sectional view.

The pit at locality i showed an injection structure intruding through three sedimentary units: a sand, a peat, and a silt layer (Figure 5.14). This structure splays across the present excavated floor (Figure 5.14). The grey injection structure located in the 1 m-deep pit occurs at a depth of 3 m below the pre-excavated surface. The source bed could not be identified because of safety restrictions relating to pit depth.

The pit at locality ii displays grey injection structures with fine widths and often disjointed (Figure 5.16) intruding through a thick sandy-silt layer. These paleoliquefaction features are found at a depth of 3.6 m below the pre-excavated surface. The source bed and water table is identified at locality ii (see chapter 4).

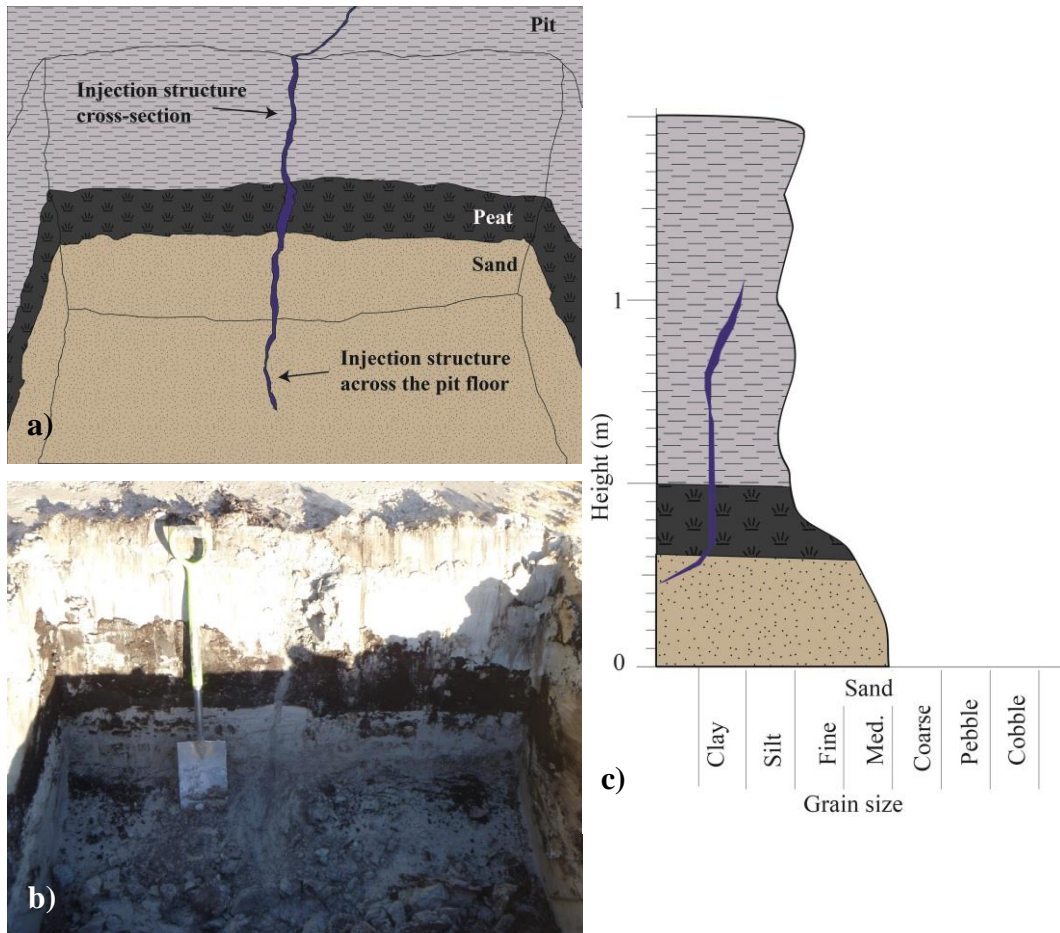


Figure 5.14: Cross-sectional view of pit at locality i, Endeavour Primary School, north Hamilton. (a) Schematic diagram of injection structure intruding through sand, peat and silt beds (see key in Figure 5.1). Dimensions: width of 3 cm, vertical height of 1.10 m and 3.30 m for the path travelled on the excavated floor (above the pit). (b) Field observation. (c) Stratigraphy of pit sequence at locality i.

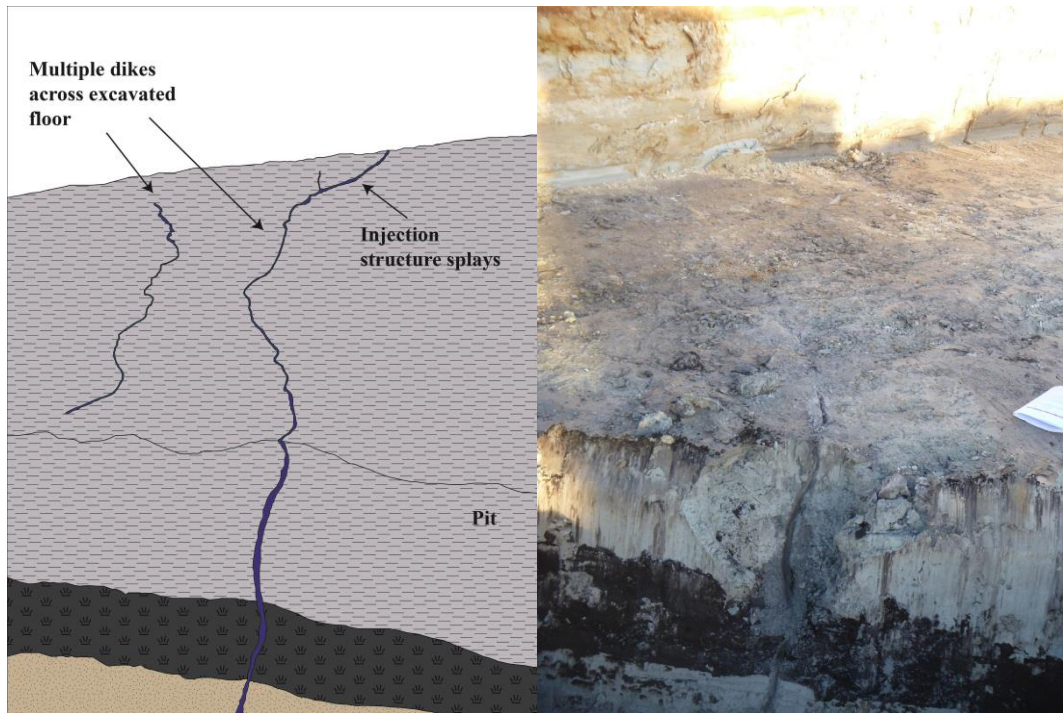


Figure 5.15: Cross-sectional view looking above pit at locality i, for Endeavour Primary School. (a) Schematic diagram of multiple paleoliquefaction features across the excavated floor, injection structure from pit splays into different directions (see key in Figure 5.1). (b) Field observation, field book ~ 30 cm in length.

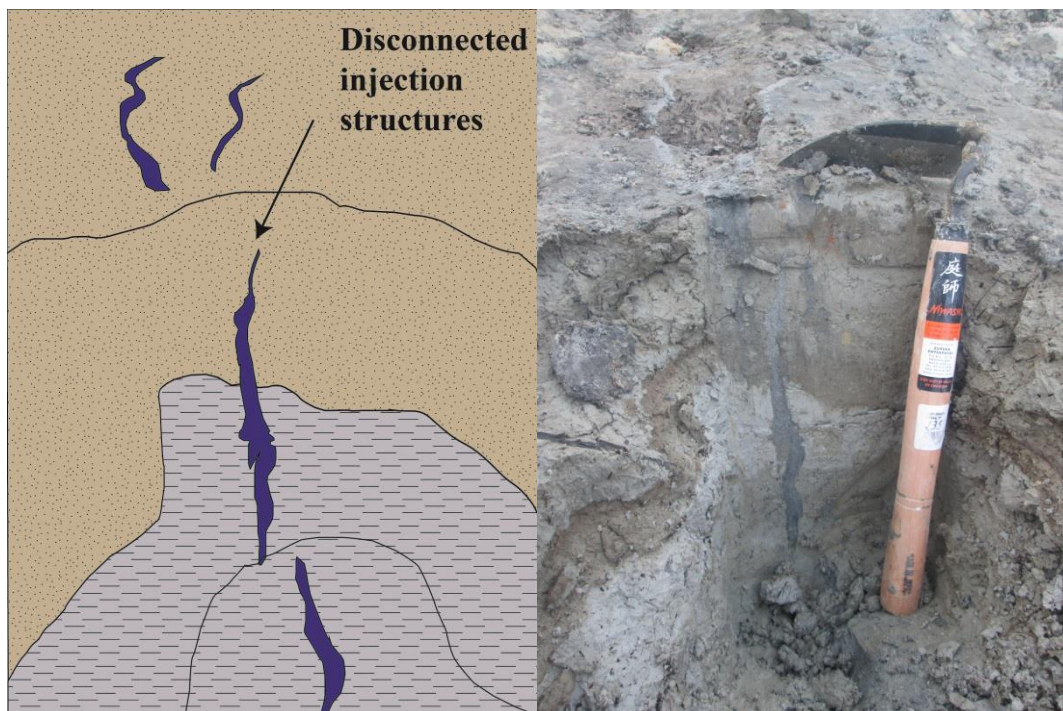


Figure 5.16: Cross-sectional view of small pit at locality ii. (a) Schematic diagram of injection structures intruding through a silt and sand layer (see key in Figure 5.1). (b) Field observations, cutting tool ~ 30 cm. Injection structures with widths of 2 cm and vertical height of 30 cm.

5.3.2 Particle size analysis

The sand layer (Sand) and the paleoliquefaction feature (Injection) are only sampled at locality i for a particle size analysis (Figure 5.17). Samples are not extracted from locality ii, as permission to analyse material from this site had not been granted. The cumulative grain size curves of both stratigraphic units, Sand and Injection, are situated within the region that suggests a high possibility of liquefaction occurring.

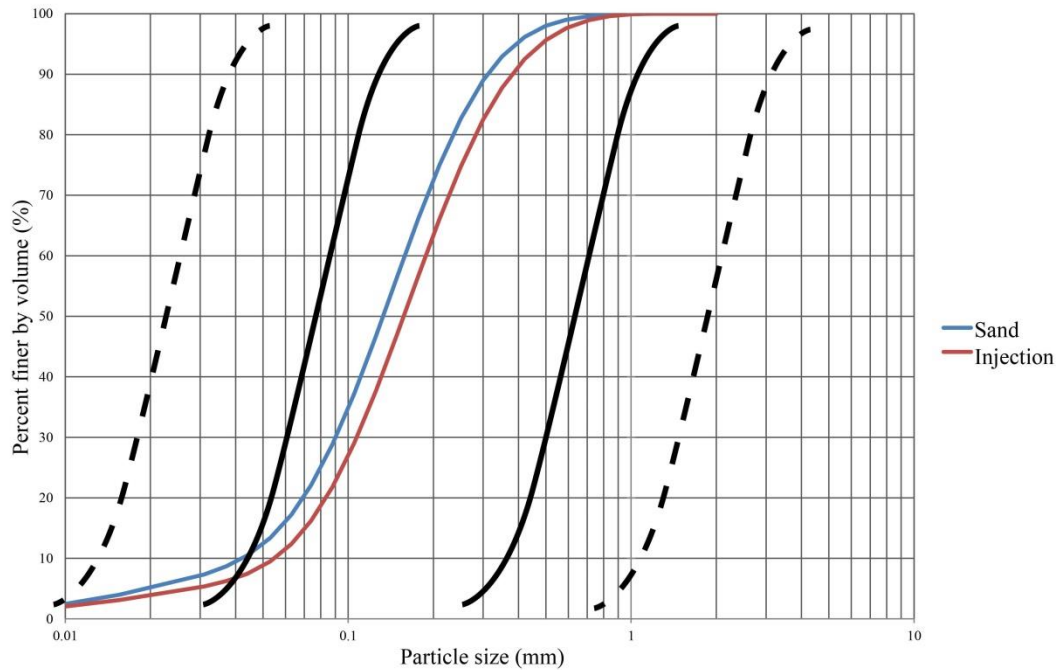


Figure 5.17: Endeavour Primary School cumulative plots of particle size analysis for stratigraphic units: Sand and Injection. Bold inner boundaries define a high possibility of liquefaction occurring and outer dotted boundary define a possibility of liquefaction occurring (boundaries reproduced by NZGS (2010) modified from MTJ (1999)).

5.3.2.1 Statistical parameters

Statistical parameters mode, mean, sorting, skewness and kurtosis for Endeavour Primary School are shown in Table 5-6. The Sand and Injection samples portray identical characteristics. Mean and mode are calculated to be fine sand, sorting is poorly sorted, skewness is dominated by fine particles (fine-skewed) and kurtosis shows excessively peaked characteristics (leptokurtic).

Table 5-6: Mode, mean, sorting, skewness and kurtosis at locality i, Endeavour Primary School. Measurements of particle size are determined using Udden-Wentworth scale, values in phi units (ϕ) unless stated.

Sample	Mode	Mean	Sorting	Skewness	Kurtosis
Sand	2.88	2.98 (0.127mm)	1.18	0.18	1.26
	Fine sand	Very fine to fine sand	Poorly sorted	Fine-skewed	Leptokurtic
Injection	2.63	2.71 (0.153mm)	1.14	0.13	1.20
	Fine sand	Fine sand	Poorly sorted	Fine-skewed	Leptokurtic

5.3.3 Radiocarbon dating

Samples are collected from the peat layer at locality i for radiocarbon dating (Table 5-7). Due to cross-cutting relationships, the peat layer pre-dates the event that caused liquefaction. Therefore the liquefaction event occurred sometime after c. 19,964 years ago. Pryce (1997) reported a ^{14}C age on a ‘paludal layer’ in Hinuera Formation sediments in north Flagstaff of $16,320 \pm 170$ ^{14}C yr BP (± 1 sd), Wk-4783 (equivalent to approximately 19,670 cal. BP ± 2 sd), which is in keeping with dates reported here.

Table 5-7: Radiocarbon date for peat material at site 16 (Endeavour Primary School).

Lab sample number*	Material type	Radiocarbon age (^{14}C yr BP ± 1 sd) [§]	Calibrated age (calendar yr BP, 94.5 % probability range) [¶]
Wk39956	Peat	16,601 \pm 58	19,964 \pm 222

*Wk, University of Waikato Radiocarbon Dating Laboratory number

[§] Conventional radiocarbon age (uncalibrated)

[¶] Based on SHCal13 calibration dataset (Hogg *et al.*, 2013).

5.3.4 Liquefaction assessment

As part of the preliminary ground investigation, six piezocone penetration tests are undertaken at Endeavour Primary School. CPTu-6 is closest to the injection structures at locality i and CPTu-3 is nearest locality ii (Figure 5.18).



Figure 5.18: Site location of injection structures and CPTus at site 16.

Generally, CPTu-6 basic plots show a combination of high and low cone resistance, low friction ratios and hydrostatic pore water pressures (Figure 5.19a). High cone resistance is evident in three sections: 3 to 8 MPa at 4.1 to 5.7 m; 7 to 11 MPa at depths 7.2 to 9.0 m; 8 to 14 MPa at depths 11.0 to 15.8 m and 8 MPa at 19 to 19.8 m. Low cone resistance values are located within the first 4 m and at depths 6.2 to 6.8 m, 9.5 to 10.9 m and 16 to 19 m. Friction ratio is usually low except in the upper 2.5 m and peaks at 10.7 m. Generally, pore water pressures match hydrostatic conditions except at 4 m, 6.4 m, 9.5 to 10.8 m and 16 to 19 m. Basic plots for CPTu-3 show a mixture of low and high cone resistance, low friction ratio percentages and pore water pressures that mostly follow hydrostatic conditions (Figure 5.19b). High cone resistance are evident in three sections: 8 to 11 MPa at 4.7 to 6.5 m; 8 to 11 MPa at depths 7.0 to 9.2 m; 9 to 12 MPa at depths 11.0 to 15.0 m; and 10 MPa at 18 to 19 m. Low cone resistance values are located within the

first 4.5 m and at depths 6.5 m, 9.3 to 11 m, 15.2 to 17.8 m and below 19 m. Friction ratio plots generally display low percentages (1.5 %) throughout, except for within the first 2 m where friction ratio is rapidly decreasing from 6 to 1% and at 3 m, peaking to 7%. Pore water pressures usually follow hydrostatic conditions, but peaks occur at depths of 6.8 m, 9.5 to 10.2 m, 10.8 m, 15.2 to 18 m and 19 to 20 m.

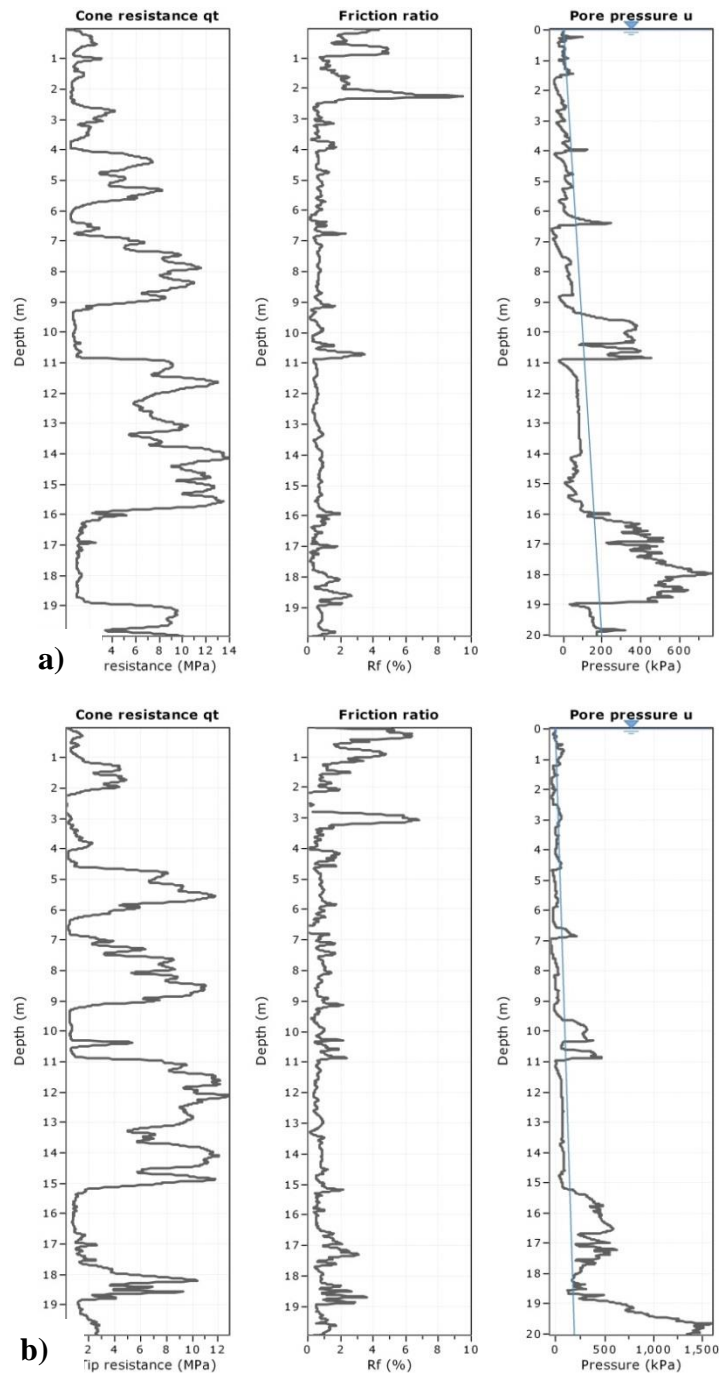


Figure 5.19: Basic plots exported from CPeT-IT presenting corrected cone resistance (q_t), friction ratio (R_f) and pore water pressure (u_2) at Endeavour Primary School. (a) Locality i- CPTu-6. (b) Locality-ii CPTu-3.

The site subsoil classification is “Class D” at Endeavour Primary School site according to surface geology and estimates of the depth to underlying rock (New Zealand Standards, 2004). Shear strength for cohesive soils is mostly less than 200 kPa which is classified as “stiff to hard” (Figure 5.20) and cohesionless soils are determined as “loose dry” from field observations. As stated previously, the Hinuera Formation can be up to 90 m in thickness, therefore exceeding depth requirements from Table 3.2 in NZ1170.5 (Standards New Zealand, 2004).

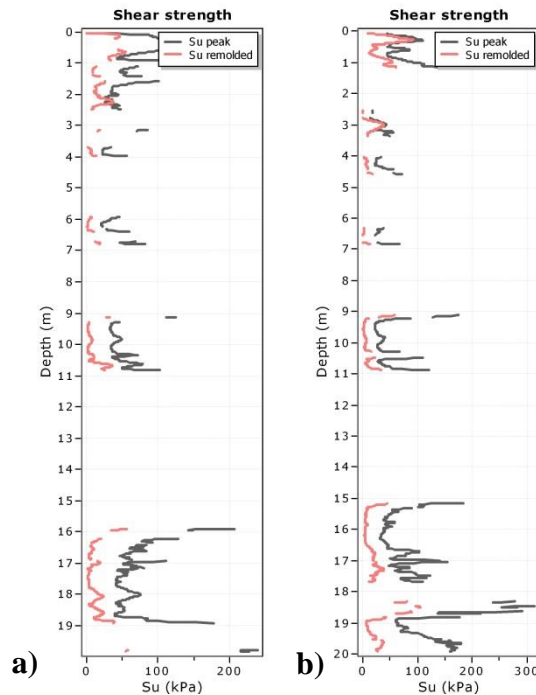


Figure 5.20: Shear strength versus depth plots for (a) CPTu-6 - locality i and (b) CPTu-3 (locality ii). Exported from CPeT-IT for Endeavour Primary School. See appendix 3 for other estimated plots.

5.3.4.1 Soil behaviour type (SBT) plots

During the site investigation at Endeavour Primary School, the source bed at locality i could not be located due to depth excavation restrictions. However, the source bed at locality ii is identified, through the principle of lateral continuity, to be the same as the source bed at locality i. Identical cumulative curves from the particle size analysis further confirm the source bed at the bottom of the pit at locality i. The critical layers for both CPTu-6 and CPTu-3 are identified using non-normalised SBT plots (Figure 5.21). CPTu-6 critical layer is defined at depths 3.00 to 3.70 m (70 cm thick) with interbedded “sand, silty sand” and “silty sand, sandy silt” material. The critical layer for CPTu-3 contains “sand, silty sand” and “silty sand, sandy silt” layers, which are defined at depths between 3.60 to 4.00 m (40 cm

thick). Note that the true depths of both critical layers are unknown and these are only best estimates, due to less control over this site. See appendix 3 for SBT plots of the other piezocone penetration tests and for the normalised SBT plots. (Note that CPTu raw data for Endeavour Primary School cannot be provided as they are provided only on a temporary basis.)

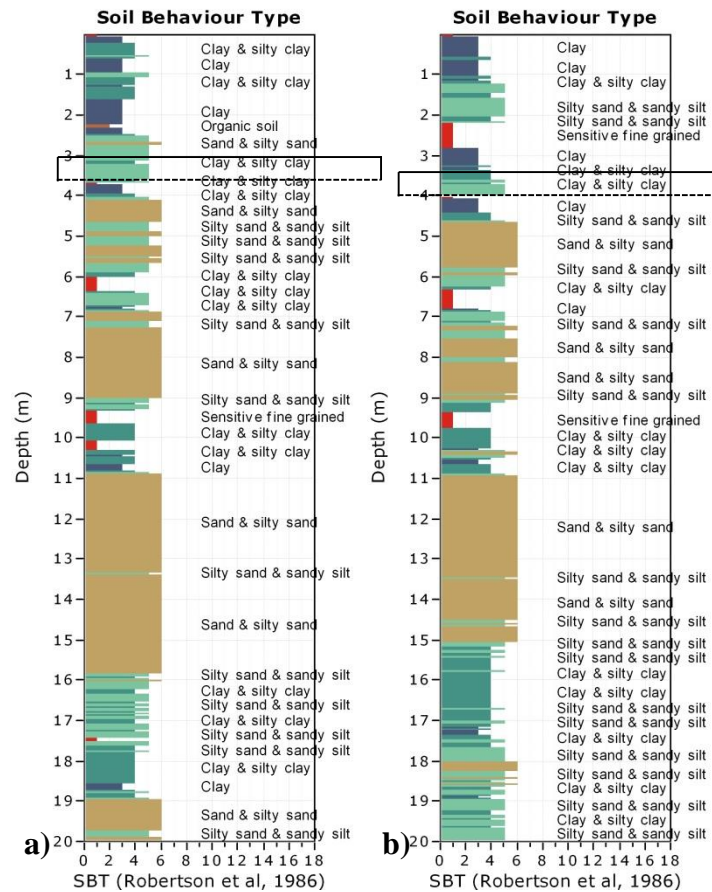


Figure 5.21: Soil behaviour type plots for locality i, CPTu-6 (left) and locality ii, CPTu-3 (right) at Endeavour Primary School. Bold black box indicates critical layers for each CPTu test. Depths defining critical layer for CPTu-6: 3.00 to 3.70 m and CPTu-3: 3.60 to 4.00 m.

5.3.4.2 Cyclic liquefaction plots

Endeavour Primary School CSR and CRR plots of ULS annual probability of exceedance are predominantly focussed on, as the SLS earthquake event predicted no liquefaction. The MCE event, like the ULS, also predicted liquefaction occurring within the entire stratigraphic sequence. Therefore, ULS is considered best suited for the liquefaction assessment as a significant amount of liquefaction is predicted to occur. See appendix 3b for cyclic liquefaction plots of all annual probabilities of exceedance (SLS, ULS and MCE).

5.3.4.2.1 Idriss and Boulanger (2008)

Implementing the calculation methods from Idriss and Boulanger (2008), showed that liquefaction would occur within the critical layers of CPTu-6 and CPTu-3 (Figure 5.22). CPTu-6 predicted liquefaction depths 2.50 to 3.14 m and 3.18 to 3.70 m, therefore liquefying the top 16 cm and lowermost 52 cm of the critical layer. For CPTu-3 data, liquefaction occurs at the upper and lower boundary of the defined critical layer, at depths between 3.45 to 4.04 m therefore liquefying the entire critical layer. LPI is within the region of high risk of liquefaction occurring for both CPTu-6 and CPTu-3.

5.3.4.2.2 Boulanger and Idriss (2014)

Boulanger and Idriss (2014) calculation methods are applied, and they demonstrate the same depths and increased amounts of predicted liquefaction for CPTu-3 and CPTu-6 (Figure 5.23). For CPTu-6, the upper 16 cm and lower 52 cm of the critical layer are predicted to liquefy, and the factor of safety became less than 1 at depths 2.50 to 3.14 m and 3.18 to 3.70 m. For CPTu-3, the entire critical layer is predicted to liquefy for depths from 3.45 to 4.04 m where the factor of safety became less than 1. LPI for both CPTu plots showed a considerable shift towards the higher values within the high risk zone.

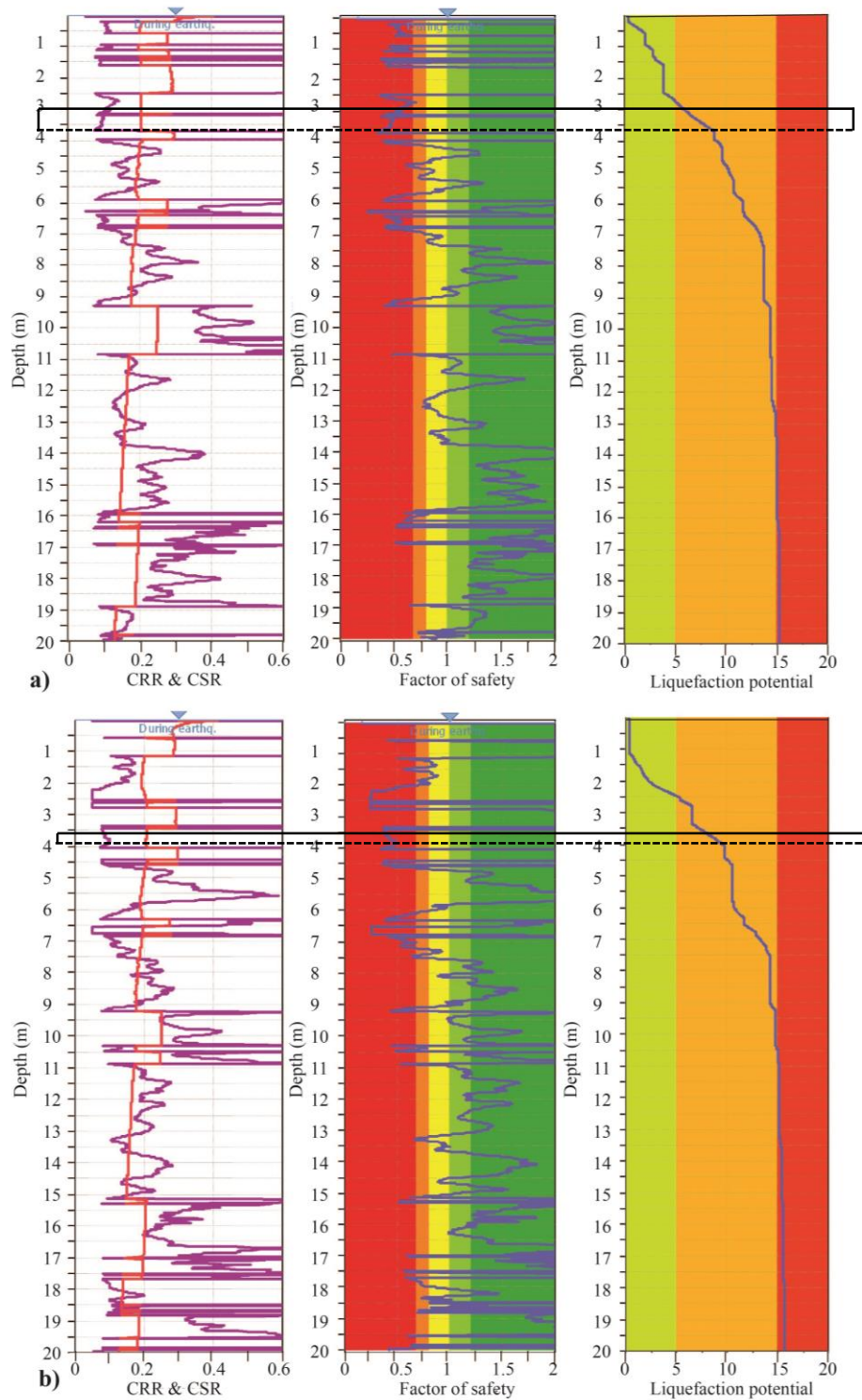


Figure 5.22: ULS (1 in 500 year return period) cyclic liquefaction plots at Endeavour Primary School, imported from CLiq (GeoLogismiki, 2006). (a) CPTu-6 and (b) CPTu-3. Liquefaction parameters: M_{eff} 5.9, ground water table 0 m and PGA 0.22, calculation method Idriss and Boulanger (2008), bold black box defining critical layer. CRR plot: red line is the CSR, purple line is CRR. LPI plot: green zone is “low risk”, orange zone is “high risk” and red zone is “very high risk” of liquefaction occurring.

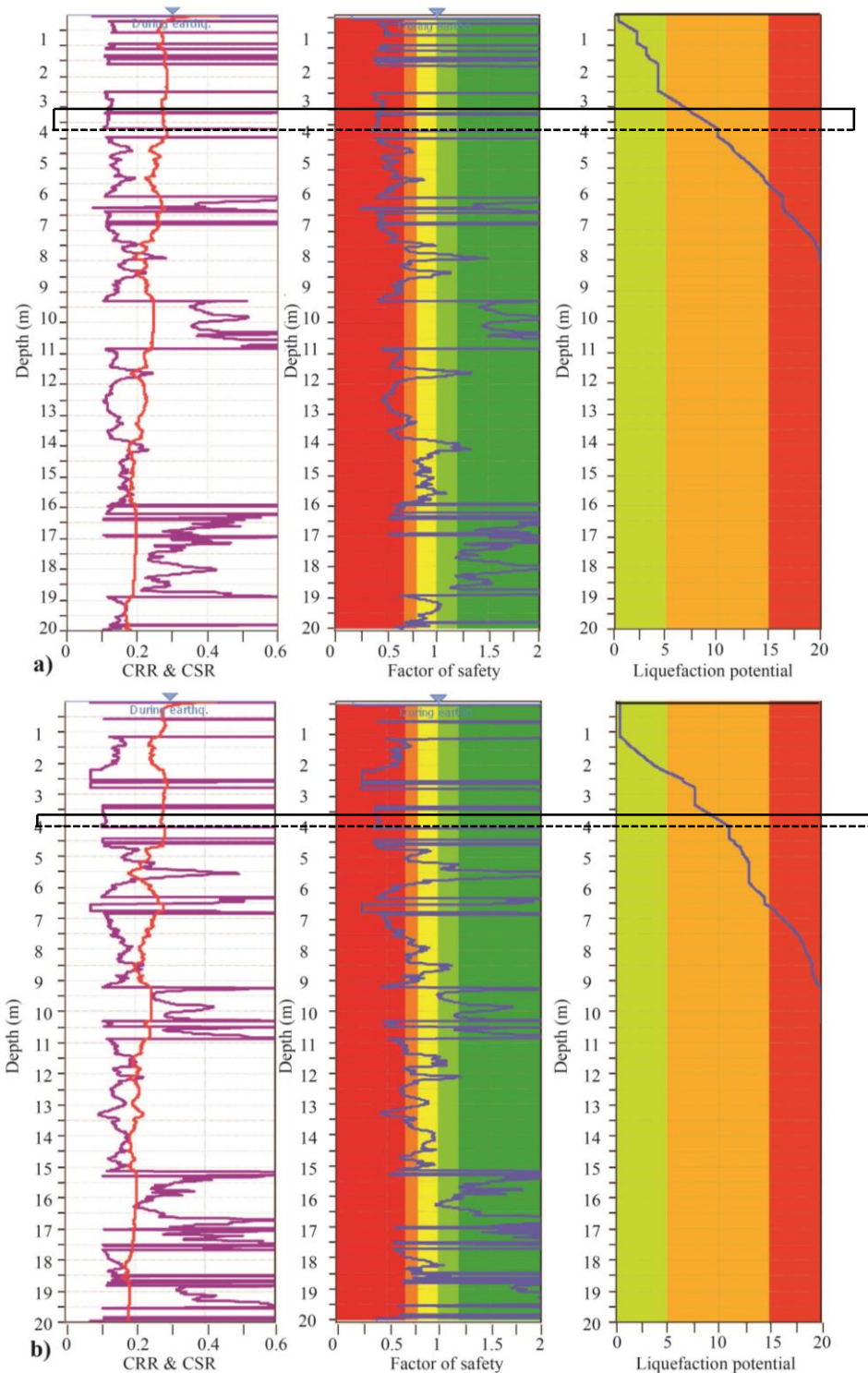


Figure 5.23: ULS (1 in 500 year return period) cyclic liquefaction plots at Endeavour Primary School, imported from CLiq (GeoLogismiki, 2006). (a) CPTu-6 and (b) CPTu-3. Liquefaction parameters: M_{eff} 5.9, ground water table 0 m and PGA 0.22, calculation method Boulanger and Idriss (2014), bold black box defining critical layer. CRR plot: red line is the CSR, purple line is CRR. LPI plot: green zone is “low risk”, orange zone is “high risk” and red zone is “very high risk” of liquefaction occurring.

5.3.4.3 Triggering earthquake (minimum PGA)

The minimum PGA required to liquefy soils within the critical layer is approximated by trial-and-error, and results are summarised in Table 5-8. Parametric graphs portray predicted settlements, LPI and LSN and are compared to PGA using both calculation methods (Idriss & Boulanger 2008; Boulanger & Idriss 2014). Values of settlements, LPI and LSN for CPTu-6 and CPTu-3 are averaged for each probability of exceedance of the design earthquake SLS, ULS, MCE and for minimum PGA.

Table 5-8: Summary of minimum PGA results for site 16

Calculation method	CPT	Minimum PGA
Idriss and Boulanger (2008)	CPTu-6	0.17
	CPTu-3	0.20
	Average	0.19
Boulanger and Idriss (2014)	CPTu-6	0.14
	CPTu-3	0.17
	Average	0.16

5.3.4.3.1 Idriss and Boulanger (2008)

Parametric graphs from the calculation method of Idriss and Boulanger (2008) are presented in Figure 5.24. Calculated liquefaction parameters for both CPTu are presented in Table 5-9. Settlement values show significant effects after calculated triggering earthquake. LPI for site 16 presents very similar values to site 15: low risk values for SLS, high risk for minimum PGA and very high risk for ULS and MCE. The LSN values for all probability of exceedance design earthquakes are off by one magnitude. Manually calculated LSN values are presented in Table 5-9, and they predict minor expression of liquefaction for all design earthquake events and minimum PGA. However, ULS and MCE are at the higher end of minor expression of liquefaction.

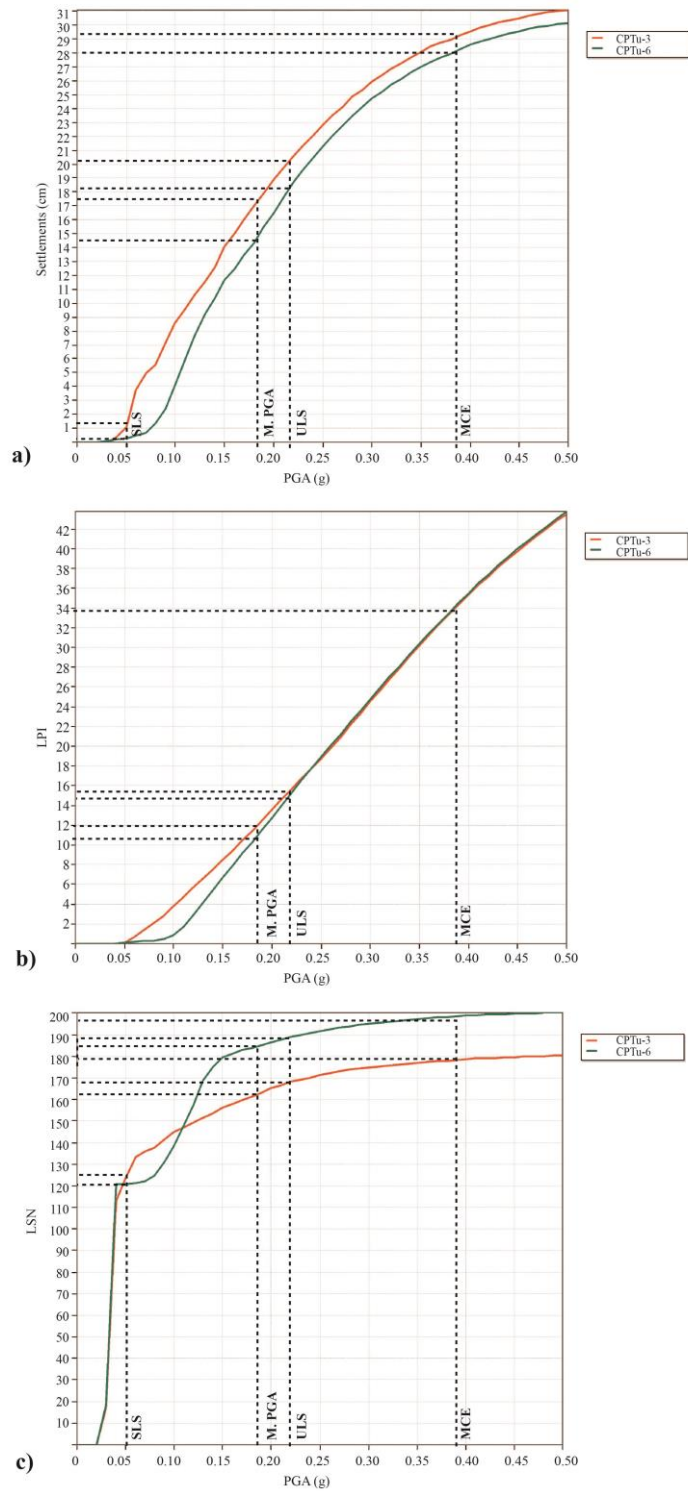


Figure 5.24: Parametric graphs of PGA verses (a) settlement, (b) LPI and (c) LSN using calculation method Idriss and Boulanger (2008) for site 16.

Table 5-9: Calculated liquefaction parameters for site 16 using Idriss and Boulanger (2008).

Liquefaction parameters	Earthquake event	CPTu-3	CPTu-6	Average	Interpretation
Settlements (cm)	SLS	1.5	0.1	0.8	Minimal
	M.PGA	17.5	14.5	16	Significant
	ULS	20.2	18.2	19.2	Significant
	MCE	29.3	28	28.65	Significant
LPI	SLS	0	0	0	Low risk
	M.PGA	12	10.8	11.4	High risk
	ULS	15.5	15	15.25	Very high risk
	MCE	33.9	33.9	33.9	Very high risk
LSN	SLS	12.4	12.1	12.3	Minor
	M.PGA	16.2	18.5	17.3	Minor
	ULS	16.8	18.9	17.9	Minor
	MCE	17.8	19.9	18.9	Minor

5.3.4.3.2 Boulanger and Idriss (2014)

Parametric graphs for the method of calculation of Boulanger and Idriss (2014) are shown in (Figure 5.25). This calculation method shows LPI at identical levels of risk to Idriss and Boulanger (2008)—that is, low risk values for SLS, high risk for minimum PGA and very high risk for ULS and MCE. All LSN values also exceed 50 (boundary for severe expression of liquefaction) but these values are again not reasonable. Liquefaction parameters for both CPTu are presented in Table 5-10, and predict minor expression of liquefaction, with ULS and MCE close to the boundary of moderate expression of liquefaction.

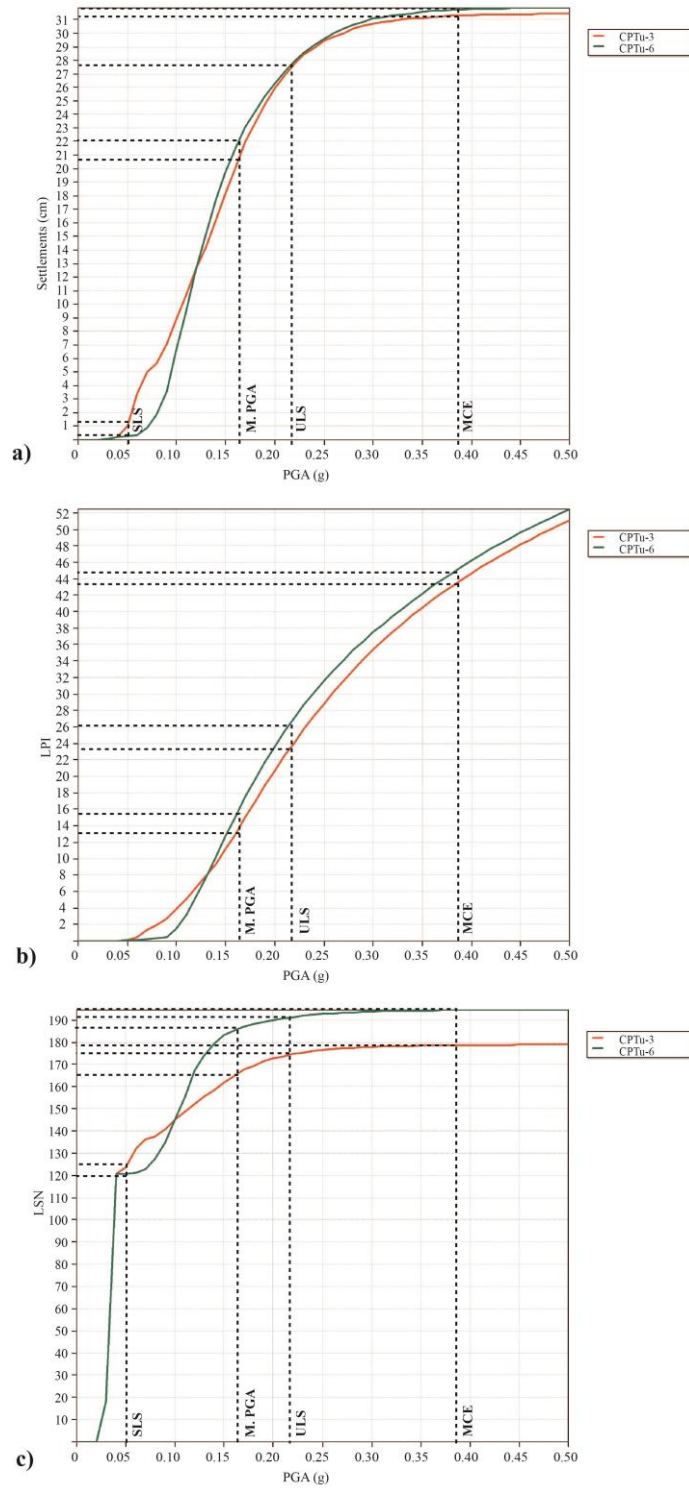


Figure 5.25: Parametric graphs of PGA verses (a) settlement, (b) LPI and (c) LSN using calculation method Boulanger and Idriss (2014) for site 16.

Table 5-10: Calculated liquefaction parameters for site 16 using Boulanger and Idriss (2014).

Liquefaction parameters	Earthquake event	CPTu-3	CPTu-6	Average	Interpretation
Settlements (cm)	SLS	0.5	1.2	0.85	Minimal
	M.PGA	20.8	22	21.4	Significant
	ULS	27.8	27.8	27.8	Significant
	MCE	31	31.5	31.25	Significant
LPI	SLS	0	0	0	Low risk
	M.PGA	13	15.8	14.4	High risk
	ULS	23	26	24.5	Very high risk
	MCE	41.5	45	43.25	Very high risk
LSN	SLS	12.3	12.1	12.2	Minor
	M.PGA	16.5	18.8	17.7	Minor
	ULS	17.5	19.1	18.3	Minor
	MCE	18.8	19.4	19.1	Minor

5.4 Summary

Site 15 (Quarry on Aspin Road) and site 16 (Endeavour Primary School) both show evidence of paleoliquefaction. The particle size analysis shows a possibility of liquefaction occurring for the injection structures (Injection-1, Injection-2a and Injection-2b), source bed (Sand-1) and upper sand bed (Sand-3) for site 15. Furthermore, site 16 shows that the grain size distribution of both the injection structure and the sand bed are identical, therefore confirming the injection structure is sourced from the sand layer. Grain size distribution of injection structures and source beds for sites 15 and 16 present optimal characteristics for the possibility of liquefaction occurring. Liquefaction assessments of ULS earthquake events predict liquefaction for source beds identified in field observations. Material variability of the Hinuera Formation is reflected in CPTu data at site 15, and this observation is not surprising. Calculation methods Boulanger and Idriss (2014) show increased predicted liquefaction compared to Idriss and Boulanger (2008), hence the updated calculation method is conservative.

Chapter 6

Discussion

6.1 Introduction

Firstly, I will discuss possible and definitive evidence of earthquake-induced paleoliquefaction features located within the sediments of the Hinuera Formation in the Hamilton and Hauraki basins (sites 7, 15, 16 and 17). In particular, I discuss how seismic and non-seismic triggers are determined from the soft-sediment deformation structures. Liquefaction assessments based on CPTu data are compared to field observations to determine the validity of this *in situ* test. Field observations revealed that definitive evidence of paleoliquefaction are manifested at locations where modern (surface) pedological soils are silty and slightly peaty on slightly lower landscape elevations. As a result, I have developed a provisional soil-landscape model to predict more widely areas that are possibly highly susceptible to liquefaction.

6.2 Soft-sediment deformation

Context-based approaches are used to determine deformation mechanisms and trigger agents for soft-sediment deformations (Owen & Moretti, 2011; Owen *et al.*, 2011). Only four sites showed evidence of soft-sediment deformation and a high water table: Tirau Sands (site 7), Endeavour Primary School (site 15), Quarry on Aspin Road (site 16) and Waikato Expressway (site 17). The soft-sediment deformation structures identified are all sand dikes with the exception of site 17 where large-scale load structures are present. The deformation mechanism is definitively liquefaction or fluidisation because other deformation mechanisms are possible only in cohesive materials (e.g. thixotropy or sensitivity, see chapter 2).

6.2.1 Possible evidence of paleoliquefaction

Determining a seismic or non-seismic trigger agent is profoundly difficult as research is limited primarily to identifying seismic triggers (Sims & Garvin, 1995; Obermeier, 1996; Tuttle, 2001; Montenat *et al.*, 2007), as opposed to a more holistic

approach that considers both (non-seismic and seismic triggers) (Moretti & Sabato, 2007; Owen *et al.*, 2011). Sites 7 and 17 are interpreted as possible evidence of paleoliquefaction as both a seismic and non-seismic trigger agent are equally plausible. The sand dike at site 7 is small (8 cm in height), suggesting a non-seismic trigger. Furthermore, the source bed is not identified at this site. However, the sand dike is located at the base of the quarry wall and deeper excavations could locate a source bed. The load structures at site 17 are inferred as earthquake induced due to large crest size (~ 50 cm in height), but a very thick (~15 m) gravelly sand overlies the silt bed enclosing the load structure. Rapid loading of a thick deposit is likely, hence also suggesting a non-seismic trigger.

6.2.2 Definitive evidence of paleoliquefaction

The sedimentary sequences at sites 15 and 16 show definitive evidence of earthquake-induced paleoliquefaction features because the facies analysis of the Hinuera Formation eliminates most non-seismic triggers. For example, pressure fluctuations caused by breaking water waves, storm waves and tsunamis are unfeasible as the study area is located large distances from the coast. Possible non-seismic triggers include: a fluctuating groundwater level which is evident from iron and manganese stained beds (minor at site 15 but significant at site 16), varying turbulence in water flow, and floods or rapid sediment loading (possible in a fluvial environment). It is also possible that earthworks at site 15 may have caused the injection structures, as the quarry manager mentioned observations of “water and sediment bubbling up”. However, if an excavator is able to cause injection structures, then an earthquake is more than capable. Multiple appearances right through site 16 reject the possibility of injection structures as a result of excavation. Therefore the two most likely trigger agents are rapid sediment loading, which is the inferred interpretation from Hume *et al.* (1975), or an earthquake event. A seismic trigger is determined to be the most likely cause of liquefaction at sites 15 and 16 because of the presence of strong indicators as suggested by Owen and Moretti (2011). The strong indicators include optimal sediment characteristics, as the particle size analysis suggests grain size within the high possibility of a liquefaction boundary (NZGS, 2010). Furthermore the injection structures showed ductile deformation, increased deformation upwards, preserved surrounding

stratification (see chapter 2) and, most importantly, identified a source bed (Tuttle, 2001).

Bastin *et al.* (2013) identified paleoliquefaction features amongst liquefaction structures produced from the 2010-2011 Canterbury earthquake sequence. The orange mottling paleoliquefaction features are cross-cut by younger grey liquefaction structures, indicating multiple earthquake events. These grey liquefaction structures (also recognised by Almond *et al.*, 2010) are very similar in appearance to the injection structures found at sites 15 and 16. Only one set of injection structures are recognised at 15 and 16. The lack of orange mottling which is characteristic of older liquefaction events in Christchurch may be due to a couple of possible causes: (a) the observed injection structures are too recent to have developed mottles; (b) water table levels may be high enough to maintain permanent saturation, thus not permitting the oxidation required to develop mottles.

Through the principle of cross-cutting relationships, depositional ages determined from radiocarbon dating suggest any seismic events that post-date deposition of organic material could be responsible for the injection structures at site 15 and 16. Therefore shallow pre-historical or historical earthquake events with \geq Mw 5.0, occurring at a time more recent than c. 20,749 calendar years ago for site 15 and c. 19,964 calendar years ago for site 16 are probable seismic sources. The Kerepehi Fault in the Hauraki Basin is inferred by de Lange and Lowe (1990) to have moved substantially at least four times in the Holocene, c. 10,000, c. 7600, c. 6400, and c. 1300 calendar years ago. Any one of these postulated events could have been responsible for the paleoliquefaction features observed at the two key sites (Quarry on Aspin Road, Endeavour Primary School) recorded here. Alternatively, the paleoliquefaction at Aspin Quarry and Endeavour Primary School could represent one or two new and previously unrecorded paleoearthquake events additional to those denoted by de Lange and Lowe (1990). Table 2-3 also lists a number of local earthquakes that have been recorded in historical times (see chapter 2). Eight of these have a magnitude of \geq 5.0, and hence could be the trigger for the liquefaction observed. The seismic event recorded at Aspin Quarry may be the same as that recorded at Endeavour Primary School, or a different (separate) event. Thus there may have been up to six paleoseismic events in the region since c. 20,000 calendar

years ago on the basis of de Lange and Lowe (1990) and the new work reported here.

Seismic energy from the recorded historical earthquakes are directed mostly towards the Hamilton Basin as opposed to the Haruaki Basin. Field observations of the Hauraki Basin (refer to chapter 4 and appendix 1) contain a higher content of pumiceous (as opposed to non-pumiceous) gravels in comparison with those of the Hamilton Basin. All sites at which possible and definitive evidence of liquefaction are recognised within the Hamilton Basin. Except for site 7; which is the most southern site investigated of the Hauraki Basin. Pumiceous material is a concern in engineering design due to high crushability and compressibility characteristics. Triaxial shear tests of pumiceous sands conducted by Orense and Pender (2013) depict increased cyclic resistance compared to sands used for empirical correlations that predict CSR by the simplified approach. Therefore recorded CPTu values may over estimate liquefaction potential. More importantly, coarser pumiceous material is simply too free-draining to allow for the development of high pore water pressure required for liquefaction. This may explain why no liquefaction is seen near the Kerepehi Fault, a location where evidence of liquefaction is expected to be most profound.

6.3 Liquefaction assessment

6.3.1 Site 15 – Quarry on Aspin Road

6.3.1.1 Soil behaviour type interpretations

The quarry on Aspin Road shows SBT sequences almost identical to field observations for CPTu-1 and CPTu-2. However, a “clay, silty clay” layer is recognised by the SBT calculations instead of organic material identified in field observations for CPTu-1. Inconsistencies between field observations and SBT interpretations for CPTu-1 did not affect cyclic predictions as both clay and organic silt are not susceptible to liquefaction. Nonetheless, it is clear that the organic materials are indicating an environment with a high water table and poor drainage conditions; a situation that is conducive to liquefaction. These conditions would not be recognised from CPT assessment alone. At CPTu-2, located on a higher bench, recognised “sensitive fine grained” materials in the upper metre transitioning into interbedded “silty sand, sandy silt” and “clay” layers which is identified as a medium sand in field observations. Not until the test reached depths of 1.5 m did the results reflect field data. The inconsistent data is a result of reworked material placed to make a temporary path. Hand augers below the present quarry floor (0 m at CPTu-1 and 1.7 m at CPTu-2) are unable to penetrate below a 30 cm depth because the hole collapsed continuously (due to the sand material being saturated).

6.3.1.2 Cyclic liquefaction interpretations

The critical layer defined from field observations presents opposing results of predicted liquefaction for CPTu-1 and CPTu-2. The test associated with injection structures (CPTu-1) clearly show predicted liquefaction of the source bed for the ULS earthquake event. Although the test located on a higher bench (CPTu-2) predicts liquefaction occurring in the upper and lower most sections, the majority of the bed does not liquefy. Furthermore, liquefaction structures are not identified at CPTu-2, showing that field observations and predicted liquefaction plots are in agreement. Other sand beds above and below the critical layer of both CPTu profiles are also predicted to liquefy. The water table is set to saturate all soils, which predicted liquefaction of the upper sediments. However, in real case circumstances the water table would not likely be at this level. Lower beds predicted to liquefy are

at depths below liquefaction susceptibility and can therefore be ignored. Despite only a 50 m distance between each test, variability of the Hinuera Formation is evident and is expected.

The triggering earthquake determined from the observed data presents a much lower PGA value (0.19) compared to the predicted PGA for a ULS earthquake event (0.25). Predicted settlements and LPI values become substantial at the approximated triggering earthquakes. LSN values calculated in CLiq show a severe liquefaction expression at site 15 (Aspin Quarry) for a SLS earthquake event, a result which is not probable (Moon and Stichbury 2012; NZTA, 2014; Standards New Zealand, 2004). Calculating LSN manually, using equation (3-3), show minor to moderate expressions of liquefaction which is a reasonable prediction. The algorithm in CLiq is producing a results one order of magnitude above those defined by Tonkin and Taylor (2013).

6.3.2 Site 16 – Endeavour Primary School

6.3.2.1 Soil behaviour type interpretations

The SBT plots at Endeavour Primary School are inconsistent with field observations. CPTu data is collected before identification of liquefaction structures; therefore CPTu injection structures are correlated to the nearest CPTu location. The differences are due to the high degree of variability in the soil sequence evident at site 16. CPTu-6 recognises sand and silty sand SBT at the base of the pit, overlain by a clay and organic soil. This sequence correlates mostly to beds identified in the pit, except for the clay and thickness of the organic soil. Clay material is not recognised in field observations and the organic soil is approximately 40 cm thick. CPTu-3 SBT interpretations are completely different from those relating to field observations.

6.3.2.2 Cyclic liquefaction interpretations

Field observations identified the source bed at locality ii (CPTu-3), within the interbedded sand and silty sand facies, 3.6 m below the pre-excavated surface. Through the particle size analysis the critical layer is identified at 3.0 m in SBT

plots for locality i (CPTu-6). Liquefaction is predicted to occur in both CPTu-6 and CPTu-3 and agrees with extensive paleoliquefaction features evident on site. Discrete patches of predicted liquefaction are occurring above and below the defined critical layer. From a depth of 1 m to the critical layer (3 m and 3.6 m for CPTu-6 and CPTu-3, respectively), all soils predicting liquefaction are very likely to occur. Below the critical layer to ~16 m depth, liquefaction is likely to occur, and below ~16 m overburden stress becomes too large for liquefaction to occur. This site shows widespread predicted liquefaction and further provides evidence of liquefaction risk within the Hinuera Formation.

The minimum earthquake size required to cause liquefaction within soils of the critical layer also presents a much lower PGA value (0.19) compared to the predicted PGA for an ULS earthquake event (0.22) for site 16 (Endeavour School). Thus, a moderate sized earthquake as opposed to a less frequent, large earthquake, would provide significant residual damage to structural buildings at lower earthquake energies. The same minimum PGA is also evident at site 15. Therefore, smaller earthquakes at more frequent occurrences is a common possible trigger for liquefaction across both sites.

6.3.3 Calculation methods

The updated deterministic methodology (Boulanger & Idriss, 2014) is encouraged to be used instead of the older calculation method (Idriss & Boulanger, 2008) for liquefaction assessment (Ministry of Business, Innovation and Employment (MBIE), 2014). The Boulanger and Idriss (2014) method refines liquefaction trigger correlations firstly by revising old case histories and secondly by integrating recent earthquake events into the database—many of which are from the 2010-2011 Christchurch earthquake sequence (case histories collected from Green *et al.*, 2014). Comparing results from the older and updated calculation method shows increased predicted liquefaction at both sites 15 and 16, primarily due to a new formulation of the Magnitude Scaling Factor (MSF). MSF incorporates soil density and duration effects, which account for the number and amplitude of cycles induced by an earthquake (Boulanger & Idriss, 2014). The results are more conservative

using the Boulanger and Idriss (2014) calculation method, and it provides a more comprehensive liquefaction assessment and will therefore be the method of choice.

6.3.4 Aging factor

From the results presented here, there seems to be little justification for assuming an “aging” factor in the liquefaction potential analysis. A sensitivity analysis of increasing aging factor against FS shows linearity (Figure 6.1). FS is taken 5 cm below the top of the defined critical layer for the Quarry on Aspin Road and Endeavour Primary School sites. That is, for Aspin Quarry: CPTu-1 at 1.78 m, CPTu-2 at 3.24 m and for Endeavour Primary; CPTu-6 at 3.05 m, CPTu-3 at 3.65 m. Applying the aging factors (1.3 to 1.4) to the Hinuera Formation as suggested by Clayton and Johnson (2013) still show FS values below 1. Note inputting an aging factor of 1 is equivalent to applying no aging factor. Therefore, implementing aging factors for the Hinuera Formation may not be due to definitive evidence of paleoliquefaction features within the Hamilton Basin. More research needs to be done to establish if an aging factor genuinely reflects changes in the sediments that reduce susceptibility to liquefaction.

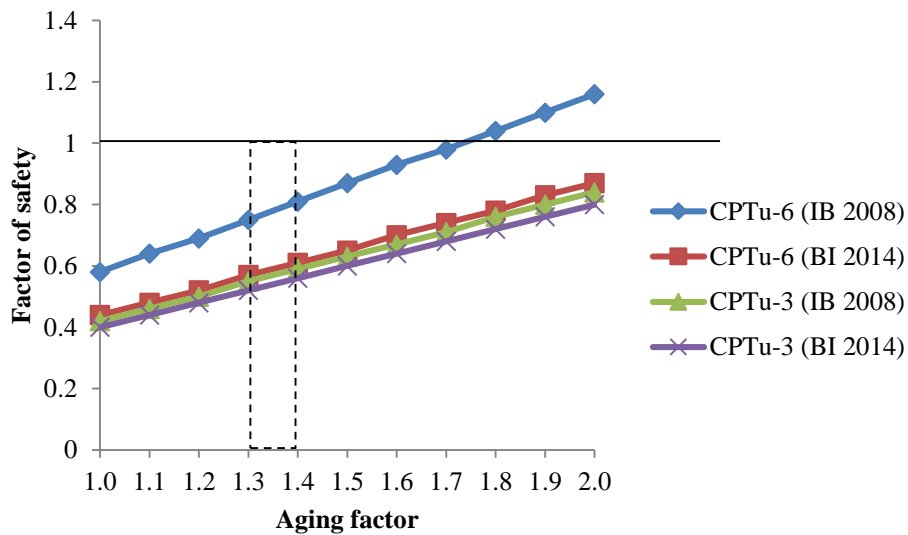
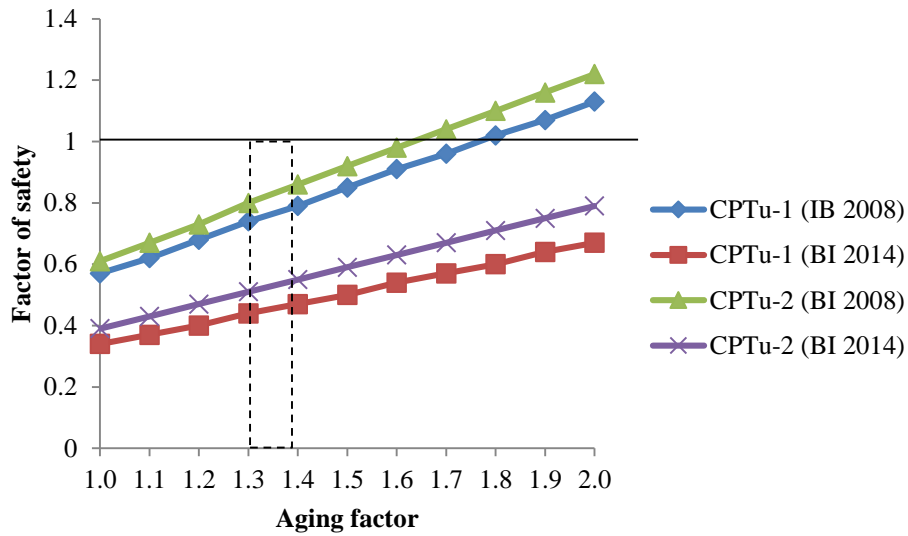


Figure 6.1: Relationship of FS verses aging factor for (a) site 15 and (b) site 16. Below FS=1, liquefaction is predicted to occur.

6.4 Soil-landscape model

Soil-landscape models project observed soil properties with their associated landforms to areas unsampled (Webb, 1994). In this case the attribute of interest is liquefaction susceptibility, and field observations showed that paleoliquefaction features are found in association with silt and organic layers. This lithological association probably relates to slow or impeded drainage and permeability. Silts originated usually as overbank flood deposits (Hume *et al.*, 1975) and can be associated with peat if they are located near the present-day land surface (e.g. Bruce,

1979). Therefore, impeded drainage is reflected in the modern pedological soil pattern. The liquefaction structures observed are at both locations where the modern (pedological) soils (Te Rapa and Te Kowhai soil series) occurred in topographic depressions on the Hinuera Surface. Therefore, this relationship enables the development of a soil-landscape model using the modern soil pattern to tentatively predict areas of higher susceptibility to liquefaction. Such a prediction relies on the assumptions that lower-lying land surfaces: (i) have a water table closer to the land surface and (ii) that the underlying deposits in such topographic positions may be more likely to be dominated by silts rather than sands or gravels. Chapman (2008) recorded that groundwater levels occur between 2 m and 6 m below the ground surface in the Hamilton Basin but that because of the Hinuera Formation's lithological variability, the deposits are characterised by a lack of lithological continuity. This lack of continuity in turn influences the behaviour of groundwater and causes change in the water table level and storage capacity over relatively short distances (see chapter 2).

Paleoliquefaction features occur at approximately 3 m depth at a location where the Te Rapa soil series occurs at the modern land surface at Endeavour Primary, and at the Quarry on Aspin Road where the soil series is not mapped. Soil characteristics of the Te Rapa series are poorly drained peaty silt loams formed on low-lying areas of flat to slightly undulating landscapes, next to abandoned river channels and ancient lakes (Singleton, 1991). The Te Kowhai series are closely related to Te Rapa soils, forming on the lowest part of the plain where water became trapped; depositing fine-grained suspended sediments. This series contains soil types characterised by a peaty silt loam and silt loam textured "A horizons". The equivalent poorly drained, peaty and silty soils in the Hauraki Basin are the Waitoa series in association with the Te Rapa series. Poorly drained Waitoa and Te Rapa series both form on low-lying areas of the Hauraki plains such as backswamps and embayments (McLeod, 1992). However, the Te Rapa soils contain a higher organic content, and hence are classed as Peaty Orthic Gley Soils in Hewitt (2010), compared to the Waitoa soils, Acidic Orthic Gley Soils in Hewitt (2010). Therefore, the distribution patterns of three soil series; namely Te Rapa, Te Kowhai, and Waitoa, are used to tentatively predict a possible high liquefaction susceptibility where silts or peaty silts occur within 2-3 m of the modern surface in low-lying

situations, and where the water table may be expected to be relatively high for much of the time (Figure 6.2).

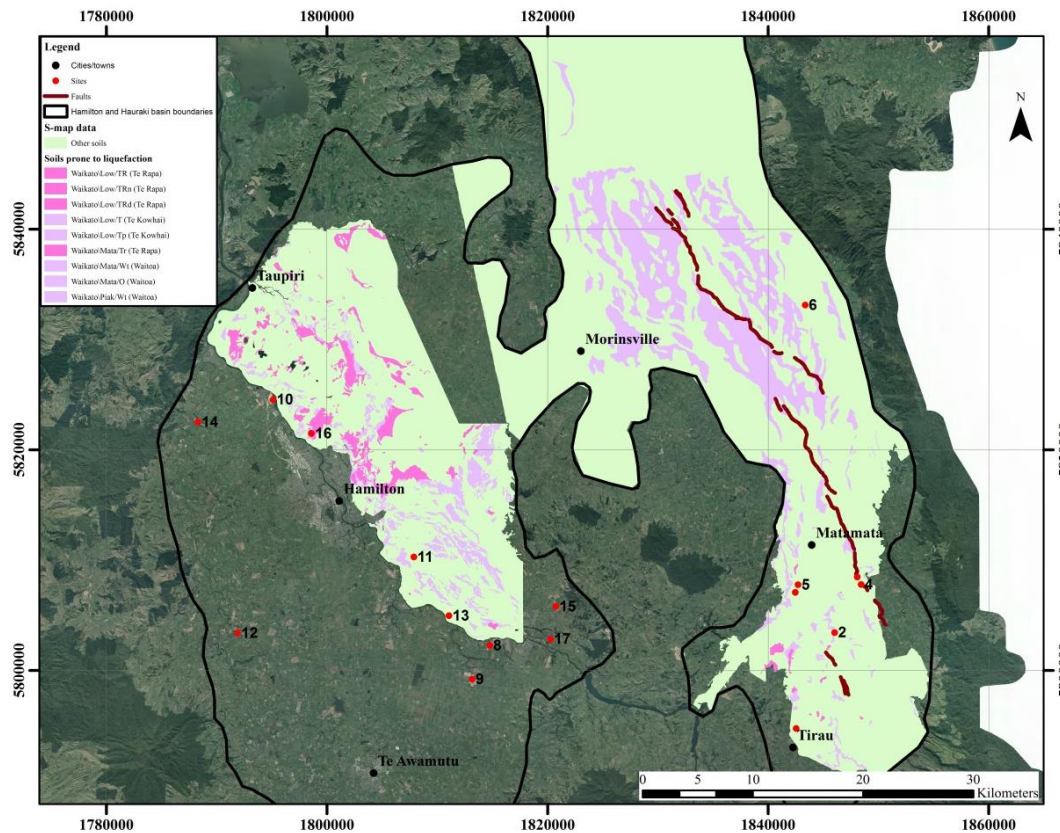


Figure 6.2: Map of soils likely to be more prone to liquefaction (pink-purple colours) on the basis of a soil-landscape model of the Hamilton and Hauraki basins.

S-map developed a partially new soil classification system to provide consistency over a national extent, with levels 4 and 5 in the New Zealand Soil Classification (NZSC) designated as “families” and “siblings” (Lilburne *et al.*, 2004). Soil series names are still widely used, and remain as legitimate nomenclature, but are not a formal part of NZSC. Within the NZSC hierarchy, soil families incorporate specific characteristics of parent material, rock type, dominant texture and permeability class, whereas siblings are, a further subdivision showing variations in drainage class, topsoil stoniness, depth class and a more detailed texture profile (Webb & Lilburne, 2011). These properties are additional to those associated with higher-level categories in the classification (namely those attributes associated with order, group, and subgroup categories). Table 6-1 correlates the previous soil series nomenclature with that of S-map.

Table 6-1: Correlation and classification of soil series.

Series	S-map family and siblings	Subgroups of NZSC	Symbol for GIS
Te Rapa	Matakana 2a.1	Peaty Orthic Gley Soil	Waikato\Low/TR or Waikato\Mata/Tr
	Te Rapa 1a.1	Peaty Orthic Gley Soil	Waikato\Low/TRn
	Utuhina 31a.1	Mellow Humic Organic Soil	Waikato\Low/TRd
Te Kowhai	Pukehina 8a.1	Typic Orthic Gley Soil	Waikato\Low/T
	Matakana 6a.1	Peaty Orthic Gley Soil	Waikato\Low/Tp
Waitoa	Eureka 9a.1	Acidic Orthic Gley Soil	Waikato\Piak/Wt
	Waitoa 1a.a	Typic Acid Gley Soil	Waikato\Mata/O

6.4.1 Limitations

The soil-landscape model for liquefaction susceptibility is subject to certain limitations. For example, to date, Hamilton S-map currently only has data available west of the Waikato River, and only part of Cambridge is covered. Furthermore, pedological soils comprise material of the uppermost metre, and liquefaction can occur to approximately 10 m in depth. The soil-landscape model therefore must be viewed as a reflection of the liquefaction susceptibility of surface materials. While conditions leading to liquefaction may well exist deeper in the profile, Tonkin and Taylor (2013) report that in Christchurch it is liquefaction of the shallowest materials that caused the greatest damage. The model's purpose is to tentatively indicate that the pedological soils in association with the geomorphology reflect areas of shallow water tables, likely associated with fine-grained sediments and impeded drainage, which are ideal conditions for liquefaction of shallow materials. The purpose is to predict the behaviour of soil systems in relation to landforms—in this case, during an earthquake.

6.5 Summary

Seismic triggers are determined through context-based approaches for injection structures located at site 15 (Aspin Quarry) and 16 (Endeavour Primary School). A pedological soil-landscape model utilises the occurrence of modern (surface) silty and peaty soils at low-lying landscape positions on the Hinuera Surface to derive a map showing (tentatively) areas of high liquefaction susceptibility. The liquefaction

assessments consistently respond to the wide lithological variability of the Hinuera Formation and are reflected in piezocone penetration tests. Boulanger and Idriss (2014) calculation methods produce a more conservative outcome compared to the older Idriss and Boulanger (2008) methodology, and therefore increased predicted liquefaction.

Chapter 7

Conclusion

7.1 Paleoliquefaction

Earthquake-induced paleoliquefaction features are identified within the Hinuera Formation at two sites: a Quarry on Aspin Road (site 15), near Cambridge, and Endeavour Primary School in Flagstaff (site 16), north Hamilton. The paleoliquefaction features are in the form of injection structures (sand dikes) and indicate the potential for future liquefaction events. Possible evidence of liquefaction is also observed at site 7 (Tirau Sands), manifested in the form of small-scaled injection structure, and further at site 17 (Waikato Expressway), where large-scale load structures show crests and troughs.

Sites with definitive and possible evidence of paleoliquefaction events are also accompanied by shallow water tables. This wetness is an important pre-requisite for liquefaction to occur and is expected to be found at such sites showing evidence of liquefaction. However, it is notable that all sites examined with high water tables had some form of soft-sediment deformation. Liquefaction also too a possible cause of deformation at these sites.

Radiocarbon dates of organic material at site 15 and 16 allowed for me to determine the maximum age of occurrence through cross-cutting relationships, as the injection structures intrude through organic-rich layers. These dates indicate a seismic event occurred sometime after c. $20,749 \pm 204$ calendar years ago for site 15, and after c. $19,964 \pm 222$ calendar years ago for site 16.

Organic material in association with silty soils is also observed at sites showing possible and definitive evidence of paleoliquefaction. Silt and organic layers are important indicators of impeded or slow drainage, thus allowing for the generation of high water tables. Silts originated usually as overbank flood deposits (Hume *et al.*, 1975) and are commonly linked with subsequently-developed peats, and, if near the present-day land surface, are reflected in the modern pedological soil pattern

(e.g. Bruce 1979). The liquefaction structures observed at site 16 are associated with the silty Te Rapa and Te Kowhai soil series, which occur in topographic depressions on the Hinuera Surface in the Hamilton Basin. Equivalent soil series in the Hauraki Basin include the Te Rapa and Waitoa soils. This soil association enabled me to develop a pedological soil-landscape model using the modern soils to predict areas of likely high susceptibility to liquefaction. Note that this model will only reflect the near-surface conditions and assumes that similar materials of high susceptibility occur deeper within the Hinuera Formation. However, near-surface liquefaction is likely to be most damaging to infrastructure (Tokin & Taylor, 2013) and so the soil-landscape model is an initial indicator of possible liquefaction in shallow soil layers.

7.2 Liquefaction assessment

Hinuera deposits show high variability and are often very complex laterally and with depth. These characteristics are reflected in the liquefaction assessment. At site 15, the critical layer defined in CPTu-1 and CPTu-2 shows contradictory liquefaction predictions. Data from CPTu-1 (test contains same stratigraphic sequence in which the injection structures are located) predict liquefaction of the source bed identified in field observations. Conversely, the critical layer in CPTu-2 (test is located on the upper bench) shows little liquefaction predicted. Injection structures are not identified at locations near CPTu-2, and therefore field observations and liquefaction assessment of the critical layer are consistent. The liquefaction assessment at site 16 presents liquefaction occurrences at the defined critical layer for CPTu-6 (locality i) and CPTu-3 (locality ii). The instrumental CPTu method provides a valid method of predicting liquefaction potential. However, the materials are highly variable over short distances and hence liquefaction is localised. Thus, it is difficult to infer ground conditions for more than a few metres from a CPTu site without further ground-truth information.

Organic-rich layers are not adequately recognised in SBT plots where they are identified as clay and silty clay soils. The association of organic material with the paleoliquefaction features are key observations at both sites 15 and 16. I suggest

that near surface (upper 3 m) organic-rich (not necessarily peaty) soils in hand auger logs should provide a clear warning of liquefaction potential.

7.3 Summary

This study has resulted in four key conclusions:

- It is clear from the newly-identified paleoliquefaction features that the Late Pleistocene Hinuera Formation in the Hamilton Basin, at least, is susceptible to earthquake-induced liquefaction (not so clear in the Hauraki Basin). This is a hazard that needs to be recognised in infrastructure development and maintenance work.
- Key conditions observed at sites with definitive evidence of paleoliquefaction features included the presence of silts associated with organic-rich materials. The high levels of silts and organic material reflect impeded or slow flowing drainage (associated ultimately with overbank silt deposition from the ancestral Waikato River), and are located at lower elevations of the land surface. Topography and the silty, organic-rich soil association are indicative of the shallow water tables required for liquefaction.
- A soil-landscape model which recognises modern pedological soil series formed under high water tables and impeded drainage may provide a first indication of areas of high liquefaction susceptibility in the near-surface materials. The Hinuera Surface represents a very low angled, braided alluvial fan (akin to a plain), and therefore deposits are highly variable. Liquefaction at deeper levels may not be well represented by the soil-landscape model.
- Instrumental CPTu data predicts a low factor of safety in known liquefied layers, and provides a good point prediction of liquefaction susceptibility using methods of Idriss and Boulanger (2008) and Boulanger and Idriss (2014). However, the soil behaviour type derived from CPTu results does not adequately identify the organic rich silts which may be a key indicator of high susceptibility. Liquefaction has clearly occurred and it is not evident from this study that applying an aging factor to the calculation of CRR is justified.

7.4 Recommendations for future study

- Test and refine the pedological soil-landscape model, by seeking evidence of paleoliquefaction features at sites with predicted high liquefaction susceptibility.
- Construct a CPTu-based hazard model in GIS, using a compilation of CPT data from the council and engineering consultants in the Waikato Region. This could then be followed by a comparison with the soil-landscape model.
- Compare liquefaction assessment result, across different *in situ* tests, such as CPT, seismic cone penetration test (SCPT) and standard penetration test (SPT) at sites prone to liquefaction or of known paleoliquefaction features.

References

- Allen, J. R. L. (1982). *Sedimentary structures, their character and physical basis*. Vol. 1. Amsterdam, Netherlands: Elsevier.
- Almond, A., Whitman, Z., Cockcroft, M., Wilson, T., Eger, A., Nobes, D., Shanhun, F., & Moot, D. (2010). Agricultural land rehabilitation following the 2010 Darfield (Canterbury) Earthquake: a preliminary report. *Bulletin of the New Zealand Society for Earthquake Engineering*, 43(4), 432.
- Ambraseys, N. N. (1988). Engineering seismology: Part II. *Earthquake engineering & structural dynamics*, 17(1), 51-105.
- Andrus, R. D., & Stokoe, K. H. (2000). Liquefaction Resistance of Soils from Shear-Wave Velocity. *Journal of Geotechnical and Geoenvironmental Engineering*, 126(11), 1015-1025.
- ASTM International. D5778 – 12, *Standard Test Method for Electronic Friction Cone and Piezocone Penetration Testing of Soils*.
- Bastin, S. H., Quigley, M. C., Bassett, K., & Green, R. A. (2013). *Characterisation of modern and paleo-liquefaction features in eastern Christchurch, NZ following the 2010-12 Canterbury earthquake sequence*. Paper presented at Proc. 19th NZGS Geotechnical Symposium. Queenstown, New Zealand.
- Beanland, S., & Berryman, K. R. (1986). *The Kerepehi Fault, Hauraki Depression*: New Zealand Geological Survey Earth Deformation Section immediate report 86/27.
- Beanland, S., Waikato (N.Z.). Regional Council., & Institute of Geological & Nuclear Sciences Limited. (1996). *Earthquake hazard analysis : Environment Waikato (Regional Council) area*. Environment Waikato technical report TR96/17. Hamilton [N.Z.]: Environment Waikato Regional Council.
- Boulangier, R. W., & Idriss, I. M. (2014). *CPT and SPT based liquefaction triggering procedures*. Report No. UCD/CGM-14.
- Bronk Ramsey, C. (2001). Development of the radiocarbon calibration program OxCal. *Radiocarbon*, 43(2A), 355-364.
- Bruce, J. G. (1979). *Soils of Hamilton City, North Island, New Zealand*. New Zealand Soil Survey Report 31. 65p + 1 sheet 1:20,000.
- Chapman, M. (2008). *Groundwater and the Hinuera Formation: a broad flat basin containing 50% water and 50% sediment - lake or land?* Guidebook for Pre-conference North Island Field Trip A1 'Ashes to Issues' (28-30 November, 2008). Massey University, Palmerston North. New Zealand Society of Soil

Science, Christchurch: Australian and New Zealand 4th Joint Soils Conference.

- Clayton, C. R. (1995). *The standard penetration test (SPT): methods and use*. CIRIA Report 143: Construction Industry Research and Information Association.
- Clayton, P. J., & Johnson, J. T. (2013). *Liquefaction resistance and possible aging effects in selected Pleistocene soils of the Upper North Island*. Paper presented at Proc. 19th NZGS Geotechnical Symposium. Queenstown, New Zealand.
- Cubrinovski, M. (2010). *Geotechnical Aspects of the 2010 Darfield (Canterbury) Earthquake*. Paper presented at Bangladesh Geotechnical Conference 2010: Natural Hazards and Countermeasures in Geotechnical Engineering. Dhaka, Bangladesh.
- Cubrinovski, M., Bradley, B., Wotherspoon, L., Green, R., Bray, J., Wood, C., Pender, M., Allen, J., Bradshaw, A., & Rix, G. (2011). Geotechnical aspects of the 22 February 2011 Christchurch earthquake. *Bulletin of the New Zealand Society for Earthquake Engineering*, 44(4).
- Dalrymple, R. W., & James, N. P. (2010). *Facies models 4*. St. John's, N.L.: Geological Association of Canada.
- de Lange, P. J., & Lowe, D. J. (1990). History of vertical displacement of Kerepehi Fault at Kopouatai bog, Hauraki Lowlands, New Zealand, since c. 10 700 years ago. *New Zealand Journal of Geology and Geophysics*, 33(2), 277-283.
- Downes, G. L., & Dowrick, D. J. (2014). *Atlas of isoseismal maps of New Zealand earthquakes - 1843-2003 Second edition (revised)*. GNS Science monograph 25. Lower Hutt, New Zealand: GNS Science.
- Dowrick, D. J. (1996). The Modified Mercalli earthquake intensity scale: Revisions arising from recent studies of New Zealand earthquakes. *Bulletin of the New Zealand National Society for Earthquake Engineering*, 29(2), 92-106.
- Dowrick, D. J., & Rhoades, D. A. (1998). Magnitudes of New Zealand earthquakes, 1901-1993. *Bulletin of the New Zealand National Society for Earthquake Engineering*, 31(4), 260-280.
- Dowrick, D. J., & Rhoades, D. A. (2005). Revised models for attenuation of modified Mercalli intensity in New Zealand earthquakes. *Bulletin of the New Zealand Society for Earthquake Engineering*, 38(4), 185-214.
- Duffy, B., Quigley, M., Barrell, D. J. A., Van Dissen, R., Stahl, T., Leprince, S., McInnes, C., & Bilderback, E. (2013). Fault kinematics and surface deformation across a releasing bend during the 2010 MW 7.1 Darfield, New Zealand, earthquake revealed by differential LiDAR and cadastral surveying. *Geological Society of America Bulletin*, 125(3-4), 420-431.

- Edbrooke, S. W. (2005). *Geology of the Waikato Area*. Institute of Geological & Nuclear Sciences 1:250 000 geological map 4 (1 sheet + 68 p). Lower Hutt, New Zealand: GNS Science.
- Eiby, G. A. (1968). An annotated list of New Zealand earthquakes, 1460–1965. *New Zealand Journal of Geology and Geophysics*, 11(3), 630-647.
- Eiby, G. A. (1977). Anomalous intensities due to the Korakonui earthquake, 5 December 1976. *Bulletin of the New Zealand National Society for Earthquake Engineering*, 10(4), 167-169.
- Folk, R. L. (1968). *Petrology of sedimentary rocks*. Austin, TX: Hemphills.
- Forsyth, P. J., Barrell, D., & Jongens, R. (2008). *Geology of the Christchurch Area*. Institute of Geological & Nuclear Sciences 1:250 000 geological map 46 (Map 16 + 67 p). Lower Hutt, New Zealand: GNS Science.
- GeoLogismiki (2006). *CLiq v.1.7*. (Computer program).
- GeoNet. (2014). Retrieved from www.geonet.org.nz
- Ghosh, S. K., Pandey, A. K., Pandey, P., Ray, Y., & Sinha, S. (2012). Soft-sediment deformation structures from the Paleoproterozoic Damtha Group of Garhwal Lesser Himalaya, India. *Sedimentary Geology*, 261–262(0), 76-89.
- Green, J. D., & Lowe, D. J. (1985). Stratigraphy and development of c. 17 000 year old Lake Maratoto, North Island, New Zealand, with some inferences about postglacial climatic change. *New Zealand Journal of Geology and Geophysics*, 28(4), 675-699.
- Green, R. A., Cubrinovski, M., Cox, B., Wood, C., Wotherspoon, L., Bradley, B., & Maurer, B. (2014). Select Liquefaction Case Histories from the 2010–2011 Canterbury Earthquake Sequence. *Earthquake Spectra*, 30(1), 131-153.
- Hewitt, A. E. (2010). *New Zealand soil classification*. Landcare Research Science Series (3 ed.) Vol. 1. Lincoln, New Zealand: Manaaki Whenua Press, Landcare Research.
- Hochstein, M. P., & Nixon, I. M. (1979). Geophysical study of the Hauraki Depression, North Island, New Zealand. *New Zealand Journal of Geology and Geophysics*, 22(1), 1-19.
- Hodder, A. P. W., & Moon, V. G. (2007). *Seismic risk to water, wastewater and stormwater pipelines in Hamilton City*. A report prepared for the Hamilton City Council. Hamilton, New Zealand: HodderBalog Consultants and The University of Waikato. 50p.
- Hogg, A. G., Lowe, D. J., & Hendy, C. H. (1987). University of Waikato radiocarbon dates I. *Radiocarbon*, 29(2), 263-301.
- Hogg, A. G., Hua, Q., Blackwell, P. G., Niu, M., Buck, C. E., Guilderson, T. P., Heaton, T. J., Palmer, J. G., Reimer, P. J., & Reimer, R. W. (2013). SHCal13

- Southern Hemisphere calibration, 0–50,000 years cal BP. *Radiocarbon*, 55(2), 1-15.
- Houghton, B. F., & Cuthbertson, A. S. (1989). Kaimai Sheet T14 BD *Geological Map of New Zealand*. (), New Zealand Geological Survey. Department of Scientific and Industrial Research. Lower Hutt.
- Hume, T. M., Sherwood, A. M., & Nelson, C. S. (1975). Alluvial sedimentology of the Upper Pleistocene Hinuera formation, Hamilton Basin, New Zealand. *Journal of the Royal Society of New Zealand*, 5(4), 421-462.
- Idriss, I. M., & Boulanger, R. W. (2008). *Soil Liquefaction During Earthquakes*. Monograph MNO-12. Oakland, CA: Earthquake Engineering Research Institute.
- Iwasaki, T., Arakawa, T., & Tokida, K. (1982). *Simplified procedures for assessing soil liquefaction during earthquakes*. Paper presented at Soil dynamics and earthquake engineering. Southampton, UK.
- Juang, C. H., Yuan, H., Li, D. K., Yang, S. H., & Christopher, R. A. (2005). Estimating severity of liquefaction-induced damage near foundation. *Soil Dynamics and Earthquake Engineering*, 25(5), 403-411.
- Kear, D., & Schofield, J. C. (1978). Geology of the Ngaruawahia Subdivision. *New Zealand Geological Survey Bulletin*, 88, 1-168.
- Leonard, G. S., Begg, J. G., & Wilson, C. J. N. (2010). *Geology of the Rotorua Area*. Institute of Geological and Nuclear Sciences 1:250 000 geological map 5. (1 sheet + 102 p). Lower Hutt, New Zealand: GNS Science.
- Liao, S., & Whitman, R. (1986). Overburden Correction Factors for SPT in Sand. *Journal of Geotechnical Engineering*, 112(3), 373-377.
- Lilburne, L., Hewitt, A., Webb, T. H., & Carrick, S. (2004). *S-map – a new soil database for New Zealand* Paper presented at SuperSoil 2004: 3rd Australian New Zealand Soils Conference, 5 – 9 December 2004. University of Sydney, Australia.
- Lowe, D. J. (1986). Controls on the rates of weathering and clay mineral genesis in airfall tephros: a review and New Zealand case study. In S. M. Colman & D. P. Dethier (Eds.), *Rates of chemical weathering of rocks and minerals* (pp. 265-330). Orlando: Academic Press.
- Lowe, D. J. (1988). Stratigraphy, age, composition, and correlation of late Quaternary tephros interbedded with organic sediments in Waikato lakes, North Island, New Zealand. *New Zealand Journal of Geology and Geophysics*, 31(2), 125-165.
- Lowe, D. J., & Green, J. D. (1992). Lakes. In J. M. Soons & M. J. Selby (Eds.), *Landforms of New Zealand, Second Edition* (pp. 107-143). Auckland: Longman Paul.

- Lowe, D. J., Neall, V. E., Hedley, M., Clothier, B., & Mackay, A. (2010). *Guidebook for pre-conference North Island, New Zealand 'Volcanoes to Ocean' field tour (27-30 July, 2010)*. Paper presented at 19th World Soils Congress, International Union of Soil Sciences. Brisbane.
- Lowe, D. R. (1975). Water escape structures in coarse-grained sediments. *Sedimentology*, 22(2), 157-204.
- Lowry, M. A., Ede, S. C., & Harris, J. S. (1989). Assessment of seismic intensities resulting from the 1987 Edgecumbe earthquake, New Zealand, and implications for modernising the intensity scale. *New Zealand Journal of Geology and Geophysics*, 32(1), 145-153.
- Lunne, T., Robertson, P. K., & Powell, M. J. J. (1997). *Cone Penetration Testing in Geotechnical Practice* London: E & FN Spon, an imprint of Routledge.
- Manville, V., & Wilson, C. J. N. (2004). The 26.5 ka Oruanui eruption, New Zealand: A review of the roles of volcanism and climate in the post - eruptive sedimentary response. *New Zealand Journal of Geology and Geophysics*, 47(3), 525-547.
- Manville, V., Hodgson, K. A., & Nairn, I. A. (2007). A review of break - out floods from volcanogenic lakes in New Zealand. *New Zealand Journal of Geology and Geophysics*, 50(2), 131-150.
- Marcuson, W. F. (1978). Definition of terms related to liquefaction. *Journal of the Geotechnical Engineering Division*, 104(9), 1197-1200.
- Maurer, B. W., Green, R. A., Cubrinovski, M., & Bradley, B. A. (2014). Evaluation of the Liquefaction Potential Index for Assessing Liquefaction Hazard in Christchurch, New Zealand. *Journal of Geotechnical and Geoenvironmental Engineering*, 140(7).
- Mayne, P. W. (2007). *Cone Penetration Testing - A synthesis of Highway Practice. National Cooperative Highway Research Program*.
- Mayne, P. W. (2014). *Interpretation of geotechnical parameters from seismic piezocone tests*. Paper presented at 3rd International Symposium on Cone Penetration Testing. CPT'14, Las Vegas, ISSMGE Technical Committee TC 102.
- Mayne, P. W., Christopher, B. R., & DeJong, J. (2001). *Manual on Subsurface Investigations*. FHWA NHI-01-031. Washington DC, National Highway Institute.
- McCraw, J. D. (1967). The surface features and soil patterns of the Hamilton Basin. *Earth Science Journal*, 1, 59-74.
- McCraw, J. D. (2011). *The Wandering River. Landforms and geological history of the Hamilton Basin*. GSNZ Guidebook 16. Levin, New Zealand: Geoscience Society of New Zealand Guidebook.

- McGlone, M. S., Nelson, C. S., & Hume, T. M. (1978). Palynology, age and environmental significance of some peat beds in the upper Pleistocene Hinuera formation, South Auckland, New Zealand. *Journal of the Royal Society of New Zealand*, 8(4), 385-393.
- McLeod, M. (1992). *Soils of part northern Matamata County, North Island, New Zealand*. DSIR Land Resources scientific report No. 18. Lower Hutt, New Zealand: DSIR Land Resources.
- McVerry, G. H., Zhao, J. X., Abrahamson, N. A., & Somerville, P. G. (2006). New Zealand acceleration response spectrum attenuation relations for crustal and subduction zone earthquakes. *Bulletin of the New Zealand Society for Earthquake Engineering*, 39(1), 1-58.
- Middleton, G. (2003). Flame structure. *Sedimentology* (pp. 457-457): Springer Netherlands. Retrieved from http://dx.doi.org/10.1007/978-1-4020-3609-5_85.
- Montenat, C., Barrier, P., Ott d' Estevou, P., & Hibsich, C. (2007). Seismites: An attempt at critical analysis and classification. *Sedimentary Geology*, 196(1 - 4), 5-30.
- Moon, V. G., & Stichbury, G. (2012). *Liquefaction hazard, Hamilton City*. ERI Report No. 8. A report prepared for the Hamilton City Council. Hamilton, New Zealand: Environmental Research Institute, Faculty of Science and Engineering, The University of Waikato.
- Moretti, M., & Sabato, L. (2007). Recognition of trigger mechanisms for soft-sediment deformation in the Pleistocene lacustrine deposits of the Sant'Arcangelo Basin (Southern Italy): Seismic shock vs. overloading. *Sedimentary Geology*, 196(1-4), 31-45.
- Moretti, M., & Ronchi, A. (2011). Liquefaction features interpreted as seismites in the Pleistocene fluvio-lacustrine deposits of the Neuquén Basin (Northern Patagonia). *Sedimentary Geology*, 235(3-4), 200-209.
- New Zealand Geotechnical Society (NZGS). (2005). *Field description of soil and rock: Guideline for the field classification and description of soils and rock for engineering purposes*. NZ Geotechnical Society Inc.
- New Zealand Geotechnical Society (NZGS). (2010). *Geotechnical earthquake engineering practice: Module 1 – Guideline for the identification, assessment and mitigation of liquefaction hazards*. New Zealand Geotechnical Society.
- New Zealand Transport Agency (NZTA). (2014). *Bridge Manual, Third Edition*. New Zealand Transport Agency
- Newnham, R., McGlone, M., Moar, N., Wilmshurst, J., & Vandergoes, M. (2013). The vegetation cover of New Zealand at the last glacial maximum. *Quaternary Science Reviews*, 74, 202-214.

- Obermeier, S. F. (1996). Use of liquefaction-induced features for paleoseismic analysis — An overview of how seismic liquefaction features can be distinguished from other features and how their regional distribution and properties of source sediment can be used to infer the location and strength of Holocene paleo-earthquakes. *Engineering Geology*, 44(1–4), 1-76.
- Obermeier, S. F., Olson, S. M., & Green, R. A. (2005). Field occurrences of liquefaction-induced features: a primer for engineering geologic analysis of paleoseismic shaking. *Engineering Geology*, 76(3–4), 209-234.
- Orense, R. P., & Pender, M. J. (2013). *Liquefaction characteristics of crushable pumice sand*. Paper presented at Proc. of the 18th International Conference on Soil Mechanics and Geotechnical Engineering. Paris, France.
- Orense, R. P., Pender, M. J., & Tai, A. (2014). Undrained cyclic shear strength of crushable sands. *International Journal of Geotechnical Engineering*, 8(4), 426-430.
- Owen, G. (1987). Deformation processes in unconsolidated sands. *Geological Society, London, Special Publications*, 29(1), 11-24.
- Owen, G. (2003). Pseudonodules. *Sedimentology* (pp. 896-899): Springer Netherlands. Retrieved from http://dx.doi.org/10.1007/978-1-4020-3609-5_165.
- Owen, G., & Moretti, M. (2011). Identifying triggers for liquefaction-induced soft-sediment deformation in sands. *Sedimentary Geology*, 235(3–4), 141-147.
- Owen, G., Moretti, M., & Alfaro, P. (2011). Recognising triggers for soft-sediment deformation: Current understanding and future directions. *Sedimentary Geology*, 235(3–4), 133-140.
- Persaud, M., Berryman, K. R., & Villamor, P. (2003). *Paleoseismology of the Kerpehi Fault, Hauraki Graben*. Paper presented at Geological Society of New Zealand Otago Conference. Otago, New Zealand.
- Pettinga, J. R., Yetton, M. D., Van Dissen, R. J., & Downes, G. (2001). Earthquake source identification and characterisation for the Canterbury region, South Island, New Zealand. *Bulletin of the New Zealand National Society for Earthquake Engineering*, 34(4), 282-317.
- Price, D. G. (2008). *Engineering geology: principles and practice*. Springer.
- Pryce, T. V. (1997). *Distribution and geotechnical properties of Quaternary volcanogenic deposits and soils, Flagstaff North, Hamilton, New Zealand*. Master of Science (Technology) in Earth Science unpublished thesis, University of Waikato.
- Quigley, M. C., Bastin, S., & Bradley, B. A. (2013). Recurrent liquefaction in Christchurch, New Zealand, during the Canterbury earthquake sequence. *Geology*, 41(4), 419-422.

- Ramsey, N. (2010). *Some issues related to application of the CPT*. Paper presented at 2nd International Symposium on Cone Penetration Testing, CPT'10. Huntington Beach, California.
- Rana, N., Bhattacharya, F., Basavaiah, N., Pant, R. K., & Juyal, N. (2013). Soft sediment deformation structures and their implications for Late Quaternary seismicity on the South Tibetan Detachment System, Central Himalaya (Uttarakhand), India. *Tectonophysics*, 592(0), 165-174.
- Robertson, P. K. (1990). Soil classification using the cone penetration test. *Canadian Geotechnical Journal*, 27(1), 151-158.
- Robertson, P. K. (2009). Interpretation of cone penetration tests — a unified approach. *Canadian Geotechnical Journal*, 46(11), 1337-1355.
- Robertson, P. K. (2010a). Evaluation of Flow Liquefaction and Liquefied Strength Using the Cone Penetration Test. *Journal of Geotechnical and Geoenvironmental Engineering*, 136(6), 842-853.
- Robertson, P. K. (2010b). *Soil behaviour type from the CPT: an update*. Paper presented at 2nd International Symposium on Cone Penetration Testing. Huntington Beach, California.
- Robertson, P. K., & Wride, C. E. (1998). Evaluating cyclic liquefaction potential using the cone penetration test. *Canadian Geotechnical Journal*, 35(3), 442-459.
- Robertson, P. K., & Cabal, K. L. (2012). *Guide to Cone Penetration Testing for Geotechnical Engineering*. (5th ed.): Gregg Drilling & Testing, Inc.
- Robertson, P. K., Campanella, R., Gillespie, D., & Greig, J. (1986). *Use of piezometer cone data*. Use of in situ tests in geotechnical engineering: ASCE.
- Schofield, J. C. (1965). The hinuera formation and associated quaternary events. *New Zealand Journal of Geology and Geophysics*, 8(5), 772-791.
- Schofield, J. C. (1972). *Ground water of Hamilton Lowland*. Wellington,: Dept. of Scientific and Industrial Research.
- Seed, H. B., & Idriss, I. M. (1971). Simplified procedure for evaluating soil liquefaction potential. *Journal of the Soil Mechanics and Foundations Division*, 97(9), 1249-1273.
- Seed, H. B., & Idriss, I. (1982). *Ground motions and soil liquefaction during earthquakes*. Vol. 5: Earthquake Engineering Research Institute Oakland, CA.
- Seed, H. B., Tokimatsu, K., Harder, L., & Chung, R. (1985). Influence of SPT Procedures in Soil Liquefaction Resistance Evaluations. *Journal of Geotechnical Engineering*, 111(12), 1425-1445.

- Seilacher, A. (1969). Fault-graded beds interpreted as seismites. *Sedimentology*, 13(1-2), 155-159.
- Seilacher, A. (1984). Sedimentary structures tentatively attributed to seismic events. *Marine Geology*, 55(1-2), 1-12.
- Selby, M. J. L., D J. (1992). The Middle Waikato Basin and Hills In J. M. Soons & M. J. Selby (Eds.), *Landforms of New Zealand* (Second Edition ed., pp. 233-256). New Zealand.
- Sims, J. D., & Garvin, C. D. (1995). Recurrent liquefaction induced by the 1989 Loma Prieta earthquake and 1990 and 1991 aftershocks: Implications for paleoseismicity studies. *Bulletin of the Seismological Society of America*, 85(1), 51-65.
- Singleton, P. L. (1991). *Soils of Ruakura - a window on the Waikato*. Lower Hutt, N.Z, DSIR Land Resources.
- Skempton, A. (1986). Standard penetration test procedures and the effects in sands of overburden pressure, relative density, particle size, ageing and overconsolidation. *Geotechnique*, 36(3), 425-447.
- Standards New Zealand. NZS1170.5: 2004, *Structural Design Actions Part 5: Earthquake actions – New Zealand*.
- Stirling, M., McVerry, G., Gerstenberger, M., Litchfield, N., Van Dissen, R., Berryman, K., Barnes, P., Wallace, L., Villamor, P., & Langridge, R. (2012). National seismic hazard model for New Zealand: 2010 update. *Bulletin of the Seismological Society of America*, 102(4), 1514-1542.
- Sylvester, Z., & Lowe, D. (2003). Dish structure. *Sedimentology* (pp. 368-370): Springer Netherlands. Retrieved from http://dx.doi.org/10.1007/978-1-4020-3609-5_70.
- Tonkin and Taylor. (2013). *Liquefaction vulnerability study*. Report prepared for: Earthquake Commission.
- Tonkin, P. J. (1970). Contorted stratification with clay lobes in volcanic ash beds, Raglan-Hamilton region, New Zealand. *Earth Science Journal*, 4(2), 129-140.
- Tuttle, M. P. (2001). The use of liquefaction features in paleoseismology: Lessons learned in the New Madrid seismic zone, central United States. *Journal of Seismology*, 5(3), 361-380.
- Vandergoes, M. J., Hogg, A. G., Lowe, D. J., Newnham, R. M., Denton, G. H., Southon, J., Barrell, D. J. A., Wilson, C. J. N., McGlone, M. S., Allan, A. S. R., Almond, P. C., Petchey, F., Dabell, K., Dieffenbacher-Krall, A. C., & Blaauw, M. (2013). A revised age for the Kawakawa/Oruanui tephra, a key marker for the Last Glacial Maximum in New Zealand. *Quaternary Science Reviews*, 74(0), 195-201.

- Villamor, P., Litchfield, N., Barrell, D., Van Dissen, R., Hornblow, S., Quigley, M., Levick, S., Ries, W., Duffy, B., Begg, J., Townsend, D., Stahl, T., Bilderback, E., Noble, D., Furlong, K., & Grant, H. (2012). Map of the 2010 Greendale Fault surface rupture, Canterbury, New Zealand: application to land use planning. *New Zealand Journal of Geology and Geophysics*, 55(3), 223-230.
- Wair, B., DeJong, J., & Shantz, T. (2012). Guidelines for Estimation of Shear Wave Velocity Profiles. *Pacific Earthquake Engineering Research (PEER) Report*, 8.
- Webb, T. H., & Lilburne, L. (2011). *Criteria for defining the soil family and soil sibling: the fourth and fifth categories of the New Zealand Soil Classification*. Vol. 3. Lincoln, New Zealand: Manaaki Whenua Press, Landcare Research.
- Webb, T. H. (Ed.). (1994). *Soil-landscape modelling in New Zealand: proceedings of a workshop held at Aokautere, New Zealand, 8-9 February 1993* (Vol. no. 5). Lincoln, N.Z: Manaaki Whenua Press.
- Youd, T., Idriss, I., Andrus, R. D., Arango, I., Castro, G., Christian, J. T., Dobry, R., Finn, W. L., Harder Jr, L. F., & Hynes, M. E. (2001). Liquefaction resistance of soils: summary report from the 1996 NCEER and 1998 NCEER/NSF workshops on evaluation of liquefaction resistance of soils. *Journal of Geotechnical and Geoenvironmental Engineering*, 127(10), 817-833.
- Youd, T. L., & Perkins, D. M. (1978). Mapping liquefaction-induced ground failure potential. *Journal of the Geotechnical Engineering Division*, 104(4), 433-446.
- Zhang, G., Robertson, P. K., & Brachman, R. W. I. (2002). Estimating liquefaction-induced ground settlements from CPT for level ground. *Canadian Geotechnical Journal*, 39(5), 1168-1180.